Mathematical Modeling and Numerical Simulation of Piezoelectrical Agitated Surface Acoustic Waves

Dissertation zur Erlangung des Doktorgrades der
Mathematisch-Naturwissenschaftlichen Fakultät der
Universität Augsburg

vorgelegt von
Andreas Gantner

Erster Gutachter:	Prof. Dr. Ronald H.W. Hoppe, Universität Augsburg,
Zweiter Gutachter:	Prof. Dr. Kunibert G. Siebert, Universität Augsburg,
Dritter Gutachter:	Prof. Dr. Axel Klawonn, Universität Duisburg-Essen,
Vierter Gutachter:	Prof. Dr. Raytcho Lazarov, Texas A&M University.

Tag der mündlichen Prüfung: 28. Juni 2005

Für Astrid

Contents

1 Introduction

In life sciences, during the past few years increasing efforts have been devoted to the development of so-called "labs-on-a-chip". By definition, these are chip-based miniature laboratories that can be controlled electronically (and thus by computers). In spite of their smallness, the chip laboratories are able to conduct complex tasks in biology and chemistry on a few square centimeters where otherwise full-size laboratories are needed.
Of course, the driving force behind these ambitions is the need for extreme miniaturization in certain assays. Sometimes, only tiny amounts of certain samples are available for investigation, e.g., in gene expression profiling analysis or forensic tasks. Drug discovery and molecular biology demand precise handling of precious sample material and costly reagents on the scale of a millionth of a liter and often, simply no full-size laboratory is at hand as, e.g., in space-flight applications.
Nearly all attempts for realizing such a "lab-on-a-chip" tried to transfer devices and systems known from the macro-world by several scales in magnitude: micropumps, microchannels or micropipettes have been realized with huge technological effort and in especially developed production processes. The aim behind all is the realization of a "total analysis system" (μTAS) which is able to perform also complex assays.

1.1 The Advalytix Biochip

The German company Advalytix AG [2] (located in Brunnthal near Munich) around the physicist Prof. Dr. Achim Wixforth [104] from the University of Augsburg, has developed a technology that brings about precise electronic control of chemical reactions on the surface of a biochip [105, 106, 107]. This feature is made possible by nanopumps utilizing so-called surface acoustic waves (SAWs) propagating on the

surface of the chip just like earthquakes would do. These SAWs can be easily excited by applying radiofrequency pulses to so-called interdigital transducers (IDTs) located on the surface of a piezoelectric substrate. As they move along, they are able to transport fluids and solid matters across the chip surface (see Figure 1.1). At first glance, this looks astonishing, since the mechanical amplitude of the SAW is tiny, just a few nanometers, compared to the liquid diameter which typically is in the region of millimeters or centimeters.

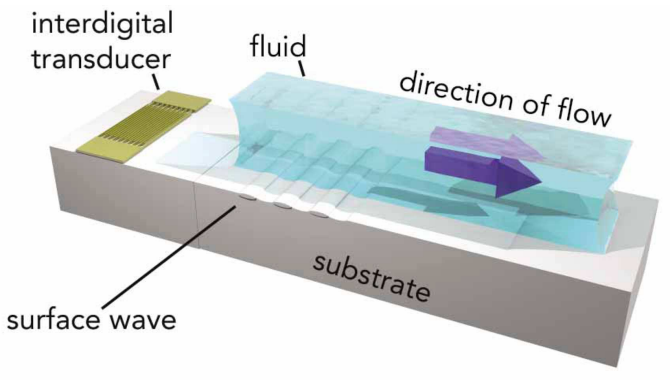

Figure 1.1: Working principle of an SAW biochip

By using lithographic techniques, the surface can be divided into hydrophilic and hydrophobic parts, changing the chips' surface chemistry in a precisely controlled way. In doing so, a fluidic network is laid out on the surface of the chip without patterning the chip mechanically, thus building predefined tracks for small droplets to ride on while driven by the SAW nanopumps (see Figure 1.2).

However, the SAW biochip technology cannot only be used for transportation processes, but also, e.g., for assays where mixing of small amounts of liquid is necessary (see Figure 1.3). This is an important task, e.g., in gene expression analysis where sample cDNA molecules bind to spotted probe molecules on a DNA microarray. In conventional assays, diffusion in the sample solution is the only mechanism for the cDNA molecules to move to the spotted DNA. Using the biochip, by microagitation of the sample solution, much better and faster results are obtained [2].

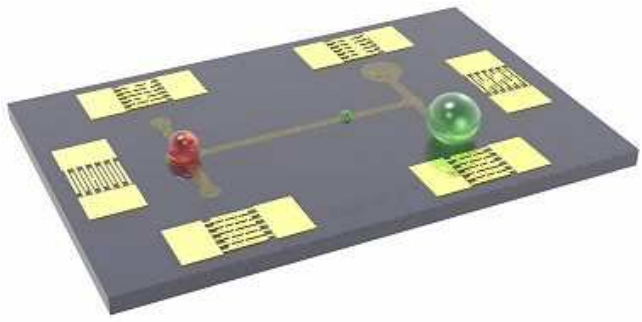

Figure 1.2: Fluidic Network

Figure 1.3: Mixing of small amounts of liquid

1.2 Mathematical Problem Treatment

Precise mathematical modeling and numerical simulations can help to achieve a precise understanding of the processes on a biochip. In this thesis, we develop a mathematical model for the SAW biochip based on the linearized equations of piezoelectricity given by

$$\begin{aligned} \rho\, u_{i,tt} - c_{ijkl}\, u_{k,lj} - e_{kij}\, \Phi_{,kj} &= 0 \ , \\ e_{ikl}\, u_{k,li} - \epsilon_{ij}\, \Phi_{,ji} &= 0 \ , \end{aligned}$$

where u_i denote the components of the mechanical displacement, Φ the electric potential, and c_{ijkl}, e_{kij} and ϵ_{ij} the components of the material moduli. Energetic considerations show that the material tensors $\boldsymbol{\epsilon}$ and $\boldsymbol{c}$ admit special ellipticity properties as well as the model analysis shows special symmetry properties for the tensors $\boldsymbol{\epsilon}$, $\boldsymbol{c}$ and $\boldsymbol{e}$.

These tensor properties will prove useful in the analysis by mathematical methods. A variational approach leeds to a formulation of the piezoelectric equations in the dual

spaces of the spatial Hilbert spaces $\boldsymbol{\mathcal{V}}$ and $\mathcal{W}$, i.e.

$$\begin{aligned} \rho\,\boldsymbol{u}_{,tt} + \boldsymbol{\mathcal{A}}\boldsymbol{u} + \boldsymbol{\mathcal{B}}\Phi &= \boldsymbol{f}\ , \qquad \text{in } \boldsymbol{\mathcal{V}}'\ , \\ \mathcal{B}'\boldsymbol{u} - \mathcal{C}\Phi &= g\ , \qquad \text{in } \mathcal{W}'\ , \end{aligned}$$

where the operators $\boldsymbol{\mathcal{A}}$ and $\mathcal{C}$ inherit their symmetry and ellipticity directly from the corresponding properties of $\boldsymbol{c}$ and $\boldsymbol{\epsilon}$ and some fundamental Sobolev space inequalities. We show that these equations admit unique solutions under very general conditions. Here, the properties of the Hilbert spaces $\boldsymbol{\mathcal{V}}$ and $\mathcal{W}$ play an essential role as well as the construction of the right-hand sides $\boldsymbol{f}$ and g.
Analytical studies of equations second order in time exist for a long time, cf. [72, 49]. However, the theories developed there cannot be applied directly: Only after a Gaussian elimination step resulting in the reduced Schur complement system

$$\rho\,\boldsymbol{u}_{,tt} \ + \ \boldsymbol{\mathcal{S}}\boldsymbol{u} \ = \ \boldsymbol{F}\ , \qquad \text{in } \boldsymbol{\mathcal{V}}'\ ,$$

the results from these books can be used. This requires an intrinsic study of the properties of the Schur complement operator $\boldsymbol{\mathcal{S}}$.

The operator $\boldsymbol{\mathcal{S}}$ also plays the all-dominant role in the analysis of the time harmonic approach,

$$\boldsymbol{u}(\boldsymbol{x},t) \ = \ \Re\,(\,\boldsymbol{u}(\boldsymbol{x})\exp(-\mathrm{i}\omega\mathrm{t})\,)\ ,$$

resulting (after an adaption of the spaces and boundary data) in the time harmonic operator relation

$$\boldsymbol{\mathcal{S}}\boldsymbol{u} \ - \ \rho\omega^2\boldsymbol{I}\boldsymbol{u} \ = \ \boldsymbol{F}\ , \qquad \text{in } \boldsymbol{\mathcal{V}}'\ .$$

We will use the Riesz-Schauder theory to derive conditions on the solvability of this equation, a technique that is well-established e.g. for the Helmholtz equation, cf. for instance [112], which is usually considered in connection to scattering problems [61, 77]. Our result will be essentially that these equations admit unique solutions except for countably many generalized real eigenvalues $\rho\omega^2$ of $\boldsymbol{\mathcal{S}}$ that cannot accumulate in $\mathbb{R}$. Even if $\rho\omega^2$ is an eigenvalue of $\boldsymbol{\mathcal{S}}$, the solvability is guaranteed under certain conditions on the boundary data. However, in these cases the solutions in general are not unique.

The study of the time-independent equations is of utmost importance for the analysis of time-harmonic and fully time-dependant problems. These equations now take the form of saddle point problems, and after a finite element discretization we get the linear system

$$\begin{aligned} \boldsymbol{A}u + \boldsymbol{B}\Phi &= f\ , \qquad \text{in } \mathcal{V} = \mathbb{R}^n\ , \\ \boldsymbol{B}^T u - \boldsymbol{C}\Phi &= g\ , \qquad \text{in } \mathcal{W} = \mathbb{R}^m\ . \end{aligned}$$

Finite element problems with $\boldsymbol{C} = \boldsymbol{0}$ were extensively studied in the literature, e.g. in [10, 22, 52]. Here, we focus on the case $\boldsymbol{C} \neq \boldsymbol{0}$. Such problem have been studied in the context of stabilized mixed finite element methods [17, 23, 31] or in the finite element modeling of slightly compressible fluids and solids [18, 65]. Also, some interior point methods in optimization result in systems with $\boldsymbol{C} \neq \boldsymbol{0}$ [108, 109]. In all of these cases the matrix $\boldsymbol{C}$ has small norm compared to the other blocks. We establish a condition number bound for the Schur complement matrix $\boldsymbol{S}$ that is independent of the meshsize parameter in the norm of the continuous Sobolev space $\boldsymbol{\mathcal{V}}$. Note that in our case there is no significant difference in the norms of $\boldsymbol{A}$ and $\boldsymbol{C}$.

The first iterative scheme for the solution of saddle point problems of a rather general type was that developed by Uzawa [98]. Uzawa type methods are stationary schemes consisting of simultaneous iterations for $\boldsymbol{u}$ and Φ. By elimination of one of the unknown vectors, they can also be interpreted as iterations for the reduced Schur complement system. Convergence results depend strongly on spectral properties of the Schur complement matrix $\boldsymbol{S}$. However, by $\boldsymbol{S} = \boldsymbol{A} + \boldsymbol{B}\boldsymbol{C}^{-1}\boldsymbol{B}^T$ each iteration step requires the solution of a system of equations with coefficient matrix $\boldsymbol{C}$. For large and sparse matrices this system is solved by an inner iteration resulting in an inexact Uzawa method [11, 40, 19].

Krylov subspace methods have turned out to be a strong alternative for the iterative solution of saddle point problems, particularly when a specially adapted preconditioner is at hand [101, 94, 67, 68].
For elliptic equations, construction principles for preconditioners are well-established, the fastest among them often resulting from domain decomposition and multilevel methods [96]. For indefinite systems we can fall back on these construction principles

and adapt the preconditioners to the indefinite setting. We use an approach similar to that in [94, 67, 68] and show that the condition number of the thus obtained Schur complement matrix $\hat{\boldsymbol{S}}$ is bounded by a constant independent of the meshsize parameter h.

SAW devices are used for a wide range of applications, particularly in high frequency signal processing [45]. Thus, pseudo-analytical studies can be found [7, 74, 78, 85] as well as finite element [4, 70, 41, 59], boundary element [57, 35] and combined finite/boundary element approaches [100, 48]. However, these approaches often use severely simplifying assumptions like an infinite size of the piezoelectric substrate, isotropic material behavior and the assumption of plane wave propagation. An interesting treatment of Love waves can be found in [16].
All the cited works lack a mathematical analysis of the underlying piezoelectric equations and often also of the used numerical methods. Thus, the mathematical modeling and numerical simulation of SAW devices is still of huge interest from an industrial as well as an analytical viewpoint.

Experimental studies of certain effects can be very expensive and time-consuming. Thus, the study of such effects lends itself to simulate the processes and analyze the numerical results. This is true all the more as quantitative statements are not possible at the current technological status quo. Finally, the effective simulation of the SAW biochip opens the door to on-demand optimization.

1.3 Outline

The remainder of this thesis is organized as follows.

In the second chapter, we shortly review the derivation of the piezoelectric field equations. Piezoelectric problems are coupled electro-mechanical problems. A mathematical treatment leeds to different mathematical formulations of the physical problem either as a indefinite saddle-point or a symmetric positive definite Schur complement problem. Finally, existence and uniqueness results for the piezoelectric equations are established.

The third chapter addresses the principles of surface acoustic wave propagation in a piezoelectric substrate. We shortly outline the usual handling used by physicists. Based on a time-harmonic approach we derive a formulation as a generalized eigenvalue problem for the Schur complement operator. Using Riesz-Schauder theory, we show that the time-harmonic equations admit unique solutions except for countably many frequencies. An Ansatz to simplify matters by a dimensional reduction is shortly described.

The forth chapter shortly reviews the principles of the finite element discretization of the coupled problem. Saddle point problems in the finite element context are considered whereas we underline the importance of Babuška's theorem. The case $\boldsymbol{C} = \boldsymbol{0}$ is well treated by the literature. We generalize the results to our situation.

In the fifth chapter, we address efficient iterative methods for the discretized problem. Special issues for saddle point problems are covered: Uzawa methods are especially adapted iterative methods for saddle point problems. However, Krylov subspace methods are often superior when they account for the special saddle point structure of the given equations by the choice of particular preconditioners.

Such preconditioners are constructed in Chapter 6. The performance of iterative methods is related to the condition number of the coefficient matrix of the system. We examine construction principles of preconditioners for the saddle point problem.

In Chapter 7, we examine the performance of the methods developed before. First, an artificial test example is chosen to show the accuracy of the methods. Then, the methods have to testify themselves in a real-life SAW device simulation.

2 Mathematical Theory Of Piezoelectricity

2.1 Linear Model of Piezoelectricity

An isolator exposed to an electric field $\boldsymbol{E}$ experiences forces on its free charges and undergoes a mechanical deformation. The origin of this piezoelectric effect is related

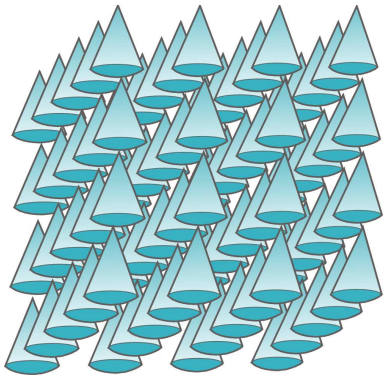

Figure 2.1: Polar axis: Rotational symmetry around each cone axis, but the two axis directions are not equivalent.

to an asymmetry in the unit cell and can only be observed in materials with a polar axis, i.e., in face of a rotational symmetry around this axis there are differences in the two directions of this axis. For an illustration, see Figure 2.1, where each cone in an infinite array of cones stands for the unit cell of a piezoelectric crystal.

Crystallographers recognize 32 classes of crystals of which 20 exhibit the piezoelectric effect. Figure 2.2 b) shows a traditional "PZT" piezoelectric material consisting of a small, tetravalent metal ion, usually titanium or zirconium, in a lattice of larger di-

valent metal ions, usually lead or barium, and O_2-ions. Such materials show a simple

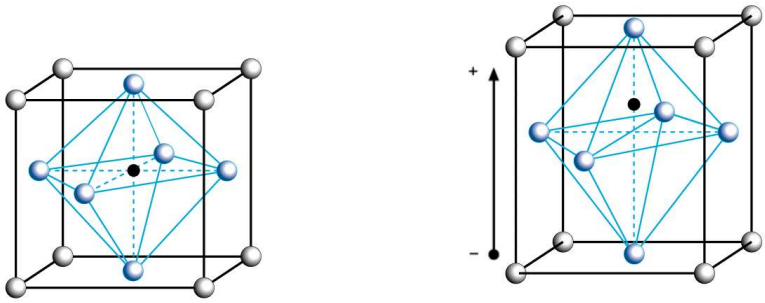

(a) Temperature above Curie point (b) Temperature below Curie point

Figure 2.2: Crystallographic structure of a "PZT" material

cubic symmetry above the Curie temperature and are thus isotropic before poling. After poling, they exhibit a tetragonal symmetry below the Curie temperature (see Figure 2.2 b). Above this temperature, they lose the piezoelectric properties again.

In piezoelectric materials, the mechanical stress $\boldsymbol{\sigma}$ depends linearly on the electric field $\boldsymbol{E}$, in contrast to non-piezoelectric materials where the effect is quadratic. Piezoelectric materials also show the reverse effect to generate an electric field when subjected to mechanical stress. These behaviors were labeled the piezoelectric effect and the inverse piezoelectric effect, respectively, from the Greek word piezein ($\pi\iota\grave{\epsilon}\zeta\varepsilon\iota\nu$), meaning to press or squeeze. Ever since the brothers Pierre and Jacques Curie [34, 33] discovered the piezoelectric effect on materials such as tourmaline or quartz, piezoelectric devices have become the basis for many daily life objects of utility. Although the magnitudes of piezoelectric voltages, movements, or forces are small, and often require amplification (for instance, a typical disc of piezoelectric ceramic will increase or decrease in thickness by only a small fraction of a millimeter), piezoelectric materials have been adapted to an impressive range of applications: The piezoelectric effect is used in sensing applications, such as in force or displacement sensors. The inverse piezoelectric effect is used in actuation applications, such as in motors and devices that precisely control positioning, and in generating sonic and ultrasonic signals. Typical piezoelectric materials are quartz (SiO_2), lithium niobate ($LiNbO_3$) or barium titanate ($BaTiO_3$).

Learning from above, piezoelectric problems are elasticity problems coupled to problems from electricity. We consider a linear model for piezoelectricity in which the elastic, piezoelectric and dielectric coefficients are treated as constants independent of the magnitude and frequency of applied mechanical stresses and electric fields. The model is macroscopic, i.e., only mean values of the relevant physical magnitudes are incorporated. Real materials involve microscopic effects as well as mechanical and electric dissipation and nonlinear behavior. For further reference on piezoelectric problems see [42, 74] and the references therein.

2.1.1 Elastic Properties of Piezoelectric Crystals

Let $\Omega \subset \mathbb{R}^d$ be a spatial Lipschitz domain, where $d = 2, 3$, let $T := [0, \tau) \subset \mathbb{R}_+$ be a time interval, and let $\boldsymbol{\varphi} = \mathbf{id} + \boldsymbol{u}$ be a standard C^1-deformation, with $\boldsymbol{u} = \boldsymbol{u}(\boldsymbol{x}, t)$ denoting the mechanical displacement for $\boldsymbol{x} \in \Omega$ and $t \in T$. The Green deformation tensor $\tilde{\boldsymbol{\varepsilon}}$ is then given by

$$\tilde{\boldsymbol{\varepsilon}} := \frac{1}{2}\left((\boldsymbol{\nabla}\boldsymbol{\varphi})^T \boldsymbol{\nabla}\boldsymbol{\varphi} - \mathbf{id} \right) = \frac{1}{2}\left((\boldsymbol{\nabla}\boldsymbol{u})^T + \boldsymbol{\nabla}\boldsymbol{u} + (\boldsymbol{\nabla}\boldsymbol{u})^T \boldsymbol{\nabla}\boldsymbol{u} \right) ,$$

which contains geometrical information like volume changes (see, e.g., [73, 13, 95] for further references on elasticity). The linear theory of piezoelectricity assumes that the displacement gradients are sufficiently small and hence, the term $(\boldsymbol{\nabla}\boldsymbol{u})^T \boldsymbol{\nabla}\boldsymbol{u}$ can be omitted. This means that the underlying deformation is considered as a simple elongation and the deformation tensor $\tilde{\boldsymbol{\varepsilon}}$ becomes the infinitesimal strain tensor $\boldsymbol{\varepsilon}$:

$$\boldsymbol{\varepsilon}(\boldsymbol{u}) := \frac{1}{2}\left((\boldsymbol{\nabla}\boldsymbol{u})^T + \boldsymbol{\nabla}\boldsymbol{u} \right) . \tag{2.1.1}$$

Since a piezoelectric material is anisotropic, physical constants relate to both the direction of the applied mechanical or electric force and the directions perpendicular to the applied force. Consequently, each physical magnitude generally has two subscripts that indicate these directions. For example, a full determination of the stress state $\boldsymbol{\sigma} = (\sigma_{ij})_{i,j=1}^3$ in the vicinity of a given point within the body assumes the determination of elastic stress vectors $\boldsymbol{t}_i$ acting on three mutually perpendicular planes running through the point. The planes are usually placed in such a way that their

normal lines are parallel to the three rectangular coordinate axes x_1, x_2 and x_3 as in Figure 2.3. More general, the traction $\boldsymbol{t}(\boldsymbol{n})$ in direction $\boldsymbol{n}$ is given by the relation $\boldsymbol{t}(\boldsymbol{n}) = \boldsymbol{\sigma} \cdot \boldsymbol{n}$.

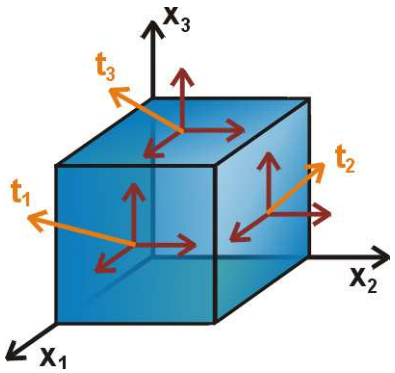

Figure 2.3: Stresses on the unit cube

One of the basic principles of mechanics is the balance of momentum. In the presence of a body force $\boldsymbol{b}$, this law takes the form

$$\rho\, \boldsymbol{u}_{,tt} \;=\; \boldsymbol{b} + \boldsymbol{\nabla} \cdot \boldsymbol{\sigma}\ , \qquad \text{or} \qquad \rho\, \boldsymbol{u}_{i,tt} \;=\; b_i + \sigma_{ij,j}\ , \tag{2.1.2}$$

where we have used the Einstein summation convention for repeated tensor indices and the notation $v_{,i}$ for the partial differentiation of a function v with respect to the direction x_i, if $i = 1, 2, 3$, or with respect to t, if $i = t$. The mass per unit volume is denoted by ρ, and will be a constant throughout this work.

The generalized Hooke's law states that the mechanical stresses can be calculated as a linear combination from the infinitesimal strain tensor. As mentioned above, in piezoelectric materials, an electric field $\boldsymbol{E} = \boldsymbol{E}(\boldsymbol{x}, t)$ produces an additional mechanical stress in a linear way. Thus, the overall stress $\boldsymbol{\sigma}$ can be calculated as

$$\sigma_{ij}(\boldsymbol{u}, \boldsymbol{E}) \;=\; c_{ijkl}\varepsilon_{kl}(\boldsymbol{u}) \;-\; e_{kij}\boldsymbol{E}_{,k}\ . \tag{2.1.3}$$

Here, $\boldsymbol{c}$ is the forth-order elasticity tensor (or elastic stiffness tensor) with components c_{ijkl} (the elastic modules), $\boldsymbol{e}$ is the third-order piezoelectric tensor with components e_{kij}.

In view of the symmetry of the stress $\boldsymbol{\sigma}$ and the strain $\boldsymbol{\varepsilon}$, we get the symmetry properties

$$\text{for } \boldsymbol{c}: \qquad c_{ijkl} = c_{klij} , \qquad \text{(major symmetry)} , \tag{2.1.4}$$

$$c_{ijkl} = c_{jikl} , \qquad c_{ijkl} = c_{ijlk} , \qquad \text{(minor symmetry)} , \tag{2.1.5}$$

$$\text{for } \boldsymbol{e}: \qquad e_{ikl} = e_{ilk} . \tag{2.1.6}$$

Additionally, the tensor $\boldsymbol{c}$ is positive definite:

$$c_{ijkl}\xi_{ij}\xi_{kl} \geq \mathfrak{c}\,\xi_{ij}^2 , \qquad \forall \xi_{ij} \text{ satisfying } \xi_{ij} = \xi_{ji} . \tag{2.1.7}$$

2.1.2 Dielectric Properties of Piezoelectric Crystals

The electromagnetic field is governed by the four Maxwell's equations

$$\boldsymbol{\nabla} \times \boldsymbol{H} = \boldsymbol{D}_{,t} + \boldsymbol{J} , \tag{2.1.8}$$

$$\boldsymbol{\nabla} \times \boldsymbol{E} = -\boldsymbol{B}_{,t} , \tag{2.1.9}$$

$$\nabla \cdot \boldsymbol{B} = 0 , \tag{2.1.10}$$

$$\nabla \cdot \boldsymbol{D} = \rho_e , \tag{2.1.11}$$

where $\boldsymbol{E} = \boldsymbol{E}(\boldsymbol{x}, t)$ denotes the electric field as before, $\boldsymbol{D} = \boldsymbol{D}(\boldsymbol{x}, t)$ the electric displacement, $\boldsymbol{H} = \boldsymbol{H}(\boldsymbol{x}, t)$ the magnetic field, $\boldsymbol{B} = \boldsymbol{B}(\boldsymbol{x}, t)$ the magnetic induction, $\boldsymbol{J} = \boldsymbol{J}(\boldsymbol{x}, t)$ the current density and ρ_e the electric charge density. The magnetic field and the magnetic induction are related by $B_i = \mu_{ij} H_j$, where $\boldsymbol{\mu}$ is the permeability tensor. The electric field $\boldsymbol{E}$ and the electric displacement are related by

$$D_i = \epsilon_{ij} E_j + P_i , \tag{2.1.12}$$

where $\boldsymbol{P}$ is the electric polarization, which in the case of a piezoelectric material stems from an external stress, and $\boldsymbol{\epsilon}$ is the (symmetric positive definite) permittivity tensor. For further details on Maxwell's equations, we refer to [58, 27, 77]; treatments from a more physical viewpoint can be found e.g. in [63, 84].

In piezoelectric materials, the frequency of the occurring electric field wave is considered sufficiently small so that the coupling of electro-magnetic waves and elastic waves can be neglected. This means that local perturbations in the electro-magnetic field are felt almost instantaneously throughout the domain, so that the electric field can be treated as quasi-static. Mathematically, this can be achieved by setting the magnetic permeability to zero, corresponding to an infinite speed of the electro-magnetic wave. Maxwell's second equation $(2.1.9)$ then reduces to

$$\boldsymbol{\nabla} \times \boldsymbol{E} \;=\; \mathbf{0}\;,$$

i.e., the electric field is irrotational and thus can be represented as the gradient of an electric scalar potential according to

$$\boldsymbol{E} \;=\; -\boldsymbol{\nabla}\Phi\;. \tag{2.1.13}$$

When the electric field $\boldsymbol{E}$ is known, the magnetic field $\boldsymbol{H}$ can be obtained from the equation $(2.1.8)$. However, the magnetic field is rarely of interest in piezoelectric calculations and is therefore not considered further. Moreover, piezoelectric substrates are nearly perfect isolators, i.e., the density of free electric charges ρ_e and the current density $\boldsymbol{J}$ can be completely neglected. Thus, bearing $(2.1.13)$ in mind, the only relevant Maxwell equation is

$$\nabla \cdot \boldsymbol{D} \;=\; 0\;. \tag{2.1.14}$$

An important feature of piezoelectricity is the material law $(2.1.12)$. Figure 2.1.2 shows a schematic explanation for the formation of a polarization $\boldsymbol{P}$ in an atomic

Figure 2.4: The formation of a electric dipole by pressure

structure when subjected to external stress: In both cases one can see six "point

charges", "red" indicating positive and "green" negative charges. In a relaxed state with no forces acting on them, they are arranged at the vertices of an hexagon. In some distance, the positive and negative array of charges will cancel each other out and the potential Φ will be zero. If a compressive force is applied to the hexagon, the array is distorted in such a way as to bring two of the positive charges closer together at one end and the negative charges at the other. This forms a dipole where one end of the array is positive and the other one is negative. One can easily imagine a crystal structure made up of these hexagonal arrangements of ions.
In piezoelectric materials, the polarization according to external strain is linear. In analogy to the inverse effect $(2.1.3)$, we set

$$D_i(\boldsymbol{u}, \boldsymbol{E}) \;=\; e_{ikl}\varepsilon_{kl}(\boldsymbol{u}) + \;\epsilon_{ij}E_j \;. \tag{2.1.15}$$

2.1.3 Coupled Piezoelectric Equations

Summarizing, the constitutive equations can be written as follows (compare [42, 74]):

$$\sigma_{ij}(\boldsymbol{u}, \Phi) \;=\; c_{ijkl}\varepsilon_{kl}(\boldsymbol{u}) \;+\; e_{kij}\Phi_{,k} \;, \tag{2.1.16}$$

$$D_i(\boldsymbol{u}, \Phi) \;=\; e_{ikl}\varepsilon_{kl}(\boldsymbol{u}) \;-\; \epsilon_{ij}\Phi_{,j} \;. \tag{2.1.17}$$

In this case, the energy density is given by

$$\Sigma \;=\; \frac{1}{2}\left(\sigma_{ij}\varepsilon_{ij} \;+\; D_iE_i\right) \;=\; \frac{1}{2}c_{ijkl}\varepsilon_{ij}\varepsilon_{kl} \;+\; \frac{1}{2}\epsilon_{ij}E_iE_j \;. \tag{2.1.18}$$

The symmetry properties of the tensors are as follows:

$$c_{ijkl} \;=\; c_{klij} = \; c_{jikl} \;, \qquad e_{ikl} \;=\; e_{ilk} \;, \qquad \epsilon_{ij} \;=\; \epsilon_{ji} \;. \tag{2.1.19}$$

Moreover, the tensors $\boldsymbol{c}$ and $\boldsymbol{\epsilon}$ are positive definite:

$$c_{ijkl}\xi_{ij}\xi_{kl} \;\geq\; \mathfrak{c}\,\xi_{ij}^2 \;, \qquad \epsilon_{ij}\zeta_i\zeta_j \;\geq\; \mathfrak{e}\,\zeta_i^2 \;, \tag{2.1.20}$$

for all $\xi_{ij}, \zeta_i \in \mathbb{R}$, where $\xi_{ij} = \xi_{ji}$. Note that this can be derived from $(2.1.18)$ and the requirement for a positive energy.

Substituting the constitutive equations $(2.1.16)$,$(2.1.17)$ into $(2.1.14)$,$(2.1.2)$, we arrive at the field equations for piezoelectricity:

Problem 2.1.1 (Linear Field Equations for Piezoelectricity)
In a space-time domain $Q = \Omega \times T$, $\Omega \subset \mathbb{R}^d$, $T = (0, \tau)$, find a vector field $\boldsymbol{u} = \boldsymbol{u}(\boldsymbol{x}, t)$ and a scalar field $\Phi = \Phi(\boldsymbol{x}, t)$ satisfying

$$\rho\, u_{i,tt} - c_{ijkl}\, u_{k,lj} - e_{kij}\, \Phi_{,kj} = b_i \ , \tag{2.1.21}$$

$$e_{ikl}\, u_{k,li} - \epsilon_{ij}\, \Phi_{,ji} = 0 \ . \tag{2.1.22}$$

These equations are supplemented by the decoupled boundary conditions

$$\begin{aligned} \mathbf{u}|_{\Gamma_u} &= \boldsymbol{u}_\Gamma \ , \ \textit{(displacement)} \\ \boldsymbol{\sigma} \cdot \boldsymbol{n}|_{\Gamma_\sigma} &= \boldsymbol{\sigma}_n \ , \ \textit{(traction)} \end{aligned} \qquad \textit{where } \partial\Omega = \Gamma_u \dot{\cup} \Gamma_\sigma \ , \tag{2.1.23}$$

$$\begin{aligned} \Phi|_{\Gamma_\Phi} &= \Phi_\Gamma \ , \ \textit{(potential)} \\ \boldsymbol{D} \cdot \boldsymbol{n}|_{\Gamma_D} &= D_n \ , \end{aligned} \qquad \textit{where } \partial\Omega = \Gamma_\Phi \dot{\cup} \Gamma_D \ , \tag{2.1.24}$$

and by the initial conditions

$$\boldsymbol{u}(\boldsymbol{x}, 0) = \boldsymbol{u}_0(\boldsymbol{x}) \ , \qquad \boldsymbol{u}_{,t}(\boldsymbol{x}, 0) = \dot{\boldsymbol{u}}_0(\boldsymbol{x}) \ . \tag{2.1.25}$$

The Voigt Notation

Sometimes, it is useful to adopt a compressed notation for the piezoelectric moduli, the Voigt notation (see, e.g., [42, 74, 113]). By utilizing the symmetry properties of the third- and forth-order tensors they can be reduced to higher dimensional second-order matrices. To this end, we use the identification $I = (ij)$, where

(ij)	(11)	(22)	(33)	$(23) = (32)$	$(13) = (31)$	$(12) = (21)$
I	1	2	3	4	5	6

i.e., $c_{IK} = c_{ijkl}$, $e_{iK} = e_{ikl}$ and $\epsilon_I = \epsilon_{ij}$. With this notation, the characteristic

properties of a linear piezoelectric substrate are completely determined by the material matrix

$$\begin{pmatrix} c_{IK} & e_{Ki}^T \\ e_{iK} & \epsilon_{ij} \end{pmatrix} = \left(\begin{bmatrix} c_{11} & c_{12} & c_{13} & c_{14} & c_{15} & c_{16} \\ c_{12} & c_{22} & c_{23} & c_{24} & c_{25} & c_{26} \\ c_{13} & c_{23} & c_{33} & c_{34} & c_{35} & c_{36} \\ c_{14} & c_{24} & c_{34} & c_{44} & c_{45} & c_{46} \\ c_{15} & c_{25} & c_{35} & c_{45} & c_{55} & c_{56} \\ c_{16} & c_{26} & c_{36} & c_{46} & c_{56} & c_{66} \end{bmatrix} \quad \begin{bmatrix} e_{11} & e_{21} & e_{31} \\ e_{12} & e_{22} & e_{32} \\ e_{13} & e_{23} & e_{33} \\ e_{14} & e_{24} & e_{34} \\ e_{15} & e_{25} & e_{35} \\ e_{16} & e_{26} & e_{36} \end{bmatrix} \right.$$
$$\left. \begin{bmatrix} e_{11} & e_{12} & e_{13} & e_{14} & e_{15} & e_{16} \\ e_{21} & e_{22} & e_{23} & e_{24} & e_{25} & e_{26} \\ e_{31} & e_{32} & e_{33} & e_{34} & e_{35} & e_{36} \end{bmatrix} \quad \begin{bmatrix} \epsilon_{11} & \epsilon_{12} & \epsilon_{13} \\ \epsilon_{12} & \epsilon_{22} & \epsilon_{23} \\ \epsilon_{13} & \epsilon_{23} & \epsilon_{33} \end{bmatrix} \right).$$

The matrices c_{IK} and ϵ_{ij} are symmetric with respect to the main diagonal and hence, there are $21 + 18 + 6 = 45$ independent moduli for the most general piezoelectric substrates. Appendix A lists the material matrices for some commonly used piezoelectric crystals.

2.2 Mathematical Modeling of Piezoelectricity

2.2.1 Spatial Functional Framework

The standard Sobolev spaces on a Lipschitz domain D are denoted by $H^s(D)$ and $\boldsymbol{H}^s(D) := (H^s(D))^d$, $s \geq 0$, with inner products $(\cdot,\cdot)_{s;D}$ and $(\cdot,\cdot)_{s;D}$, and norms $\|\cdot\|_{s;D}$ and $\|\cdot\|_{s;D}$, respectively. Set $(\cdot,\cdot) := (\cdot,\cdot)_\Omega := (\cdot,\cdot)_{0;\Omega}$ and $\|\cdot\| := \|\cdot\|_{0;\Omega}$. The same notations in bold style are used in the vectorial case. Dual spaces, i.e. the set of all linear and bounded mappings from the original space onto $\mathbb{R}$, will be denoted by a prime, e.g., $H^s(D)'$ will be the dual space of $H^s(D)$ etc. These spaces are equipped by the usual dual norm, for instance, for $\psi \in H^s(D)'$,

$$\|\psi\|_{H^s(D)'} \;=\; \sup_{\varphi\in H^s(D)} \frac{|\psi(\varphi)|}{\|\varphi\|_{s;\Omega}} \;.$$

For results on Sobolev spaces and associated trace spaces we refer [72, 1, 53, 21].

Let $\Omega \subset \mathbb{R}^d$, $d = 2, 3$, be a Lipschitz domain, let $T := (0,\tau) \subset \mathbb{R}_+$ be a time interval, and let $Q := \Omega \times T$. According to the boundary conditions $(2.1.23)$-$(2.1.24)$ we decompose the boundary into two disjoint sets in two different ways by

$$\begin{aligned} \partial\Omega \;&=\; \Gamma_u \cup \Gamma_\sigma \;, \qquad \Gamma_\sigma \;=\; \partial\Omega \setminus \Gamma_u \;, \\ \partial\Omega \;&=\; \Gamma_\Phi \cup \Gamma_D \;, \qquad \Gamma_D \;=\; \partial\Omega \setminus \Gamma_\Phi \,, \end{aligned}$$

where the Dirichlet boundaries Γ_u and Γ_Φ are assumed to be closed and with non-vanishing $d-1$-dimensional measure. For a smooth and closed subset $\Gamma \subset \partial\Omega$ of the boundary, there exists a unique and stable restriction $\mathcal{R}_\Gamma\varphi \in H^{\frac{1}{2}}(\Gamma)$ of functions $\varphi \in H^1(\Omega)$ to the boundary, i.e. the well-known trace operator for functions in $C^\infty(\bar\Omega)$ can also be applied in $H^1(\Omega)$ and there exists a constant $C > 0$ such that

$$\|\mathcal{R}_\Gamma\varphi\|_{\frac{1}{2};\Omega} \;\leq\; C\|\varphi\|_{1;\Omega} \;, \qquad \forall\varphi \in H^1(\Omega) \;. \tag{2.2.1}$$

Often, we will simply use the notation $\varphi|_\Gamma := \mathcal{R}_\Gamma\varphi$. There exists a thereto right inverse extension operator $\mathcal{E}_\Gamma : H^{\frac{1}{2}}(\Gamma) \to H^1(\Omega)$ which is also stable and thus yields for $\varphi \in H^{\frac{1}{2}}(\Gamma)$ an extension $\mathcal{E}_\Gamma\varphi \in H^1(\Omega)$ with constant $c > 0$ such that

$$\|\mathcal{E}_\Gamma\varphi\|_{1;\Omega} \;\leq\; c\|\varphi\|_{\frac{1}{2};\Gamma} \;, \qquad \forall\varphi \in H^{\frac{1}{2}}(\Gamma) \;. \tag{2.2.2}$$

The same results hold analogously in the vectorial case for the function spaces $\boldsymbol{H}^1(\Omega)$ and $\boldsymbol{H}^{\frac{1}{2}}(\Gamma)$, and we will use the same symbols for the trace and extension, respectively, but in bold style.

Now, we introduce the following function spaces:

$$\boldsymbol{\mathcal{V}} \;:=\; \boldsymbol{H}^1_{0;\Gamma_u}(\Omega) \;:=\; \left\{\, \boldsymbol{v} \in \boldsymbol{H}^1(\Omega) \middle|\; \boldsymbol{v}|_{\Gamma_u} \;=\; 0 \,\right\} \,, \tag{2.2.3}$$

$$\mathcal{W} \;:=\; H^1_{0;\Gamma_\Phi}(\Omega) \;:=\; \left\{\, \varphi \in H^1(\Omega) \middle|\; \varphi|_{\Gamma_\Phi} \;=\; 0 \,\right\} \,. \tag{2.2.4}$$

Additionally, set

$$\boldsymbol{\mathcal{V}}_{\Gamma_u} \;:=\; \boldsymbol{\mathcal{E}}_{\Gamma_u}\boldsymbol{u}_\Gamma \,+\, \boldsymbol{\mathcal{V}} \,, \qquad \text{and} \qquad \mathcal{W}_{\Gamma_\Phi} \;:=\; \mathcal{E}_{\Gamma_\Phi}\Phi_\Gamma \,+\, \mathcal{W} \,,$$

that account for the given Dirichlet data on the boundaries. The space of zero traces is then defined as $H^1_0(\Omega) := H_{0;\partial\Omega}(\Omega)$ with dual space $H^{-1}(\Omega) := H^1_0(\Omega)'$. Now, the continuous embeddings

$$H^1_0(\Omega) \;\subset\; \mathcal{W} \;\subset\; H^1(\Omega) \;\subset\; L^2(\Omega) \;\subset\; H^1(\Omega)' \;\subset\; \mathcal{W}' \;\subset\; H^{-1}(\Omega) \,,$$

allow the usage of the norms $\|\cdot\|_{1;\Omega}$ in $\mathcal{W}$ and $\|\cdot\|_{-1;\Omega}$ in $\mathcal{W}'$. Moreover, the continuous and dense embeddings (by identifying $L^2(\Omega)' = L^2(\Omega)$)

$$\mathcal{W} \;\subset\; L^2(\Omega) \;\subset \mathcal{W}' \,,$$

imply that the dual pairing can be seen to take place in $L^2(\Omega)$. Again, similar notations are used in the vectorial case.

Note, for the Neumann boundary part $\Gamma_D \subset \partial\Omega$ the trace operator in $\mathcal{W} = H^1_{0;\Gamma_\Phi}(\Omega)$ is not surjective onto $H^{\frac{1}{2}}(\Gamma_D)$. The appropriate space for this would be $H^{\frac{1}{2}}_{00}(\Gamma_D)$, i.e. the space of functions whose trivial extension $\tilde{\varphi}$ by zero to all of $\partial\Omega$ is in $H^{\frac{1}{2}}(\partial\Omega)$. The norm for this space is given by

$$\|\varphi\|^2_{H^{\frac{1}{2}}_{00}(\Gamma_D)} \;=\; \|\varphi\|^2_{H^{\frac{1}{2}}(\Gamma_D)} \,+\, \int_{\Gamma_D} \frac{\varphi^2(\boldsymbol{x})}{d(\boldsymbol{x},\partial\Gamma_D)} \mathrm{d}s_{\boldsymbol{x}} \,,$$

and $d(\boldsymbol{x},\partial\Gamma_D)$ denotes distance of $\boldsymbol{x}$ to $\partial\Gamma_D$. The trace and extension inequalities (2.2.1)-(2.2.2) then hold true accordingly if we replace $H^{\frac{1}{2}}(\Gamma_D)$ by $H^{\frac{1}{2}}_{00}(\Gamma_D)$. Again,

the same results apply for the vectorial case.

We have to require some properties on the boundary data and the mechanical load vector, i.e., in some sense we have to specify their degree of smoothness. This will be done in the following formulation of some standard assumptions holding throughout this work:

Assumption 2.2.1 *Throughout this work, we will make the following standard assumptions on the time-independent boundary conditions:*

$$\begin{aligned} &\textit{Elastic boundary data:} && \boldsymbol{u}_\Gamma \in \boldsymbol{H}^{\frac{1}{2}}(\Gamma_u)\,, \qquad \boldsymbol{\sigma}_n \in \boldsymbol{H}_{00}^{\frac{1}{2}}(\Gamma_\sigma)'\,, \\ &\textit{Electric boundary data:} && \Phi_\Gamma \in H^{\frac{1}{2}}(\Gamma_\Phi)\,, \qquad D_n \in H_{00}^{\frac{1}{2}}(\Gamma_D)'\,, \\ &\textit{Mechanical force:} && \boldsymbol{b} \in \boldsymbol{\mathcal{V}}'\,. \end{aligned}$$

2.2.2 Functional Framework Including Time

Up til now, we have only considered functions in $\boldsymbol{x} \in \Omega$ for fixed $t \in T$, so far neglecting the dependence on the time variable t. We use the well-known notation $L^2(T, \mathcal{W})$ for functions $\varphi(\boldsymbol{x}, t)$ satisfying $\varphi(t) \in \mathcal{W}$ for all times $t \in T$ and $\|\varphi(t)\|_{\mathcal{W}} \in L^2(T)$. This is a Banach space equipped with the norm

$$\|\varphi\|_{L^2(T,\mathcal{W})} \;=\; \left(\int_0^\tau \|\varphi(t)\|_{\mathcal{W}}^2 \,\mathrm{d}t \right)^{\frac{1}{2}}\,.$$

Note, $L^2(Q) \subset L^2(T; L^2(\Omega))$. Similar notations are used in the vectorial case.

In the analysis of time-dependant problems the concept of an evolution triple plays an essential role, which is given here by the continuous and dense embeddings

$$\boldsymbol{\mathcal{V}} \;\subset\; \boldsymbol{L}^2(\Omega) \;\subset \boldsymbol{\mathcal{V}}'\,. \tag{2.2.5}$$

We introduce the function space of all functions $\boldsymbol{v} \in L^2(T; \boldsymbol{\mathcal{V}})$ with generalized derivatives $\boldsymbol{v}_{,t}$ in $L^2(T; \boldsymbol{\mathcal{V}}')$, i.e.

$$W^1\left(T; \boldsymbol{\mathcal{V}}, \boldsymbol{L}^2(\Omega)\right) \;:=\; \{\, \boldsymbol{v} \in \boldsymbol{\mathcal{V}} \mid\; \boldsymbol{v}_{,t} \in \boldsymbol{\mathcal{V}}' \,\}\,. \tag{2.2.6}$$

This space is a Banach space equipped with the norm

$$\|\boldsymbol{v}\|_{W^1(T;\boldsymbol{\mathcal{V}},\boldsymbol{L}^2(\Omega))} \;:=\; \|\boldsymbol{v}\|_{L^2(T;\boldsymbol{\mathcal{V}})} \,+\, \|\boldsymbol{v}_{,t}\|_{L^2(T;\boldsymbol{\mathcal{V}}')} \;.$$

Of course, by identifying $\boldsymbol{\mathcal{V}}$ and $\boldsymbol{\mathcal{V}}'$, spaces $W^1\left(T;\boldsymbol{L}^2(\Omega),\boldsymbol{\mathcal{V}}'\right)$ can be defined analogously. Note, the embedding

$$W^1\left(T;\boldsymbol{\mathcal{V}},\boldsymbol{L}^2(\Omega)\right) \;\subset\; C(\bar{T};\boldsymbol{L}^2(\Omega))\;, \tag{2.2.7}$$

is continuous. Thus, we require for the displacement solution $\boldsymbol{u}$ (here assuming homogeneous boundary conditions) to satisfy

$$\boldsymbol{u} \,\in\, L^2(T;\boldsymbol{\mathcal{V}})\,, \quad \boldsymbol{u}_{,t} \,\in\, L^2(T;\boldsymbol{L}^2(\Omega))\,, \quad \boldsymbol{u}_{,tt} \,\in\, L^2(T;\boldsymbol{\mathcal{V}}')\,,$$

which yields

$$\boldsymbol{u} \,\in\, W^1(T;\boldsymbol{\mathcal{V}},\boldsymbol{L}^2(\Omega))\,, \qquad \boldsymbol{u}_{,t} \,\in\, W^1(T;\boldsymbol{L}^2(\Omega),\boldsymbol{\mathcal{V}}')\;,$$

and therefore

$$\boldsymbol{u} \,\in\, C(\bar{T};\boldsymbol{L}^2(\Omega))\,, \qquad \boldsymbol{u}_{,t} \,\in\, C(\bar{T};\boldsymbol{\mathcal{V}}')\;. \tag{2.2.8}$$

On account of this, the initial conditions

$$\boldsymbol{u}(0) \,=\, \boldsymbol{u}_0 \in \boldsymbol{\mathcal{V}} \subset \boldsymbol{L}^2(\Omega)\,, \qquad \boldsymbol{u}_{,t}(0) \,=\, \dot{\boldsymbol{u}}_{\boldsymbol{0}} \in \boldsymbol{L}^2(\Omega) \subset \boldsymbol{\mathcal{V}}'\;,$$

are meaningful. For further reference see e.g. [72, 49, 112, 43].

As will be seen in the following section, the electric potential Φ can be regained from the displacement solution $\boldsymbol{u}$ and the boundary data D_n. Hence, the time regularity of the electric potential is simply inherited.

As before, we make some standard assumptions on the regularity of the boundary and initial data:

Assumption 2.2.2 *Throughout this work, we will make the following standard assumptions on the initial conditions and time-dependant boundary conditions*

$$\begin{aligned}
\textit{Elastic boundary data:}\quad & \boldsymbol{\mathcal{E}}_{\Gamma_u}\boldsymbol{u}_\Gamma \in W^1\left(T;\boldsymbol{H}^1(\Omega),\boldsymbol{L}^2(\Omega)\right)\ ,\quad \boldsymbol{\mathcal{E}}_{\Gamma_u}\boldsymbol{u}_{\Gamma,tt} \in L^2\left(T;\boldsymbol{\mathcal{V}}'\right)\ ,\\
& \boldsymbol{\sigma}_n \in L^2\left(T;\boldsymbol{H}^{\frac{1}{2}}_{00}(\Gamma_\sigma)'\right)\ ,\\
\textit{Initial displacement:}\quad & \boldsymbol{u}_0 \in \boldsymbol{\mathcal{V}}_{\Gamma_u}\ ,\ \dot{\boldsymbol{u}}_0 \in \boldsymbol{L}^2(\Omega)\ ,\\
\textit{Electric boundary data:}\quad & \Phi_\Gamma \in L^2\left(T;H^{\frac{1}{2}}(\Gamma_\Phi)\right)\ ,\quad D_n \in L^2\left(T;H^{\frac{1}{2}}_{00}(\Gamma_D)'\right)\ ,\\
\textit{Mechanical force:}\quad & \boldsymbol{b} \in L^2\left(T;\boldsymbol{\mathcal{V}}'\right)\ .
\end{aligned}$$

2.2.3 Variational Problem Formulation

Now, being provided with some functional analytic framework, we multiply our physical problem $(2.1.21)$-$(2.1.24)$ by a test function out of the function spaces $\boldsymbol{H}^1(\Omega)$ and $H^1(\Omega)$, respectively, and integrate by parts over the spatial domain Ω yielding

$$\int_\Omega c_{ijkl}\, v_{k,lj}\, w_i \;=\; -\int_\Omega c_{ijkl}\, v_{k,l}\, w_{i,j} \;+\; \int_{\partial\Omega} c_{ijkl}\, v_{k,l}\, w_i\, n_j\ , \tag{2.2.9}$$

$$\int_\Omega e_{kij}\, v_{i,jk}\, \varphi \;=\; -\int_\Omega e_{kij}\, v_{i,j}\, \varphi_{,k} \;+\; \int_{\partial\Omega} e_{kij}\, v_{i,j}\, \varphi\, n_k\ , \tag{2.2.10}$$

$$\int_\Omega \epsilon_{ij}\, \varphi_{,ji}\, \psi \;=\; -\int_\Omega \epsilon_{ij}\, \varphi_{,j}\, \psi_{,i} \;+\; \int_{\partial\Omega} \epsilon_{ij}\, \varphi_{,j}\, \psi n_i\ . \tag{2.2.11}$$

We introduce the following bilinear forms,

$$a(\boldsymbol{v},\boldsymbol{w}) \;:=\; \int_\Omega c_{ijkl}\, \varepsilon_{kl}(\boldsymbol{v})\, \varepsilon_{ij}(\boldsymbol{w})\ , \qquad \forall \boldsymbol{v},\boldsymbol{w} \in \boldsymbol{H}^1(\Omega)\ , \tag{2.2.12}$$

$$b(\varphi,\boldsymbol{v}) \;:=\; \int_\Omega e_{kij}\, \varphi_{,k}\, \varepsilon_{ij}(\boldsymbol{v})\ , \qquad \forall \varphi \in H^1(\Omega),\ \boldsymbol{v} \in \boldsymbol{H}^1(\Omega), \tag{2.2.13}$$

$$c(\varphi,\psi) \;:=\; \int_\Omega \epsilon_{ij}\, \varphi_{,i}\, \psi_{,j}\ , \qquad \forall \varphi,\psi \in H^1(\Omega)\ . \tag{2.2.14}$$

We note that due to the symmetry properties of $\boldsymbol{c}$ and $\boldsymbol{\varepsilon}$, we have

$$a(\boldsymbol{v},\boldsymbol{w}) \;:=\; \int_\Omega c_{ijkl}\, \varepsilon_{kl}(\boldsymbol{v})\, \varepsilon_{ij}(\boldsymbol{w}) \;=\; \int_\Omega c_{ijkl}\, v_{k,l}\, w_{i,j}\ .$$

A similar argument applies to the bilinear form $b(\cdot,\cdot)$.

We are now able to state the variational form of the piezoelectric problem:

Problem 2.2.3 (Variational Formulation) *Under Assumption 2.2.2, find solutions* $\boldsymbol{u} \in L^2(T, \boldsymbol{\mathcal{V}}_{\Gamma_u})$, *and* $\Phi \in L^2(T, \mathcal{W}_{\Gamma_\Phi})$, *satisfying* $\boldsymbol{u}_{,t} \in L^2(T, \boldsymbol{L}^2(\Omega))$, $\boldsymbol{u}_{,tt} \in L^2(T, \boldsymbol{\mathcal{V}}')$ *and*

$$\begin{aligned} (\rho \boldsymbol{u}_{,tt}, \boldsymbol{v}) + a(\boldsymbol{u}, \boldsymbol{v}) + b(\Phi, \boldsymbol{v}) &= (\boldsymbol{b}, \boldsymbol{v}) + (\boldsymbol{\sigma}_n, \boldsymbol{v}|_{\Gamma_\sigma})_{0;\Gamma_\sigma} , \quad \forall \boldsymbol{v} \in \boldsymbol{\mathcal{V}} , \\ b(\psi, \boldsymbol{u}) - c(\Phi, \psi) &= (D_n, \psi|_{\Gamma_D})_{0;\Gamma_D} , \qquad \forall \psi \in \mathcal{W} . \end{aligned}$$

The variational formulation of the piezoelectric problem is the starting point for the numerical approximation by finite element methods. We will choose a nodal basis for the function spaces $\boldsymbol{\mathcal{V}}$ and $\mathcal{W}$ leading to a linear system of equations that has to be solved by efficient iterative methods.

In a standard Riesz fashion, operators are associated with the above bilinearforms:

$$\boldsymbol{\mathcal{A}} : \boldsymbol{H}^1(\Omega) \to \boldsymbol{\mathcal{V}}' , \qquad (\boldsymbol{\mathcal{A}}\boldsymbol{v}, \boldsymbol{w}) := a(\boldsymbol{v}, \boldsymbol{w}) , \qquad \forall \boldsymbol{w} \in \boldsymbol{\mathcal{V}} , \tag{2.2.15}$$

$$\mathcal{B}' : \boldsymbol{H}^1(\Omega) \to \mathcal{W}' , \qquad (\varphi, \mathcal{B}'\boldsymbol{v}) := b(\varphi, \boldsymbol{v}) , \qquad \forall \varphi \in \mathcal{W} , \tag{2.2.16}$$

$$\boldsymbol{\mathcal{B}} : H^1(\Omega) \to \boldsymbol{\mathcal{V}}' , \qquad (\boldsymbol{\mathcal{B}}\varphi, \boldsymbol{v}) := b(\varphi, \boldsymbol{v}) , \qquad \forall \boldsymbol{v} \in \boldsymbol{\mathcal{V}} , \tag{2.2.17}$$

$$\mathcal{C} : H^1(\Omega) \to \mathcal{W}' , \qquad (\mathcal{C}\varphi, \psi) := c(\varphi, \psi) , \qquad \forall \psi \in \mathcal{W} . \tag{2.2.18}$$

For the analysis of the above operators, the analysis of the strain tensor is of utmost importance. We cite [39, 83] for a significant result concerning the ellipticity of the strain tensor $\boldsymbol{\sigma}$ in Sobolev spaces:

Lemma 2.2.4 (Korn's Inequality) *If* Ω *is as above and the measure of* $\Gamma_{\boldsymbol{u}} \subset \partial\Omega$ *is non-vanishing, i.e.,* $|\Gamma_{\boldsymbol{u}}|_{d-1} \neq 0$, *there exists a positive constant* $C = C(\Omega, \Gamma)$ *such that for* $\boldsymbol{v} \in \boldsymbol{\mathcal{V}} = \boldsymbol{H}^1_{0;\Gamma_u}(\Omega)$

$$\| \boldsymbol{\varepsilon}(\boldsymbol{v}) \| \geq C \, \| \boldsymbol{v} \|_{1;\Omega} .$$

Then, the following result follows readily:

Lemma 2.2.5 *The operators $\boldsymbol{\mathcal{A}}$, $\boldsymbol{\mathcal{B}}$ and $\mathcal{C}$ are bounded, and $\boldsymbol{\mathcal{A}}$ and $\mathcal{C}$ are symmetric and elliptic in $\boldsymbol{\mathcal{V}}$ and $\mathcal{W}$, respectively.*

Proof. We get the continuity of $\boldsymbol{\mathcal{A}}$ by the Cauchy Schwarz inequality

$$(\boldsymbol{\mathcal{A}}\boldsymbol{v},\boldsymbol{w}) = \int_\Omega c_{ijkl}\, v_{k,l}\, w_{i,j} \;\leq (\max_{i,j,k,l}|c_{ijkl}|) \sum_{i,j,k,l} \int_\Omega v_{k,l}\, w_{i,j} \leq C\|\boldsymbol{v}\|_{1;\Omega}\|\boldsymbol{w}\|_{1;\Omega}\;.$$

The symmetry directly follows from the symmetry properties $(2.1.19)$ of the tensor $\boldsymbol{c}$, whereas the $\boldsymbol{\mathcal{V}}$-ellipticity is obtained by the positive definiteness $(2.1.20)$ of $\boldsymbol{c}$ and Korn's inequality

$$(\boldsymbol{\mathcal{A}}\boldsymbol{v},\boldsymbol{v}) = \int_\Omega c_{ijkl}\,\varepsilon_{kl}(\boldsymbol{v})\varepsilon_{ij}(\boldsymbol{v}) \geq \mathfrak{c}\int_\Omega \varepsilon_{kl}(\boldsymbol{v})\varepsilon_{kl}(\boldsymbol{v}) = \mathfrak{c}\|\boldsymbol{\varepsilon}(\boldsymbol{v})\|^2 \geq C\|\boldsymbol{v}\|^2_{1;\Omega}\;.$$

Similarly, $\boldsymbol{\mathcal{B}}$ and $\mathcal{C}$ are bounded by the Cauchy Schwarz inequality, $\mathcal{C}$ being symmetric by the symmetry property $(2.1.19)$, and $\mathcal{W}$-elliptic in view of $(2.1.20)$ and Friedrichs' inequality. □

We denote the ellipticity constant of $\boldsymbol{\mathcal{A}}$ and $\mathcal{C}$ by $\mathfrak{a}$ and $\mathfrak{c}$, respectively, and the constants in the continuity bounds of $\boldsymbol{\mathcal{A}}$, $\boldsymbol{\mathcal{B}}$ and $\mathcal{C}$ by $\|\boldsymbol{\mathcal{A}}\|$, $\|\boldsymbol{\mathcal{B}}\|$ and $\|\mathcal{C}\|$, respectively. For example, in case of the operator $\boldsymbol{\mathcal{A}}$ this means that we have the inequalities

$$(\boldsymbol{\mathcal{A}}\boldsymbol{v},\boldsymbol{w}) \;\leq\; \|\boldsymbol{\mathcal{A}}\|\;\|\boldsymbol{v}\|_{1;\Omega}\;\|\boldsymbol{w}\|_{1;\Omega}\;, \qquad (\boldsymbol{\mathcal{A}}\boldsymbol{v},\boldsymbol{v}) \;\geq\; \mathfrak{a}\;\|\boldsymbol{v}\|^2_{1;\Omega}\;.$$

For the treatment of the boundary conditions we introduce the adjoint of the trace operators by

$$\boldsymbol{\mathcal{R}}'_{\Gamma_\sigma} : \boldsymbol{H}^{\frac{1}{2}}_{00}(\Gamma_\sigma)' \to \boldsymbol{\mathcal{V}}'\;,\quad (\boldsymbol{\mathcal{R}}'_{\Gamma_\sigma}\boldsymbol{z},\boldsymbol{v}) := (\boldsymbol{z},\boldsymbol{\mathcal{R}}_{\Gamma_\sigma}\boldsymbol{v})_{0;\Gamma_\sigma}\;, \qquad \forall \boldsymbol{v}\in\boldsymbol{\mathcal{V}}'\;,\quad (2.2.19)$$

$$\mathcal{R}'_{\Gamma_D} : H^{\frac{1}{2}}_{00}(\Gamma_D)' \to \mathcal{W}'\;,\quad (\mathcal{R}'_{\Gamma_D}z,\varphi) := (z,\mathcal{R}_{\Gamma_D}\varphi)_{0;\Gamma_D}\;, \qquad \forall \varphi\in\mathcal{W}'\;.\quad (2.2.20)$$

Then, we are able to formulate the piezoelectric problem alternatively in operator notation:

Problem 2.2.6 (Operator Formulation) *Under Assumption 2.2.2, find solutions* $\boldsymbol{u} \in L^2(T, \boldsymbol{\mathcal{V}}_{\Gamma_u})$, *and* $\Phi \in L^2(T, \mathcal{W}_{\Gamma_\Phi})$, *satisfying* $\boldsymbol{u}_{,t} \in L^2(T, \boldsymbol{L}^2(\Omega))$, $\boldsymbol{u}_{,tt} \in L^2(T, \boldsymbol{\mathcal{V}}')$ *and*

$$\begin{aligned} \rho \boldsymbol{u}_{,tt} + \boldsymbol{\mathcal{A}}\boldsymbol{u} + \boldsymbol{\mathcal{B}}\Phi &= \boldsymbol{b} + \boldsymbol{\mathcal{R}}'_{\Gamma_\sigma}\boldsymbol{\sigma}_n \ , && \text{in } \boldsymbol{\mathcal{V}}' \ , \\ \mathcal{B}'\boldsymbol{u} - \mathcal{C}\Phi &= \mathcal{R}'_{\Gamma_D} D_n \ , && \text{in } \mathcal{W}' \ . \end{aligned}$$

Since the ellipticity properties of $\boldsymbol{\mathcal{A}}$ and $\mathcal{C}$ only hold in the linear spaces $\boldsymbol{\mathcal{V}}$ and $\mathcal{W}$ (and not in $\boldsymbol{\mathcal{V}}_{\Gamma_u}$ and $\mathcal{W}_{\Gamma_\Phi}$), respectively, it is easier to integrate the boundary conditions into the right-hand side, yielding

$$\begin{aligned} \boldsymbol{f} &:= \boldsymbol{b} + \boldsymbol{\mathcal{R}}'_{\Gamma_\sigma}\boldsymbol{\sigma}_n - \boldsymbol{\mathcal{A}}\boldsymbol{\mathcal{E}}_{\Gamma_u}\boldsymbol{u}_\Gamma - \boldsymbol{\mathcal{B}}\mathcal{E}_{\Gamma_\Phi}\Phi_\Gamma - \rho\boldsymbol{\mathcal{E}}_{\Gamma_u}\boldsymbol{u}_{\Gamma,tt} \ , \\ g &:= \mathcal{R}'_{\Gamma_D} D_n - \mathcal{B}'\boldsymbol{\mathcal{E}}_{\Gamma_u}\boldsymbol{u}_\Gamma + \mathcal{C}\mathcal{E}_{\Gamma_\Phi}\Phi_\Gamma \ . \end{aligned}$$

Moreover, we assume ρ to be constant in space and time and thus set $\rho = 1$ for simplicity of presentation. Then, we arrive at a different operator formulation:

Problem 2.2.7 (Operator Formulation II) *Under Assumption 2.2.2, find solutions* $\boldsymbol{u} \in L^2(T, \boldsymbol{\mathcal{V}})$, *and* $\Phi \in L^2(T, \mathcal{W})$, *satisfying* $\boldsymbol{u}_{,t} \in L^2(T, \boldsymbol{L}^2(\Omega))$, $\boldsymbol{u}_{,tt} \in L^2(T, \boldsymbol{\mathcal{V}}')$ *and*

$$\begin{aligned} \boldsymbol{u}_{,tt} + \boldsymbol{\mathcal{A}}\boldsymbol{u} + \boldsymbol{\mathcal{B}}\Phi &= \boldsymbol{f} \ , && \text{in } \boldsymbol{\mathcal{V}}' \ , \\ \mathcal{B}'\boldsymbol{u} - \mathcal{C}\Phi &= g \ , && \text{in } \mathcal{W}' \ . \end{aligned}$$

The overall solution satisfying the boundary conditions is then obtained as $\boldsymbol{u} + \boldsymbol{\mathcal{E}}_{\Gamma_u}\boldsymbol{u}_\Gamma$ and $\Phi + \mathcal{E}_{\Gamma_\Phi}\Phi_\Gamma$.

For the time-independent problem, if the coupling operator $\boldsymbol{\mathcal{B}}$ is assumed to be zero, the Lax-Milgram theorem assures that both equations

$$\begin{aligned} \boldsymbol{\mathcal{A}}\boldsymbol{u} &= \boldsymbol{f} \ , && \text{in } \boldsymbol{\mathcal{V}}' \ , \\ \mathcal{C}\Phi &= g \ , && \text{in } \mathcal{W}' \ , \end{aligned}$$

admit unique solutions in $\boldsymbol{\mathcal{V}}$ and $\mathcal{W}$, respectively. Consequently, we are able to define inverse operators $\boldsymbol{\mathcal{A}}^{-1} : \boldsymbol{\mathcal{V}}' \to \boldsymbol{\mathcal{V}}$ and $\mathcal{C}^{-1} : \mathcal{W}' \to \mathcal{W}$. The operator $\boldsymbol{\mathcal{A}}^{-1}$ is obviously symmetric and bounded by the ellipticity of $\boldsymbol{\mathcal{A}}$, i.e., by

$$\mathfrak{a}\|\boldsymbol{\mathcal{A}}^{-1}\boldsymbol{f}\|_{1;\Omega} \;\leq\; \frac{(\boldsymbol{\mathcal{A}}\boldsymbol{\mathcal{A}}^{-1}\boldsymbol{f}, \boldsymbol{\mathcal{A}}^{-1}\boldsymbol{f})}{\|\boldsymbol{\mathcal{A}}^{-1}\boldsymbol{f}\|_{1;\Omega}} \;=\; \frac{(\boldsymbol{f}, \boldsymbol{\mathcal{A}}^{-1}\boldsymbol{f})}{\|\boldsymbol{\mathcal{A}}^{-1}\boldsymbol{f}\|_{1;\Omega}} \;\leq\; \|\boldsymbol{f}\|_{-1;\Omega} \,.$$

Moreover, $\boldsymbol{\mathcal{A}}^{-1}$ is $\boldsymbol{\mathcal{V}}'$-elliptic by

$$\inf_{0\neq\boldsymbol{f}\in\boldsymbol{\mathcal{V}}'} \frac{(\boldsymbol{f}, \boldsymbol{\mathcal{A}}^{-1}\boldsymbol{f})}{\|\boldsymbol{f}\|^2_{-1;\Omega}} \;=\; \inf_{0\neq\boldsymbol{v}\in\boldsymbol{\mathcal{V}}} \frac{(\boldsymbol{\mathcal{A}}\boldsymbol{v}, \boldsymbol{v})}{\|\boldsymbol{\mathcal{A}}\boldsymbol{v}\|^2_{-1;\Omega}} \;\geq\; \frac{\mathfrak{a}}{\|\boldsymbol{\mathcal{A}}\|^2} \,.$$

By the same arguments, $\mathcal{C}^{-1}$ is symmetric, bounded by $\|\mathcal{C}^{-1}\| \leq 1/\mathfrak{c}$ and $\mathcal{W}'$-elliptic with ellipticity constant $\geq \frac{\mathfrak{c}}{\|\mathcal{C}\|^2}$.

Hence, the latter equation in Problem 2.2.7 can be solved for Φ resulting in

$$\Phi \;=\; \mathcal{C}^{-1}\mathcal{B}'\boldsymbol{u} \,-\, \mathcal{C}^{-1}g \,. \tag{2.2.21}$$

This is then inserted into the first equation, and we arrive at a different operator problem, the equivalent potential-free formulation of the underlying equations:

Problem 2.2.8 (Schur Complement System) *Under Assumption 2.2.2, find a solution* $\boldsymbol{u} \in L^2(T, \boldsymbol{\mathcal{V}}_{\Gamma_u})$, *satisfying* $\boldsymbol{u}_{,t} \in L^2(T, \boldsymbol{L}^2(\Omega))$, $\boldsymbol{u}_{,tt} \in L^2(T, \boldsymbol{\mathcal{V}}')$ *and*

$$\boldsymbol{u}_{,tt} \;+\; \boldsymbol{\mathcal{S}}\boldsymbol{u} \;=\; \boldsymbol{F} \,,$$

where the Schur complement operator $\boldsymbol{\mathcal{S}}$ and the right-hand side $\boldsymbol{F}$ are given by

$$\boldsymbol{\mathcal{S}} \;:=\; \boldsymbol{\mathcal{A}} + \boldsymbol{\mathcal{B}}\mathcal{C}^{-1}\mathcal{B}' \,, \tag{2.2.22}$$

$$\boldsymbol{F} \;=\; \boldsymbol{f} \,+\, \boldsymbol{\mathcal{B}}\mathcal{C}^{-1}g \,, \tag{2.2.23}$$

respectively. Note that the electric potential Φ can be easily regained from the displacement vector $\boldsymbol{u}$ by $(2.2.21)$.

2.2.4 Mathematical Solution Theory for the Time-Independent Problem

The Schur complement operator will play an essential role in the solution theory for our problem. It will be useful to put some properties of this operator on record:

Lemma 2.2.9 *The Schur complement operator* $\boldsymbol{\mathcal{S}} : \boldsymbol{H}^1(\Omega) \to \boldsymbol{\mathcal{V}}'$,

$$\boldsymbol{\mathcal{S}} = \boldsymbol{\mathcal{A}} + \boldsymbol{\mathcal{B}}\mathcal{C}^{-1}\mathcal{B}' \ ,$$

is symmetric, $\boldsymbol{\mathcal{V}}$*-elliptic and bounded. For the ellipticity constant* $\mathfrak{s}$*, the lower bound* $\mathfrak{s} \geq \mathfrak{a}$ *and for the continuity constant* $\|\boldsymbol{\mathcal{S}}\|$ *the upper bound* $\|\boldsymbol{\mathcal{S}}\| \leq \|\boldsymbol{\mathcal{A}}\| + \|\boldsymbol{\mathcal{B}}\|^2/\mathfrak{c}$ *hold true.*

Proof. For $\boldsymbol{v} \in \boldsymbol{\mathcal{V}}$, we get

$$(\boldsymbol{\mathcal{S}}\boldsymbol{v}, \boldsymbol{v}) \ = \ (\boldsymbol{\mathcal{A}}\boldsymbol{v}, \boldsymbol{v}) \ + \ (\boldsymbol{\mathcal{B}}\mathcal{C}^{-1}\mathcal{B}'\boldsymbol{v}, \boldsymbol{v}) \ = \ (\boldsymbol{\mathcal{A}}\boldsymbol{v}, \boldsymbol{v}) \ + \ (\mathcal{C}^{-1}\mathcal{B}'\boldsymbol{v}, \mathcal{B}'\boldsymbol{v}) \ .$$

Since $\mathcal{C}$ is invertible, there is a unique $\psi := \mathcal{C}^{-1}\mathcal{B}'\boldsymbol{v} \in \mathcal{W}$. From its symmetry and $\mathcal{W}$-ellipticity it follows $(\mathcal{C}^{-1}\mathcal{B}'\boldsymbol{v}, \mathcal{B}'\boldsymbol{v}) = (\psi, \mathcal{C}\psi) \geq 0$. The operator $\boldsymbol{\mathcal{A}}$ is $\boldsymbol{\mathcal{V}}$-elliptic, which yields $(\boldsymbol{\mathcal{A}}\boldsymbol{v}, \boldsymbol{v}) \geq \mathfrak{a}\|\boldsymbol{v}\|^2_{1;\Omega}$. Altogether, we obtain $(\boldsymbol{\mathcal{S}}\boldsymbol{v}, \boldsymbol{v}) \geq \mathfrak{a}\|\boldsymbol{v}\|^2_{1;\Omega}$.
The symmetry of $\boldsymbol{\mathcal{S}}$ follows immediately from the symmetry of the operators $\boldsymbol{\mathcal{A}}$ and $\mathcal{C}$, whereas the boundedness follows from the boundedness of $\boldsymbol{\mathcal{A}}$, $\boldsymbol{\mathcal{B}}$ and $\mathcal{C}^{-1}$. In fact:

$$(\boldsymbol{\mathcal{S}}\boldsymbol{v}, \boldsymbol{w}) \ = \ (\boldsymbol{\mathcal{A}}\boldsymbol{v}, \boldsymbol{w}) + (\mathcal{C}^{-1}\mathcal{B}'\boldsymbol{v}, \mathcal{B}'\boldsymbol{w}) \ \leq \ \left(\|\boldsymbol{\mathcal{A}}\| + \|\mathcal{C}^{-1}\| \, \|\mathcal{B}'\|^2\right) \|\boldsymbol{v}\|_{1;\Omega}\|\boldsymbol{w}\|_{1;\Omega} \, .$$

The result follows by $\|\boldsymbol{\mathcal{B}}\| = \|\mathcal{B}'\|$ and $\|\mathcal{C}^{-1}\| \leq 1/\mathfrak{c}$. □

For the time-independent problem, an existence result follows readily:

Theorem 2.2.10 *Under Assumption 2.2.1, there is a unique solution* $\boldsymbol{u} \in \boldsymbol{\mathcal{V}}$ *for the time-independent Schur complement problem*

$$\boldsymbol{\mathcal{S}}\boldsymbol{u} \ = \ \boldsymbol{F} \qquad \text{in } \boldsymbol{\mathcal{V}}' \ . \tag{2.2.24}$$

Proof. The righthand side $\boldsymbol{F} = \boldsymbol{f} + \boldsymbol{\mathcal{B}}\mathcal{C}^{-1}g$ is bounded and $\boldsymbol{\mathcal{S}}$ is bounded and $\boldsymbol{\mathcal{V}}$-elliptic by Lemma 2.2.9. The result follows from the Lax-Milgram lemma. □

As before, the solution is bounded by the right-hand side, since $\mathfrak{a}\|\boldsymbol{u}\|_{1;\Omega} \leq \|\boldsymbol{F}\|_{-1;\Omega}$, i.e. by a constant that does not depend on the ellipticity constant of $\mathcal{C}$. This only enters by the construction of $\boldsymbol{F}$ according to $(2.2.23)$.

A different approach for treating the time-independent problem would be to consider the following bilinear form in the product space $\boldsymbol{\mathcal{V}} \times \mathcal{W}$:

$$k\left(\begin{pmatrix}\boldsymbol{v}\\ \boldsymbol{\varphi}\end{pmatrix}, \begin{pmatrix}\mathbf{w}\\ \psi\end{pmatrix}\right) \;:=\; a(\boldsymbol{v},\boldsymbol{w}) \,+\, b(\varphi,\boldsymbol{w}) \,-\, b(\psi,\boldsymbol{v}) \,+\, c(\varphi,\psi)\ .$$

Obviously, $k(\cdot,\cdot)$ is bounded and elliptic with ellipticity constant $\mathfrak{k} \geq \min\{\mathfrak{a},\mathfrak{c}\}$. The dependence of the solution on $\mathfrak{c}$ now enters more clearly by Babuška's Theorem 4.1.1 (cf., e.g., [8, 9]). Babuška's theorem also delivers a unique solution for the corresponding saddle point problem:

Theorem 2.2.11 *Under Assumption 2.2.1, there is a unique solution* $(\boldsymbol{u},\Phi) \in \boldsymbol{\mathcal{V}} \times \mathcal{W}$ *for the time-independent problem*

$$\begin{pmatrix}\boldsymbol{\mathcal{A}} & \boldsymbol{\mathcal{B}}\\ -\mathcal{B}' & \mathcal{C}\end{pmatrix}\begin{pmatrix}\boldsymbol{u}\\ \Phi\end{pmatrix} \;=\; \begin{pmatrix}\boldsymbol{f}\\ -g\end{pmatrix}\ .$$

2.2.5 Solution Theory for the Full Problem

Now, consider again the time-dependent equation

$$\boldsymbol{u}_{,tt} + \boldsymbol{\mathcal{S}}\boldsymbol{u} \;=\; \boldsymbol{F}\;, \qquad \text{in } \boldsymbol{\mathcal{V}}'\;. \tag{2.2.25}$$

By formally setting $\dot{\boldsymbol{u}} := \boldsymbol{u}_{,t} \in \boldsymbol{L}^2(\Omega)$, the problem can be equivalently reformulated as

$$\begin{pmatrix} \boldsymbol{u} \\ \dot{\boldsymbol{u}} \end{pmatrix}_{,t} + \underbrace{\begin{pmatrix} \mathbf{0} & \mathbf{id} \\ \boldsymbol{\mathcal{S}} & \mathbf{0} \end{pmatrix}}_{=:\boldsymbol{G}} \begin{pmatrix} \boldsymbol{u} \\ \dot{\boldsymbol{u}} \end{pmatrix} \;=\; \begin{pmatrix} \mathbf{0} \\ \boldsymbol{F} \end{pmatrix}\;, \tag{2.2.26}$$

or

$$\frac{\mathrm{d}\tilde{\boldsymbol{u}}}{\mathrm{d}t} + \boldsymbol{G}\tilde{\boldsymbol{u}} \;=\; \tilde{\boldsymbol{F}}\;, \tag{2.2.27}$$

with the new unknown vector $\tilde{\boldsymbol{u}} = (\boldsymbol{u}, \dot{\boldsymbol{u}})^T \in \boldsymbol{\mathcal{V}} \times \boldsymbol{L}^2(\Omega)$. With this formulation, semigroup theory can be applied, cf. [97, 88, 60]. We describe this approach in a very condensed fashion. The main idea is to make use of the famous Lumer-Phillips theorem which makes sense for dissipative operators, i.e. for operators $\mathcal{O}$ with dense domain $\mathcal{D}(\mathcal{O})$ in a Hilbert space $\mathcal{H}$ satisfying

$$\Re\,(\mathcal{O}v, v)_{\mathcal{H}} \;\leq\; 0\;, \qquad \forall v \in \mathcal{D}(\mathcal{O}) \;:$$

Theorem 2.2.12 (Lumer-Phillips) *A closed operator $\mathcal{O}$ in a Hilbert space $\mathcal{H}$ is the generator of a contraction semigroup if and only if $(\mathcal{O} - \lambda)(\mathcal{H}) = \mathcal{H}$ for some λ with $\Re\lambda > 0$ and $\mathcal{O}$ is dissipative.*

In our case, we set the domain of $\boldsymbol{G}$ to

$$\mathcal{D}(\boldsymbol{G}) \;:=\; \{\; \tilde{\boldsymbol{u}} = (\boldsymbol{u}, \dot{\boldsymbol{u}})^T \in \boldsymbol{\mathcal{V}} \times \boldsymbol{L}^2(\Omega) \;|\; \boldsymbol{\mathcal{S}}\boldsymbol{u} \in \boldsymbol{L}^2(\Omega),\, \dot{\boldsymbol{u}} \in \boldsymbol{\mathcal{V}} \;\}\;,$$

which is dense in $\mathcal{H} := \boldsymbol{\mathcal{V}} \times \boldsymbol{L}^2(\Omega)$. If we equip the space $\boldsymbol{\mathcal{V}}$ with the inner product $(\boldsymbol{v}, \boldsymbol{w})_{\boldsymbol{\mathcal{V}}} = (\boldsymbol{\mathcal{S}}\boldsymbol{v}, \boldsymbol{w})$ it gets immediately clear that $\boldsymbol{G}$ is dissipative,

$$(\boldsymbol{G}\tilde{\boldsymbol{u}}, \tilde{\boldsymbol{u}})_{\mathcal{H}} \;=\; (-\dot{\boldsymbol{u}}, \boldsymbol{u})_{\boldsymbol{\mathcal{V}}} + (\boldsymbol{\mathcal{S}}\boldsymbol{u}, \dot{\boldsymbol{u}}) \;=\; 0\;.$$

Moreover, for every $\tilde{\boldsymbol{f}} \in \mathcal{H}$ there is at least one solution for the equation $(\boldsymbol{G} + \mathbf{id})\tilde{\boldsymbol{u}} = \tilde{\boldsymbol{f}}$, i.e. for

$$-\dot{\boldsymbol{u}} \;+\; \boldsymbol{u} \;=\; \boldsymbol{f}_1\;, \qquad \boldsymbol{\mathcal{S}}\boldsymbol{u} = \;\boldsymbol{f}_2\;,$$

which can be easily seen by first solving the latter equation by an application of the Lax-Milgram theorem, cf. Theorem 2.2.10. The Lumer-Phillips theorem now proves the existence and uniqueness of a solution for problem $(2.2.26)$.

Note that equation $(2.2.25)$ is equivalent to the variational problem

$$(\boldsymbol{u}_{,tt}, \boldsymbol{v}) \, + \, (\boldsymbol{\mathcal{S}u}, \boldsymbol{v}) \; = \; (\boldsymbol{F}, \boldsymbol{v}) \; , \qquad \forall \boldsymbol{v} \in \boldsymbol{\mathcal{V}} \; .$$

Setting $\boldsymbol{v} := \dot{\boldsymbol{u}}$ and using the symmetry of $\boldsymbol{\mathcal{S}}$, we get

$$(\boldsymbol{\mathcal{S}u}, \dot{\boldsymbol{u}}) \, + \, (\boldsymbol{\mathcal{S}}\dot{\boldsymbol{u}}, \boldsymbol{u}) \, + \, \frac{\partial}{\partial t}(\dot{\boldsymbol{u}}, \dot{\boldsymbol{u}}) \; = \; 2(\boldsymbol{F}, \dot{\boldsymbol{u}}) \; .$$

The first two terms can be substituted by $\frac{\partial}{\partial t}(\boldsymbol{\mathcal{S}u}, \boldsymbol{u})$. After an integration in time, we arrive at

$$\begin{aligned} (\boldsymbol{\mathcal{S}u}, \boldsymbol{u}) \, + \, \|\dot{\boldsymbol{u}}\|^2 \; &= \; (\boldsymbol{\mathcal{S}u}_0, \boldsymbol{u}_0) \, + \, \|\dot{\boldsymbol{u}}_0\|^2 \, + \, 2 \int_0^t (\boldsymbol{F}, \dot{\boldsymbol{u}}) \; , \\ &\leq \; \|\boldsymbol{\mathcal{S}}\| \, \|\boldsymbol{u}_0\|_{1;\Omega}^2 \, + \, \|\dot{\boldsymbol{u}}_0\|^2 \, + \, 2 \int_0^t \|\boldsymbol{F}\| \, \|\dot{\boldsymbol{u}}\| \; . \end{aligned}$$

In view of $\mathfrak{s}\|\boldsymbol{u}\|_{1;\Omega}^2 \leq (\boldsymbol{\mathcal{S}u}, \boldsymbol{u}) \leq \|\boldsymbol{\mathcal{S}}\| \, \|\boldsymbol{u}\|_{1;\Omega}^2$ and using Young's inequality [5]

$$\|\boldsymbol{u}\|_{1;\Omega}^2 \, + \, \|\dot{\boldsymbol{u}}\|^2 \; \leq \; c \left(\|\boldsymbol{u}_0\|_{1;\Omega}^2 + \|\dot{\boldsymbol{u}}_0\|^2 + \int_0^t \|\boldsymbol{F}\|^2 + \int_0^t (\|\boldsymbol{u}\|_{1;\Omega}^2 + \|\dot{\boldsymbol{u}}\|^2) \right) .$$

Finally, by an application of Gronwall's lemma [56] we obtain the following energy estimate:

$$\|\boldsymbol{u}\|_{1;\Omega}^2 \, + \, \|\dot{\boldsymbol{u}}\|^2 \; \leq \; C \left(\|\boldsymbol{u}_0\|_{1;\Omega}^2 \, + \, \|\dot{\boldsymbol{u}}_0\|^2 \, + \, \int_0^t \|\boldsymbol{F}\|^2 \right) \; . \tag{2.2.28}$$

A similar result is obtained in the context of semigroups by an application of Stone's theorem, cf. [97, 88, 60]. This energy estimate ensures that the solution exists for all times $t \in T$. We get the following result:

Theorem 2.2.13 *Under Assumption 2.2.2, there is a unique solution* $(\boldsymbol{u}, \Phi) \in L^2\left(T; \boldsymbol{\mathcal{V}} \times \mathcal{W}\right)$ *with* $\boldsymbol{u}_{,t} \in L^2\left(T; \boldsymbol{L}^2(\Omega)\right)$ *and* $\boldsymbol{u}_{,tt} \in L^2(T, \boldsymbol{\mathcal{V}}')$ *satisfying*

$$\begin{pmatrix} \boldsymbol{u}_{,tt} \\ 0 \end{pmatrix} \, + \, \begin{pmatrix} \boldsymbol{\mathcal{A}} & \boldsymbol{\mathcal{B}} \\ \boldsymbol{\mathcal{B}}' & -\mathcal{C} \end{pmatrix} \begin{pmatrix} \boldsymbol{u} \\ \Phi \end{pmatrix} \; = \; \begin{pmatrix} \boldsymbol{f} \\ g \end{pmatrix} \; , \tag{2.2.29}$$

or equivalently,

$$\boldsymbol{u}_{,tt} \; + \; \boldsymbol{\mathcal{S}}\boldsymbol{u} \; = \; \boldsymbol{F} \; . \tag{2.2.30}$$

Proof. Since the operator $\boldsymbol{\mathcal{S}}$ is symmetric, $\boldsymbol{\mathcal{V}}$-elliptic and bounded by Lemma 2.2.9, Problem 2.2.30 admits a unique solution $\boldsymbol{u}$ satisfying the required properties above (cf. the discussions above and also complementary [72, 49]). Since $\mathcal{C}$ is symmetric positive definite and bounded we get from $\Phi = \mathcal{C}^{-1}\mathcal{B}'\boldsymbol{u} - C^{-1}g$ the relation $\Phi \in L^2(T;\mathcal{W})$. □

Remark 2.2.14 *On the account of the discussions around* $(2.2.8)$ *we gain*

$$\boldsymbol{u} \; \in \; C(\bar{T};\boldsymbol{\mathcal{V}}) \; , \qquad \boldsymbol{u}_{,t} \; \in \; C(\bar{T};\boldsymbol{L}^2(\Omega)) \; ,$$

since the boundary data also shows the same regularity in time. The same immediately applies for Φ*, again by* $\Phi = \mathcal{C}^{-1}\mathcal{B}'\boldsymbol{u} - C^{-1}g$*.*

3 Mathematical Theory Of Piezoelectrically Driven Surface Acoustic Waves

3.1 Surface Acoustic Wave Devices

Surface acoustic waves (SAWs) are modes of elastic energy propagating at the surface of a solid body. Being the nanometer size analogon of earthquakes, they have been made available to industrial applications during the last two decades. The underlying technique is relatively new, although the first theoretical treatments on the propagation of surface acoustic waves at the free surface of a homogenous isotropic elastic solid date back approximately 150 years (cf. [90]). But it was not before White and Voltmer [103] succeeded in the production of SAWs on the surface of a piezoelectric substrate that the use of this technology became clear. Nowadays, piezoelectric SAW devices are very popular in signal-processing applications (see, e.g., [25, 47, 66, 79]), which is mostly due to the fact that on homogenous substrates the velocity of SAWs is independent of their frequency.

SAWs are easily excited on piezoelectric solids, because piezoelectric substrates deform due to the application of an electric field. Rapid changes of these electric fields are efficiently converted into a real 'nanoquake on a chip'. Such rapid changes can be generated by a metallic electrode comb structure, called interdigital transducer (IDT), deposited on the surface of the piezoelectric material (see Figure 3.1).
By applying an alternating voltage to the IDT, a surface acoustic wave is excited. Typical frequencies range in the hundred MHz regime, typical wavelengths of SAW are micrometers. Since the SAW components can be manufactured using advanced

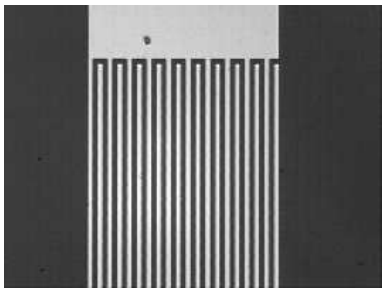

Figure 3.1: Interdigital transducer

photolithographic techniques, they meet the requirements of small size and weight. This is also the reason why SAW devices can be mass produced using the same techniques as in semiconductor microfabrication. They receive outstanding response characteristics, especially in filter applications.

Unfortunately, the excitation of an IDT on a piezoelectric substrate can lead to the generation of bulk acoustic waves (BAWs) as well as surface waves. In most applications, such BAWs are certainly undesirable, e.g., in signal processing applications they seriously degrade the filter response. In most analytical treatments, BAWs are neglected.

The typical dimensions of a SAW chip is only a few millimeters, depending on the operating frequency. A wide range of piezoelectric materials are used for the production of SAW devices, among them lithium niobate ($LiNbO_3$), lithium tantalate ($LiTaO_3$), and quartz (SiO_2) monocrystals.

3.1.1 Physical Modeling of Rayleigh Waves

The type of surface waves considered here are so-called Rayleigh waves (see, e.g., [7, 13, 71]), i.e., these are waves polarized in the sagittal plane and propagating at the free surface at a speed less than that of volume shear elastic waves. These waves usually are considered in a semi-infinite, isotropic and homogenous linear elastic space, which will be fixed as in Figure 3.2 a).

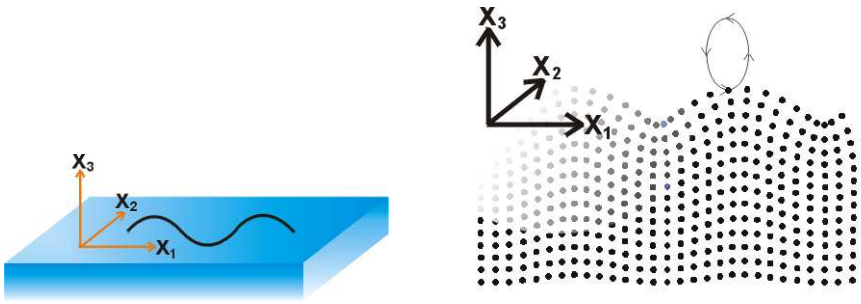

(a) Coordinate System (b) Rayleigh Wave

Figure 3.2: Modeling of Surface Acoustic Waves

The sagittal plane is the plane spanned by the unit surface normal and the real wavevector $\boldsymbol{k}$, i.e., the (x_1, x_3)-plane in Figure 3.2 a). SAWs are strictly confined to the limiting surface of the piezoelectric substrate and practically nil outside a relatively narrow zone. To be precise, the amplitude of the displacement $\boldsymbol{u}$ decays exponentially with depth into the substrate [46, 74]. In true Rayleigh waves, most of the energy (90%) is concentrated within one wavelength from the surface. Thus, both the mechanical displacements $\boldsymbol{u}$ and the electric potential Φ should vanish as $x_3 \to \infty$. Moreover, since x_1 is the direction of propagation of the wave solutions, there is no dependence of $\boldsymbol{u}$ and Φ on the x_2 coordinate, since here the surface is assumed to be infinite.

Remark 3.1.1 *We note that in the physical modeling of surface acoustic waves the assumption of an x_2-independence is extremely simplifying, since piezoelectric materials are in general anisotropic and pure Rayleigh surface acoustic waves can be observed only in rare crystal cuts.*

The two wave motions in the x_1- and x_3-direction are 90° out of phase in the time domain: if one wave component is at its maximum for a given instant, the other will be zero. Moreover, the displacement in the x_3-direction will be larger than that in the x_1-direction.

These considerations lead to

$$\begin{aligned} u_i &= \alpha_i \exp(-\beta k x_3) \exp(\mathrm{i}(\omega \mathrm{t} - \mathrm{k} x_1)) \ , \\ \Phi &= \alpha_4 \exp(-\beta k x_3) \exp(\mathrm{i}(\omega \mathrm{t} - \mathrm{k} x_1)) \ , \end{aligned}$$

where $\Re(\beta) > 0$. Hence, in some sense the factor β measures the rate of exponential decay into the substrate. We insert these functions into the piezoelectric equations, which are given as in Problem 2.1.1 by

$$\begin{aligned} \rho\, u_{i,tt} - c_{ijkl}\, u_{k,lj} - e_{kij}\, \Phi_{,kj} &= 0 \ , \\ e_{ikl}\, u_{k,li} - \epsilon_{ij}\, \Phi_{,ji} &= 0 \ . \end{aligned}$$

This leads to a linear system for the coefficients α_i of the form

$$\boldsymbol{M}\,\boldsymbol{\alpha} = 0 \ .$$

Here, $\boldsymbol{\alpha} = (\alpha_i) \in \mathbb{C}^4$, $\boldsymbol{M} = (M_{kl}) \in \mathbb{C}^{4\times 4}$, and the coefficients M_{kl} are quadratic functions in β. For the existence of nontrivial solutions, we have to require that $\det \boldsymbol{M} = 0$. Accounting for $\Re(\beta) > 0$, we get 4 possible values for β. For each such β, there is an eigenvector $\boldsymbol{\alpha}$.
The general solution is then obtained as a linear combination of these solutions

$$\begin{aligned} u_i &= \exp(\mathrm{i}(\omega \mathrm{t} - \mathrm{k} x_1)) \sum_{\mathrm{m}=1}^{4} \mathrm{c}^{(\mathrm{m})} \alpha_{\mathrm{i}}^{(\mathrm{m})} \boldsymbol{u}_{\mathrm{i}}^{0(\mathrm{m})} \exp(-\beta^{(\mathrm{m})} \mathrm{k} x_3) \ , \\ \Phi &= \exp(\mathrm{i}(\omega \mathrm{t} - \mathrm{k} x_1)) \sum_{\mathrm{m}=1}^{4} \mathrm{c}^{(\mathrm{m})} \alpha_{4}^{(\mathrm{m})} \Phi^{0(\mathrm{m})} \exp(-\beta^{(\mathrm{m})} \mathrm{k} x_3) \ , \end{aligned}$$

where the weighting factors $c^{(m)}$, the value of the phase velocity v, have to be chosen according to the boundary conditions.

We remark that the use of anisotropic materials causes many differences in detail even though the occurring surface waves share many features. For instance, the waves are still elliptically polarized at each depth and the displacement amplitude decays exponentially into the substrate. But in anisotropic materials, the phase velocity depends on the direction of propagation and in general, the vector of energy flow is not parallel to the wave vector. Moreover, the plane of the elliptical polarization

of the displacement does not necessarily correspond to the sagittal plane, but even when it does, the principal axes of the ellipse are not necessarily x_1 and x_3.

3.2 Mathematical Model of Piezoelectric SAWs

A precise modeling of the underlying physical equations as in Section 2.1 leads to the linear piezoelectric equations. In the absence of forces, they are given by

$$\rho\, u_{i,tt} - c_{ijkl}\, u_{k,lj} - e_{kij}\, \Phi_{,kj} = 0 \;, \tag{3.2.1}$$

$$e_{ikl}\, u_{k,li} - \epsilon_{ij}\, \Phi_{,ji} = 0 \;. \tag{3.2.2}$$

Introducing vector spaces $\boldsymbol{\mathcal{V}}_{\Gamma_u}$ and $\mathcal{W}_{\Gamma_\Phi}$ (the standard Sobolev spaces complying to the boundary conditions) and by an integration by parts, we arrive at the variational formulation as given in Problem 2.2.3: Under Assumption 2.2.2, find solutions $\boldsymbol{u} \in L^2(T, \boldsymbol{\mathcal{V}}_{\Gamma_u})$, and $\Phi \in L^2(T, \mathcal{W}_{\Gamma_\Phi})$, satisfying $\boldsymbol{u}_{,t} \in L^2(T, \boldsymbol{L}^2(\Omega))$, $\boldsymbol{u}_{,tt} \in L^2(T, \boldsymbol{\mathcal{V}}')$ and

$$\begin{aligned} (\boldsymbol{u}_{,tt}, \boldsymbol{v}) + a(\boldsymbol{u}, \boldsymbol{v}) + b(\Phi, \boldsymbol{v}) &= (\boldsymbol{\sigma}_n, \boldsymbol{v}|_{\Gamma_\sigma})_{0;\Gamma_\sigma} \;, \quad \forall \boldsymbol{v} \in \boldsymbol{\mathcal{V}} \;, \\ b(\psi, \boldsymbol{u}) - c(\Phi, \psi) &= (D_n, \psi|_{\Gamma_D})_{0;\Gamma_D} \;, \quad \forall \psi \in \mathcal{W} \;. \end{aligned}$$

Here, $a(\cdot,\cdot)$, $b(\cdot,\cdot)$ and $c(\cdot,\cdot)$ are the bilinear forms naturally arising from partial integration, compare Section 2.2.3.

3.2.1 Time Harmonic Ansatz

Either by using the Fourier transform, or because SAWs are usually excited by a source IDT operating at a fixed frequency $\omega > 0$, we consider time harmonic solutions given in the form

$$\boldsymbol{u}(\boldsymbol{x},t) \;=\; \Re\,(\,\boldsymbol{u}(\boldsymbol{x})\exp(-\mathrm{i}\omega\mathrm{t})\,)\;, \tag{3.2.3}$$

$$\Phi(\boldsymbol{x},t) \;=\; \Re\,(\,\Phi(\boldsymbol{x})\exp(-\mathrm{i}\omega\mathrm{t})\,)\;, \tag{3.2.4}$$

introducing some ambiguity in the notation of the physical symbols $\boldsymbol{u}$ and Φ, in the one case denoting complex valued functions, in the other not. Here, $\mathrm{i} = \sqrt{-1}$ and $\Re(\cdot)$ denotes the real part of the expression in parentheses.

This, of course, includes that the boundary data is also given in time harmonic form. To this end, we decompose the boundary into two disjoint sets in two different ways by

$$\partial\Omega \;=\; \Gamma_u \cup \Gamma_\sigma\;, \qquad \Gamma_\sigma \;=\; \partial\Omega \setminus \Gamma_u\;,$$
$$\partial\Omega \;=\; \Gamma_\Phi \cup \Gamma_D\;, \qquad \Gamma_D \;=\; \partial\Omega \setminus \Gamma_\Phi\,,$$

where the Dirichlet boundaries Γ_u and Γ_Φ are assumed to be closed and with non-vanishing $d-1$-dimensional measure. Then, the same trace and extension properties hold as in Section 2.2.1. Again, for $\Gamma \subset \partial\Omega$ the trace operator is denoted by $\mathcal{R}_\Gamma$ and the extension operator by $\mathcal{E}_\Gamma$, with bold style notations in the vectorial case. For the boundary data we set

$$\boldsymbol{\mathcal{R}}_{\Gamma_u}\boldsymbol{u}(\boldsymbol{x},t) \;=\; \Re\,(\,\boldsymbol{u}_\Gamma(\boldsymbol{x})\exp(-\mathrm{i}\omega\mathrm{t})\,)\;, \tag{3.2.5}$$

$$\boldsymbol{\mathcal{R}}_{\Gamma_\sigma}(\boldsymbol{\sigma}(\boldsymbol{x},t)\cdot\boldsymbol{n}) \;=\; \Re\,(\,\boldsymbol{\sigma}_n(\boldsymbol{x})\exp(-\mathrm{i}\omega\mathrm{t})\,)\;, \tag{3.2.6}$$

$$\mathcal{R}_{\Gamma_\Phi}\Phi(\boldsymbol{x},t) \;=\; \Re\,(\,\Phi_\Gamma(\boldsymbol{x})\exp(-\mathrm{i}\omega\mathrm{t})\,)\;, \tag{3.2.7}$$

$$\mathcal{R}_{\Gamma_D}(\boldsymbol{D}(\boldsymbol{x},t)\cdot\boldsymbol{n}|_{\Gamma_D}) \;=\; \Re\,(\,D_n(\boldsymbol{x})\exp(-\mathrm{i}\omega\mathrm{t})\,)\;. \tag{3.2.8}$$

The physical equations $(3.2.1)$-$(3.2.2)$ can then be solved for the complex electric potential and displacements, taking only the real parts of the thus obtained solutions.

3.2.2 Mathematical Problem Formulation

In order to derive a variational formulation of the piezoelectric problem, we again introduce two function spaces (compare Section 2.2):

$$\boldsymbol{\mathcal{V}} \;:=\; \boldsymbol{H}^1_{0;\Gamma_u}(\Omega) \;:=\; \left\{\, \boldsymbol{v} \in \boldsymbol{H}^1(\Omega) \middle|\; \boldsymbol{v}|_{\Gamma_u} \;=\; 0 \,\right\} , \tag{3.2.9}$$

$$\mathcal{W} \;:=\; H^1_{0;\Gamma_\Phi}(\Omega) \;:=\; \left\{\, \varphi \in H^1(\Omega) \middle|\; \varphi|_{\Gamma_\Phi} \;=\; 0 \,\right\} , \tag{3.2.10}$$

where now the Sobolev spaces are spaces of complex valued functions. Additionally, set

$$\boldsymbol{\mathcal{V}}_{\Gamma_u} \;:=\; \boldsymbol{\mathcal{E}}_{\Gamma_u}\boldsymbol{u}_\Gamma \,+\, \boldsymbol{\mathcal{V}} \,, \qquad \text{and} \qquad \mathcal{W}_{\Gamma_\Phi} \;:=\; \mathcal{E}_{\Gamma_\Phi}\Phi_\Gamma \,+\, \mathcal{W} \,,$$

that account for the given Dirichlet data on the boundaries.

Again, we have to demand some properties from the boundary data. This will be done in the following assumption (compare Assumption 2.2.1):

Assumption 3.2.1 *Throughout this work we will make the following standard assumptions on the boundary conditions:*

$$\begin{aligned} &\textit{Elastic boundary data:} && \boldsymbol{u}_\Gamma \in \boldsymbol{H}^{\frac{1}{2}}(\Gamma_u) \,, \quad \sigma_n \in \boldsymbol{H}^{\frac{1}{2}}_{00}(\Gamma_\sigma)' \,, \\ &\textit{Electric boundary data:} && \Phi_\Gamma \in H^{\frac{1}{2}}(\Gamma_\Phi) \,, \quad D_n \in \boldsymbol{H}^{\frac{1}{2}}_{00}(\Gamma_D)' \,. \end{aligned}$$

Of course, we have to switch to complex scalar products and the bilinear forms in $(2.2.12)$-$(2.2.12)$ become

$$a(\boldsymbol{v},\boldsymbol{w}) \;:=\; \int_\Omega c_{ijkl}\,\varepsilon_{kl}(\boldsymbol{v})\,\varepsilon_{ij}(\bar{\boldsymbol{w}}) \,, \qquad \forall \boldsymbol{v},\boldsymbol{w} \in \boldsymbol{H}^1(\Omega) \,, \tag{3.2.11}$$

$$b(\varphi,\boldsymbol{v}) \;:=\; \int_\Omega e_{kij}\,\varphi_{,k}\,\varepsilon_{ij}(\bar{\boldsymbol{v}}) \,, \qquad \forall \varphi \in H^1(\Omega),\, \boldsymbol{v} \in \boldsymbol{H}^1(\Omega), \tag{3.2.12}$$

$$c(\varphi,\psi) \;:=\; \int_\Omega \epsilon_{ij}\,\varphi_{,i}\,\bar{\psi}_{,j} \,, \qquad \forall \varphi,\psi \in H^1(\Omega) \,, \tag{3.2.13}$$

now being complex valued sesquilinear forms on $\boldsymbol{H}^1(\Omega)\times\boldsymbol{H}^1(\Omega)$, $H^1(\Omega)\times\boldsymbol{H}^1(\Omega)$ and $H^1(\Omega)\times H^1(\Omega)$, respectively, and $a(\cdot,\cdot)$ and $c(\cdot,\cdot)$ being symmetric. Here, $\bar{a}$

denotes the complex conjugation of a value $a \in \mathbb{C}$.

The variational formulation of the problem of piezoelectrically driven surface acoustic waves then reads

Problem 3.2.2 (Variational Formulation) *Under Assumption 3.2.1, find solutions* $\boldsymbol{u} \in \boldsymbol{\mathcal{V}}_{\Gamma_u}$, $\Phi \in \mathcal{W}_{\Gamma_\Phi}$, *satisfying*

$$\begin{aligned} a(\boldsymbol{u},\boldsymbol{v}) + b(\Phi,\boldsymbol{v}) \,-\, \omega^2(\boldsymbol{u},\boldsymbol{v}) \;&=\; (\boldsymbol{\sigma}_n, \boldsymbol{v}|_{\Gamma_\sigma})_{0;\Gamma_\sigma}\;, \qquad \forall \boldsymbol{v} \in \boldsymbol{\mathcal{V}}\;, \\ b(\psi,\boldsymbol{u}) - c(\Phi,\psi) \;&=\; (D_n, \psi|_{\Gamma_D})_{0;\Gamma_D}\;, \qquad \forall \psi \in \mathcal{W}\;. \end{aligned}$$

Again, we associate operators $\boldsymbol{\mathcal{A}} : \boldsymbol{H}^1(\Omega) \to \boldsymbol{\mathcal{V}}'$, $\mathcal{B}' : \boldsymbol{H}^1(\Omega) \to \mathcal{W}'$, $\mathcal{B} : H^1(\Omega) \to \boldsymbol{\mathcal{V}}'$ and $\mathcal{C} : H^1(\Omega) \to \mathcal{W}'$ to the above sesquilinear forms as in $(2.2.15)$-$(2.2.18)$, whereupon $\boldsymbol{\mathcal{A}}, \boldsymbol{\mathcal{B}}$, $\mathcal{B}'$ and $\mathcal{C}$ are linear operators. As before, we formally define the linear Schur complement operator $\boldsymbol{\mathcal{S}}$ according to

$$\boldsymbol{\mathcal{S}} \;:=\; \boldsymbol{\mathcal{A}} + \boldsymbol{\mathcal{B}}\mathcal{C}^{-1}\mathcal{B}'\;, \tag{3.2.14}$$

momentarily assuming the operator $\mathcal{C}$ to be invertible. This, of course, is true due to the complex version of the Lax-Milgram lemma and the following result:

Lemma 3.2.3 *The operators* $\boldsymbol{\mathcal{A}}$, $\boldsymbol{\mathcal{B}}$, $\mathcal{C}$ *and* $\boldsymbol{\mathcal{S}}$ *are bounded with constants* $\|\boldsymbol{\mathcal{A}}\|$, $\|\boldsymbol{\mathcal{B}}\|$, $\|\mathcal{C}\|$ *and* $\|\boldsymbol{\mathcal{S}}\|$, *respectively. The operators* $\boldsymbol{\mathcal{A}}$ *and* $\boldsymbol{\mathcal{S}}$ *are* $\boldsymbol{\mathcal{V}}$*-elliptic, and* $\mathcal{C}$ *is* $\mathcal{W}$*-elliptic with ellipticity constants* $\mathfrak{a}$, $\mathfrak{s}$ *and* $\mathfrak{c}$, *respectively. Furthermore,*

$$\|\boldsymbol{\mathcal{S}}\| \;\leq\; \|\boldsymbol{\mathcal{A}}\| + \frac{\|\boldsymbol{\mathcal{B}}\|^2}{\mathfrak{c}}\;, \qquad\qquad \mathfrak{s} \;\geq\; \mathfrak{a}\;.$$

Proof. Repeat the proof of Lemma 2.2.5 and Lemma 2.2.9 in the complex case. □

Introducing adjoint operators $\boldsymbol{\mathcal{R}}'_{\Gamma_\sigma} : \boldsymbol{H}^{\frac{1}{2}}_{00}(\Gamma_\sigma)' \to \boldsymbol{\mathcal{V}}'$ and $\mathcal{R}'_{\Gamma_D} : H^{\frac{1}{2}}_{00}(\Gamma_D)' \to \mathcal{W}'$ of the trace operators as in $(2.2.19)$-$(2.2.20)$, we are able to integrate the boundary conditions into the right-hand sides, yielding

$$\begin{aligned} \boldsymbol{f} &:= \boldsymbol{\mathcal{R}}'_{\Gamma_\sigma}\boldsymbol{\sigma}_n \,-\, (\boldsymbol{\mathcal{A}} - \omega^2\boldsymbol{I})\boldsymbol{\mathcal{E}}_{\Gamma_u}\boldsymbol{u}_\Gamma \,-\, \boldsymbol{\mathcal{B}}\mathcal{E}_{\Gamma_\Phi}\Phi_\Gamma \;, \\ g &:= \mathcal{R}'_{\Gamma_D}D_n \,-\, \mathcal{B}'\boldsymbol{\mathcal{E}}_{\Gamma_u}\boldsymbol{u}_\Gamma \,+\, \mathcal{C}\mathcal{E}_{\Gamma_\Phi}\Phi_\Gamma \;. \end{aligned} \tag{3.2.15}$$

where $\boldsymbol{I}$ denotes the identification $\boldsymbol{v} \in \boldsymbol{H}^1(\Omega) \to \boldsymbol{I}\boldsymbol{v} \in \boldsymbol{\mathcal{V}}'$.

Now, the problem of piezoelectrically driven surface acoustic waves can be formulated as

Problem 3.2.4 (Operator Formulation) *Under Assumption 3.2.1, find solutions* $\boldsymbol{u} \in \boldsymbol{\mathcal{V}}$, $\Phi \in \mathcal{W}$, *satisfying*

$$\begin{aligned} \boldsymbol{\mathcal{A}}\boldsymbol{u} + \boldsymbol{\mathcal{B}}\Phi \;-\omega^2\boldsymbol{I}\boldsymbol{u} &= \;\; \boldsymbol{f} \;, \qquad \text{in } \boldsymbol{\mathcal{V}}' \;, \\ \mathcal{B}'\boldsymbol{u} - \mathcal{C}\Phi \qquad\qquad\quad &= \;\; g \;, \qquad \text{in } \mathcal{W}' \;, \end{aligned}$$

or equivalently,

$$\begin{aligned} \boldsymbol{\mathcal{S}}\boldsymbol{u} \;-\; \omega^2\boldsymbol{u} &= \; \boldsymbol{F} \;, \qquad\qquad \text{in } \boldsymbol{\mathcal{V}}' \;, \\ \mathcal{C}\Phi \;&=\; \mathcal{B}'\boldsymbol{u} \,-\, g \;, \qquad \text{in } \mathcal{W}' \;. \end{aligned}$$

where the right-hand side $\boldsymbol{F}$ is again given by

$$\boldsymbol{F} \;=\; \boldsymbol{f} \;+\; \boldsymbol{\mathcal{B}}\mathcal{C}^{-1}g \;.$$

3.2.3 Mathematical Solution Theory

In the analysis of the time harmonic approach, the Schur complement operator $\boldsymbol{\mathcal{S}}$ will again play an essential role. It is convenient to introduce a sesquilinear form $s(\cdot,\cdot) : \boldsymbol{H}^1(\Omega) \times \boldsymbol{\mathcal{V}} \to \mathbb{C}$, given by

$$s(\boldsymbol{v},\boldsymbol{w}) \;:=\; (\boldsymbol{\mathcal{S}}\boldsymbol{v},\boldsymbol{w}) \;, \qquad\qquad \forall \boldsymbol{v} \in \boldsymbol{H}^1(\Omega)\,,\; \boldsymbol{w} \in \boldsymbol{\mathcal{V}} \;. \tag{3.2.16}$$

Note that the sesquilinear form $s(\cdot,\cdot)$ inherits the symmetry, continuity and $\boldsymbol{\mathcal{V}}$-ellipticity directly from the corresponding properties of $\boldsymbol{\mathcal{S}}$ (cf. Lemma 3.2.3). Including the frequency of the surface acoustic wave into the sesquilinear form, leads to a modified sesquilinear form $s_\omega(\cdot,\cdot) : \boldsymbol{H}^1(\Omega) \times \boldsymbol{\mathcal{V}} \to \mathbb{C}$, defined by

$$s_\omega(\boldsymbol{v},\boldsymbol{w}) \;:=\; ((\boldsymbol{\mathcal{S}} - \omega^2\boldsymbol{I})\boldsymbol{v},\boldsymbol{w}) \;, \qquad\qquad \forall \boldsymbol{v} \in \boldsymbol{H}^1(\Omega)\,,\; \boldsymbol{w} \in \boldsymbol{\mathcal{V}} \;, \tag{3.2.17}$$

where $\boldsymbol{I}$ denotes the identification $\boldsymbol{v} \in \boldsymbol{H}^1(\Omega) \to \boldsymbol{I}\boldsymbol{v} \in \boldsymbol{\mathcal{V}}'$. Note, the function spaces $\boldsymbol{\mathcal{V}}$, $\boldsymbol{L}^2(\Omega)$ and $\boldsymbol{\mathcal{V}}'$ form a Gelfand triple

$$\boldsymbol{\mathcal{V}} \;\subset\; \boldsymbol{L}^2(\Omega) \;\subset\; \boldsymbol{\mathcal{V}}' \;,$$

i.e., the occurring embeddings are continuous and dense. In this work, we always deal with Lipschitz domains, thus yielding a compact embedding $\boldsymbol{\mathcal{V}} \subset \boldsymbol{L}^2(\Omega)$.

Setting $\boldsymbol{F} = \boldsymbol{0}$ in Problem 3.2.4, the question of finding a solution $\boldsymbol{u} \in \boldsymbol{\mathcal{V}}$ is transformed to

$$\boldsymbol{\mathcal{S}}\boldsymbol{u} \;=\; \omega^2\boldsymbol{I}\boldsymbol{u} \;, \qquad \text{in } \boldsymbol{\mathcal{V}}' \;,$$

i.e. to the question of finding an eigensolution $\boldsymbol{u} \in \boldsymbol{\mathcal{V}} \subset \boldsymbol{\mathcal{V}}'$ for the operator $\boldsymbol{\mathcal{S}}$ and the eigenvalue ω^2. We remark that it follows immediately from the symmetry of $\boldsymbol{\mathcal{S}}$ that all eigenvalues of $\boldsymbol{\mathcal{S}}$ are real and the eigensolutions for different eigenvalues are orthogonal in the $\boldsymbol{L}^2$-inner product. Moreover, $(\boldsymbol{\mathcal{S}}\boldsymbol{v},\boldsymbol{v}) \in \mathbb{R}$ due to the symmetry of $\boldsymbol{\mathcal{S}}$.

It is immediately clear that the symmetric operator

$$\boldsymbol{\mathcal{S}}_\omega \;:=\; \boldsymbol{\mathcal{S}} - \omega^2\boldsymbol{I} \;,$$

loses its definiteness for sufficiently large ω. In fact, it satisfies a classical Gårding inequality, i.e.

$$(\boldsymbol{\mathcal{S}}_\omega \boldsymbol{v}, \boldsymbol{v}) \;+\; \omega^2 \|\boldsymbol{v}\|^2 \;\geq\; \mathfrak{s} \|\boldsymbol{v}\|_{1;\Omega}^2 \,, \qquad \forall \boldsymbol{v} \in \boldsymbol{\mathcal{V}} \,.$$

Thus, $\boldsymbol{\mathcal{S}}_\omega$ is a $\boldsymbol{\mathcal{V}}$-coercive sesquilinear form in the Gelfand triple $\boldsymbol{\mathcal{V}} \subset \boldsymbol{L}^2(\Omega) \subset \boldsymbol{\mathcal{V}}'$.

Only in case the ellipticity constant $\mathfrak{s}$ of $\boldsymbol{\mathcal{S}}$ is large enough, e.g., $\mathfrak{s} > \omega^2$, then $\boldsymbol{\mathcal{S}}_\omega$ is $\boldsymbol{\mathcal{V}}$-elliptic due to

$$\begin{aligned} s_\omega(\boldsymbol{v}, \boldsymbol{v}) \;&=\; s(\boldsymbol{v}, \boldsymbol{v}) \,-\, \omega^2 (\boldsymbol{v}, \boldsymbol{v}) \;\;=\; (\boldsymbol{\mathcal{S}} \boldsymbol{v}, \boldsymbol{v}) \,-\, \omega^2 \|\boldsymbol{v}\|^2 \\ &\geq\; (\mathfrak{s} \,-\, \omega^2) \|\boldsymbol{v}\|_{1;\Omega}^2 \;=:\; \mathfrak{s}_\omega \|\boldsymbol{v}\|_{1;\Omega}^2 \,. \end{aligned}$$

In this case, we get a unique solution by the Lax-Milgram theorem. This solution is bounded by the ellipticity constant and the norm of the right-hand side:

$$(\mathfrak{s} - \omega^2) \, \|\boldsymbol{u}\|_{1;\Omega} \;\leq\; \frac{s(\boldsymbol{u}, \boldsymbol{u}) - \omega^2 (\boldsymbol{u}, \boldsymbol{u})}{\|\boldsymbol{u}\|_{1;\Omega}} \;=\; \frac{(\boldsymbol{F}, \boldsymbol{u})}{\|\boldsymbol{u}\|_{1;\Omega}} \;\leq\; \|\boldsymbol{F}\|_{-1;\Omega} \,.$$

The other way around, if ω is sufficiently large, i.e., $\|\boldsymbol{\mathcal{S}}\| < \omega^2$, and if moreover $\boldsymbol{F} \in \mathcal{D}(\boldsymbol{\mathcal{S}}) \;:=\; \{\boldsymbol{v} \in \boldsymbol{\mathcal{V}} \,|\, \boldsymbol{\mathcal{S}} \boldsymbol{v} \in \boldsymbol{\mathcal{V}}\}$, then the problem can be equivalently written as

$$\left(\boldsymbol{I} - \frac{\boldsymbol{\mathcal{S}}}{\omega^2} \right) \boldsymbol{u} \;=\; \frac{-\boldsymbol{F}}{\omega^2} \,, \tag{3.2.18}$$

and the solution is given by the Neumann series

$$\boldsymbol{u} \;=\; -\left(\sum_{k=0}^{\infty} \frac{\boldsymbol{\mathcal{S}}^k}{\omega^{2(k+1)}} \right) \boldsymbol{F} \,. \tag{3.2.19}$$

This immediately provides a bound for the solution $\boldsymbol{u}$:

$$\|\boldsymbol{u}\|_{1;\Omega} \;\leq\; \sum_{k=0}^{\infty} \frac{\|\boldsymbol{\mathcal{S}}\|^k}{\omega^{2(k+1)}} \|\boldsymbol{F}\|_{1;\Omega} \;=\; \frac{\|\boldsymbol{F}\|_{1;\Omega}}{\omega^2 - \|\boldsymbol{\mathcal{S}}\|} \,.$$

We summarize the above results into the following theorem:

Theorem 3.2.5 *Under Assumption 3.2.1 and if one of the two conditions*

$$(i) \quad \mathfrak{s} \, > \, \omega^2 \, , \qquad \textit{or} \qquad (ii) \quad \|\boldsymbol{\mathcal{S}}\| \, < \, \omega^2 \, , \; \boldsymbol{F} \in \mathcal{D}(\boldsymbol{\mathcal{S}}) \, ,$$

holds true, there is a unique solution $\boldsymbol{u} \in \boldsymbol{\mathcal{V}}$ *to the time harmonic equation*

$$\left(\boldsymbol{\mathcal{S}} \, - \, \omega^2 \boldsymbol{I} \right) \boldsymbol{u} \; = \; \boldsymbol{F} \, ,$$

which admits the following bounds in the respective cases:

$$(i) \quad \|\boldsymbol{u}\|_{1;\Omega} \; \leq \; \frac{\|\boldsymbol{F}\|_{-1;\Omega}}{\mathfrak{s} - \omega^2} \, , \qquad (ii) \quad \|\boldsymbol{u}\|_{1;\Omega} \; \leq \; \frac{\|\boldsymbol{F}\|_{1;\Omega}}{\omega^2 - \|\boldsymbol{\mathcal{S}}\|} \, .$$

Riesz-Schauder Analysis

We remark that the embeddings $\boldsymbol{\mathcal{V}} \subset \boldsymbol{L}^2(\Omega) \subset \boldsymbol{\mathcal{V}}'$ are compact in our setting considering Lipschitz domains. In this case, the inclusion $\boldsymbol{I} : \boldsymbol{\mathcal{V}} \to \boldsymbol{\mathcal{V}}'$ is compact and the classical Riesz-Schauder theory can be used to investigate the solution behavior.

We cite a very well-known result in the general setting of compact linear operators within Banach spaces $\mathcal{H}$, i.e. for operators $\mathcal{O} \in \mathcal{L}(\mathcal{H})$ satisfying that $\overline{\mathcal{O}(b)}$ is compact for all bounded subsets $b \subset \mathcal{H}$. The significance of these compact operators lies in the fact that the equation $\mathcal{O}x - \lambda x = b$ has properties analogous to the finite dimensional case, cf. [5, 55, 112]:

Theorem 3.2.6 (Fredholm Alternative) *For* $\lambda \in \mathbb{C}$*, let* $(\lambda \, \mathrm{id} - \mathcal{O}) : \mathcal{H} \to \mathcal{H}$ *be a bounded linear operator on the Banach space* $\mathcal{H}$*,* $\mathcal{O}$ *being a compact linear operator and* id *the identity. Then, only one of the following both situations may occur:*

(1) The trivial solution is the only solution for the eigenvalue equation $\mathcal{O}x = \lambda x$*. In this case, for every* $b \in \mathcal{H}$ *the equation* $(\lambda \, \mathrm{id} - \mathcal{O})x = b$ *admits a unique solution* $x \in \mathcal{H}$ *depending continuously on* b*.*

(2) There are a finite number M *of linear independent eigenfunctions* $x_1, \dots x_M$ *satisfying* $\mathcal{O}x_m = \lambda x_m$. *In this case, if* $\bar{x}$ *is a solution of* $(\lambda \,\mathrm{id} - \mathcal{O})x = b$ *(i.e. if the equation is solvable), the general solution can be obtained with arbitrary* $\alpha_m \in \mathbb{R}$ *by* $x = \bar{x} + \sum_{m=1}^{M} \alpha_m x_m$.

By the Fredholm alternative, the existence of a solution immediately follows from its uniqueness. Moreover, the nullspace $N(\mathcal{O})$ is either empty or finite dimensional. From the Hilbert-Schmidt theory of eigenvalues we get the following supplementing result [112, 75]:

Theorem 3.2.7 *Let* $\mathcal{O} : \mathcal{H} \to \mathcal{H}$ *be a linear compact and self-adjoint operator in a Hilbert space* $\mathcal{H}$. *Then, there exists a possibly finite sequence of eigenfunctions* $x_1, x_2, \dots \neq 0$ *and real eigenvalues* $\lambda_1, \lambda_2, \dots$ *such that* $\mathcal{O}x_j = \lambda_j x_j$ *and*

(1) $|\lambda_1| \geq |\lambda_2| \geq \cdots > 0$,

(2) if the sequence of eigenvalues is infinite, then $\lim_{j\to\infty} \lambda_j = 0$, *and* $\mathcal{O}x = \sum_{j=1}^{\infty} \lambda_j (x, x_j)_{\mathcal{H}} x_j$,

(3) $\mathcal{H} = \overline{\mathrm{span}\{x_j\}_{j=1}^{\infty}} \oplus N(\mathcal{O})$.

However, in our setting the results above cannot be applied immediately because the Schur complement operator $\boldsymbol{\mathcal{S}} : \boldsymbol{\mathcal{V}} \to \boldsymbol{\mathcal{V}}'$ is no self-adjoint endomorphism between Banach spaces. By an application of the Lax-Milgram theorem we introduce an operator $\boldsymbol{s}^{-1} : \boldsymbol{L}^2(\Omega) \to \boldsymbol{\mathcal{V}} \subset \boldsymbol{L}^2(\Omega)$ that is inverse to $\boldsymbol{\mathcal{S}}$ in some special sense, i.e. $\boldsymbol{\mathcal{S}}\boldsymbol{s}^{-1}\boldsymbol{v} = \boldsymbol{v}$ for all $\boldsymbol{v} \in \boldsymbol{L}^2(\Omega)$. This operator is symmetric and bounded in $\boldsymbol{L}^2(\Omega)$ by

$$(\boldsymbol{s}^{-1}\boldsymbol{v}, \boldsymbol{w}) = (\boldsymbol{s}^{-1}\boldsymbol{v}, \boldsymbol{\mathcal{S}}\boldsymbol{s}^{-1}\boldsymbol{w}) = (\boldsymbol{\mathcal{S}}\boldsymbol{s}^{-1}\boldsymbol{v}, \boldsymbol{s}^{-1}\boldsymbol{w}) = (\boldsymbol{v}, \boldsymbol{s}^{-1}\boldsymbol{w}) ,$$

for all $\boldsymbol{v}, \boldsymbol{w} \in \boldsymbol{L}^2(\Omega)$, and

$$\mathfrak{s}\|\boldsymbol{s}^{-1}\boldsymbol{v}\|^2 \leq \mathfrak{s}\|\boldsymbol{s}^{-1}\boldsymbol{v}\|_{1;\Omega}^2 \leq s(\boldsymbol{s}^{-1}\boldsymbol{v}, \boldsymbol{s}^{-1}\boldsymbol{v}) = (\boldsymbol{v}, \boldsymbol{s}^{-1}\boldsymbol{v}) \leq \|\boldsymbol{v}\|\|\boldsymbol{s}^{-1}\boldsymbol{v}\| .$$

Moreover, for a generalized eigenvalue $\omega^2 \neq 0$ and a corresponding eigenfunction $\boldsymbol{u} \in \boldsymbol{\mathcal{V}}$ of $\boldsymbol{\mathcal{S}}$, the operator $\boldsymbol{s}^{-1}$ satisfies the inverse eigenvalue problem

$$\boldsymbol{s}^{-1}\boldsymbol{u} \;=\; \frac{1}{\omega^2}\boldsymbol{u}\ .$$

On the other hand, if $\boldsymbol{u} \in \boldsymbol{L}^2(\Omega)$ satisfies an equation like the one above, then $\boldsymbol{u} \in \boldsymbol{\mathcal{V}}$ (since $\boldsymbol{s}^{-1}(\boldsymbol{L}^2(\Omega)) \subset \boldsymbol{\mathcal{V}}$) and $\boldsymbol{u}$ is an eigenfunction of $\boldsymbol{\mathcal{S}}$. The operator $\boldsymbol{s}^{-1}$ is compact since the embedding $\boldsymbol{\mathcal{V}} \subset \boldsymbol{L}^2(\Omega)$ is compact. Thus, $\boldsymbol{s}^{-1}$ satisfies the assumptions of Theorems 3.2.6 and 3.2.7 above. The results of the Riesz-Schauder analysis now transfer via

$$\boldsymbol{\mathcal{S}} \;-\; \omega^2\boldsymbol{I} \;=\; -\omega^2\boldsymbol{\mathcal{S}}(\boldsymbol{s}^{-1} - \frac{1}{\omega^2})\ ,$$

yielding the following theorem:

Theorem 3.2.8

a) For $\omega^2 \in \mathbb{R}$, only one of the following alternatives hold:

(1) $\boldsymbol{u} = \boldsymbol{0}$ is the only solution for the eigenvalue equation $\boldsymbol{\mathcal{S}}\boldsymbol{u} = \omega^2\boldsymbol{I}\boldsymbol{u}$. In this case, for every $\boldsymbol{F} \in \boldsymbol{\mathcal{V}}'$ the equation $(\boldsymbol{\mathcal{S}} - \omega^2\boldsymbol{I})\boldsymbol{u} = \boldsymbol{F}$ admits a unique solution $\boldsymbol{u} \in \boldsymbol{\mathcal{V}}$ depending continuously on $\boldsymbol{F}$.

(2) There are a finite number M of linear independent eigenfunctions $\boldsymbol{u}_1, \ldots \boldsymbol{u}_M$ satisfying $\boldsymbol{\mathcal{S}}\boldsymbol{u}_m = \omega^2\boldsymbol{I}\boldsymbol{u}_m$. In this case, if $\bar{\boldsymbol{u}}$ solves $(\boldsymbol{\mathcal{S}} - \omega^2\boldsymbol{I})\boldsymbol{u} = \boldsymbol{F}$ (i.e. if the equation is solvable), the general solution can be obtained with arbitrary $\alpha_m \in \mathbb{R}$ by $\boldsymbol{u} \;=\; \bar{\boldsymbol{u}} + \sum_{m=1}^{M} \alpha_m \boldsymbol{u}_m$.

b) The spectrum of $\boldsymbol{\mathcal{S}}$ consists of a sequence of countably many real eigenvalues $0 < \omega_1^2 < \omega_2^2 < \ldots$ tending to infinity, i.e. $\lim_{j\to\infty} \omega_j^2 = \infty$.

c) If $\omega^2 \in \mathbb{R}$ is an eigenvalue of $\boldsymbol{\mathcal{S}}$, the equation $(\boldsymbol{\mathcal{S}} - \omega^2\boldsymbol{I})\boldsymbol{u} = \boldsymbol{F}$ is solvable if and only if $\boldsymbol{F} \in (\boldsymbol{\mathcal{S}} - \omega^2\boldsymbol{I})(\boldsymbol{\mathcal{V}})$, i.e. iff

$$\boldsymbol{F} \;\in\; N(\boldsymbol{\mathcal{S}} - \omega^2\boldsymbol{I})^0 \;=\; \{\boldsymbol{v}' \in \boldsymbol{\mathcal{V}}' \mid (\boldsymbol{v}', \boldsymbol{v}) \;=\; 0 \quad \forall \boldsymbol{v} \in N(\boldsymbol{\mathcal{S}} - \omega^2\boldsymbol{I})\ \}\ .$$

Thus, the spectrum of $\boldsymbol{\mathcal{S}}$ has measure zero, and the solvability of the Schur complement system is guaranteed for nearly all $\omega^2 \in \mathbb{R}$. If "by accident" ω^2 is a generalized

eigenvalue of $\boldsymbol{\mathcal{S}}$, the solvability condition c) in fact is a condition on the boundary data since $\boldsymbol{F} = \boldsymbol{f} + \boldsymbol{\mathcal{B}}\mathcal{C}^{-1}g$ and by $(3.2.15)$,

$$\boldsymbol{F} \;=\; \boldsymbol{\mathcal{R}}'_{\Gamma_\sigma}\boldsymbol{\sigma}_n \;+\; \boldsymbol{\mathcal{B}}\mathcal{C}^{-1}\mathcal{R}'_{\Gamma_D}D_n \;-\; (\boldsymbol{\mathcal{S}} - \omega^2\boldsymbol{I})\boldsymbol{\mathcal{E}}_{\Gamma_u}\boldsymbol{u}_\Gamma \;.$$

3.2.4 A 2.5D Model

Surface acoustic waves propagate along the surface of a substrate. To be precise, the amplitude of the displacement $\boldsymbol{u}$ decays exponentially with depth into the substrate [46, 74]. In true Rayleigh waves, most of the energy (90%) is concentrated within one wavelength from the surface. If h is the height of the substrate with surface located at $x_3 = 0$, this leads to the definition

$$H(x_3) \;:=\; \frac{1 - e^{\frac{\alpha(x_3+h)}{h}}}{1 - e^{\alpha}} \;. \tag{3.2.20}$$

We reduce the dependency on x_3 to exponential decay:

$$\mathbf{u}(\boldsymbol{x}) \;=\; H(x_3)\,\boldsymbol{u}(x_1, x_2) \;, \tag{3.2.21}$$

$$\Phi(\boldsymbol{x}) \;=\; H(x_3)\,\Phi(x_1, x_2) \;, \tag{3.2.22}$$

where there will be some ambiguity in the notation of $\boldsymbol{u}, \Phi$ and related magnitudes. The factor α measures the rapidity of the exponential decay. The problem, of course, is to get a good guess for this parameter. In numerical simulations, we will obtain it from 2D calculations.

4 Finite Element Discretization Of The Coupled Problem

4.1 Finite Element Methods

The finite element method is a method relying on the variational formulation for the PDE problem: Given a sesquilinear form $z(\cdot,\cdot) : \mathcal{X}_1 \times \mathcal{X}_2 \to \mathbb{C}$ defined on two Hilbert spaces $\mathcal{X}_1$ and $\mathcal{X}_2$ and a right-hand side $\ell \in \mathcal{X}_2'$, find $U \in \mathcal{X}_1$ such that

$$z(U,V) \;=\; \ell(V)\;, \qquad \forall V \in \mathcal{X}_2\;. \tag{4.1.1}$$

The main tool for treating the solvability and uniqueness of solutions will be the following generalization of the Lax-Milgram theorem which is due to Babuška [8, 9, 61], but was already shown by Nečas in [81] (see also [23]):

Theorem 4.1.1 (Babuška's Theorem) *Assume that a given sesquilinear form $z : \mathcal{X}_1 \times \mathcal{X}_2 \to \mathbb{C}$ on Hilbert spaces $\mathcal{X}_1$ and $\mathcal{X}_2$ satisfies the following three conditions:*

(i) Continuity : There exists a constant $\|z\| > 0$ such that

$$|z(U,V)| \;\leq\; \|z\|\,\|U\|_{\mathcal{X}_1}\|V\|_{\mathcal{X}_2}\;, \qquad \forall U \in \mathcal{X}_1, V \in \mathcal{X}_2\;.$$

(ii) inf-sup condition : There exists a constant $\beta > 0$ such that

$$\beta\|U\|_{\mathcal{X}_1} \;\leq\; \sup_{0\neq V\in\mathcal{X}_2} \frac{|z(U,V)|}{\|V\|_{\mathcal{X}_2}}\;, \qquad \forall U \in \mathcal{X}_1\;.$$

(iii) 'transposed' inf-sup condition :

$$0 \;<\; \sup_{U\in\mathcal{X}_1} |z(U,V)|\;, \qquad \forall 0 \neq V \in \mathcal{X}_2\;.$$

If additionally $\ell \in \mathcal{X}_2'$ is an antilinear and bounded functional, then there exists a unique solution $U \in \mathcal{X}_1$ to the variational problem $(4.1.1)$ *satisfying the estimate*

$$\|U\|_{\mathcal{X}_1} \;\leq\; \frac{\|\ell\|_{\mathcal{X}_2'}}{\beta} \;.$$

The inf-sup condition is called the Ladyzhenskaya-Babuška-Brezzi (LBB) condition, the smallest corresponding constant β in *(ii)* is called the inf-sup constant, i.e.,

$$\beta \;=\; \inf_{0\neq U\in\mathcal{X}_1} \sup_{0\neq V\in\mathcal{X}_2} \frac{|z(U,V)|}{\|U\|_{\mathcal{X}_1}\|V\|_{\mathcal{X}_2}} \;. \tag{4.1.2}$$

It can be easily checked that every elliptic sesquilinear form with ellipticity constant α also satisfies the inf-sup condition with $\alpha < \beta$, i.e. in the case $\mathcal{X}_1 = \mathcal{X}_2$ the Lax-Milgram theorem immediately follows from Babuška's theorem. The converse is not true, meaning a sesquilinear form may not be elliptic but still satisfy the inf-sup condition. We refer to [18, 21, 30, 31, 55] for results concerning finite element methods.

4.1.1 Galerkin Approximations

We consider Galerkin approximations, i.e., we are looking for an approximate solution in finite dimensional subspaces $\mathcal{X}_1^N \subset \mathcal{X}_1$ and $\mathcal{X}_2^N \subset \mathcal{X}_2$ of the same dimension N. The approximate solution $U^N \in \mathcal{X}_1^N$ takes the form

$$U^N \;=\; \sum_{i=1}^{N} U_i^N \varphi_i^N \;,$$

where $\mathcal{N}_1^N = \{\varphi_i^N\}_{i=1}^N$ is a basis for the space $\mathcal{X}_1^N$. Accordingly, let $\mathcal{N}_2^N = \{\psi_i^N\}_{i=1}^N$ be a basis for the discrete space $\mathcal{X}_2^N$. Then, by formally setting $[\boldsymbol{Z}]_{ij} = z(\varphi_i^N, \psi_j^N)$, $[\boldsymbol{\ell}]_i = \ell(\psi_i^N)$ and $[\boldsymbol{U}]_i = U_i^N$, the approximate solution $\boldsymbol{U} \in \mathbb{C}^N$ can be found as the solution of the linear system

$$\boldsymbol{Z}\boldsymbol{U} \;=\; \boldsymbol{\ell} \;. \tag{4.1.3}$$

One of the most outstanding properties of Galerkin approximations is the so-called

Galerkin orthogonality,

$$z(U - U^N, V) \;=\; 0 \;, \qquad \forall V \in \mathcal{X}_2^N \;.$$

In the conforming case ($\mathcal{X} := \mathcal{X}_1 = \mathcal{X}_2$), when $z(\cdot,\cdot)$ is a bounded (with constant $\|z\|$) and elliptic (with constant $\mathfrak{z}$) sesquilinear form, the discrete equation admits a unique solution U^N, and the Galerkin orthogonality immediately gives rise to Ceá's lemma [18, 21],

$$\|U - U^N\|_{\mathcal{X}} \;\leq\; \frac{\|z\|}{\mathfrak{z}} \inf_{V \in \mathcal{X}^N} \|U - V\|_{\mathcal{X}} \;. \tag{4.1.4}$$

In the non-conforming case, according to Babuška's theorem 4.1.1, a bounded sesquilinear form should satisfy the discrete inf-sup condition,

$$\exists\, \beta^N > 0 : \qquad \beta^N \;\leq\; \sup_{0 \neq V \in \mathcal{X}_2^N} \frac{|z(U,V)|}{\|U\|_{\mathcal{X}_1} \|V\|_{\mathcal{X}_2}} \;, \qquad \forall 0 \neq U \in \mathcal{X}_1^N \;. \tag{4.1.5}$$

Then, the discrete equation admits a unique solution satisfying

$$\|U - U^N\|_{\mathcal{X}_1} \;\leq\; \left(1 + \frac{\|z\|}{\beta^N}\right) \inf_{V \in \mathcal{X}_1^N} \|U - V\|_{\mathcal{X}_1} \;. \tag{4.1.6}$$

In both cases, sequences of approximating subspaces

$$\mathcal{X}_i^1 \;\subset\; \mathcal{X}_i^2 \;\subset\; \cdots \subset\; \mathcal{X}_i^N \;\subset\; \cdots \;\subset\; \mathcal{X}_i \;, \qquad i \;= 1, 2 \;,$$

should be constructed such that the discrete inf-sup condition $(4.1.2)$ is satisfied and the following approximation property holds true:

$$\inf_{V \in \mathcal{X}_1^N} \|U - V\|_{\mathcal{X}_1} \;\longrightarrow\; 0 \;, \qquad \text{as} \;\; N \longrightarrow \infty. \tag{4.1.7}$$

As will be seen in the following sections, for a stable finite element discretization we would require that $(4.1.5)$ is satisfied with a $\beta^N \geq \beta_{\min} > 0$.

According to Section 3.2.3, we are especially interested in coercive sesquilinear forms, i.e., in sesquilinear forms $z : \mathcal{X} \times \mathcal{X} \to \mathbb{C}$, whereat the inclusions $\mathcal{X} \subset L^2 \subset \mathcal{X}'$ form a Gelfand triple and $z(\cdot,\cdot)$ satisfies a Gårding inequality in the form

$$| z(V,V) + \lambda \|V\|_{L^2}^2 | \;\geq\; \alpha \|V\|_{\mathcal{X}}^2 \,, \qquad \forall V \in \mathcal{X} \,,$$

with constants $\lambda > 0$ and $\alpha > 0$. We cite [55] for an important result:

Theorem 4.1.2 *For the coercive sesquilinear form $z(\cdot,\cdot) : \mathcal{X} \times \mathcal{X} \to \mathbb{C}$ assume that the embeddings in the Gelfand triple $\mathcal{X} \subset L^2(\Omega) \subset \mathcal{X}'$ are compact and that the variational problem $(4.1.1)$ is solvable for all $\ell \in \mathcal{X}'$. Let $\{\mathcal{X}^N\}_{N\in\mathbb{N}}$, be an approximating sequence for $\mathcal{X}$ such that $(4.1.7)$ holds true. Then, for sufficiently large N ,the inf-sup condition is satisfied with $\beta^N \geq \beta_{\min} > 0$.*

4.1.2 Finite Element Spaces

We consider a triangulation $\mathcal{T}_h = \{ T_i \,|\, i = 1, \dots I \}$ of a polygonal or polyhedral domain $\Omega \subset \mathbb{R}^d$, $d = 2$ or $d = 3$, as a partition $\bar{\Omega} = \bigcup_{T\in\mathcal{T}_h} T$ of the domain Ω into finitely many simplices with non-overlapping interiors. We use d-simplices to form the partition, other constructions are possible like rectangular elements. By definition, an n-simplex $T \in \mathbb{R}^d$ is the convex hull of $n+1$ non-degenerated points $\boldsymbol{a}_0, \dots \boldsymbol{a}_n \in \mathbb{R}^d$,

$$T \;=\; \{\; \boldsymbol{x} \in \mathbb{R}^d \,|\, \boldsymbol{x} = \sum_{i=0}^{n} \lambda_i \boldsymbol{a}_i \,, \text{ with unique } \lambda_i \in [0,1] \text{ such that } \sum_{i=0}^{n} \lambda_i = 1 \;\} \,.$$

The vertices $\boldsymbol{a}_0, \dots \boldsymbol{a}_n$ are said to be degenerated if they are situated on a $n-1$-dimensional submanifold of $\mathbb{R}^d$. To simplify matters: A d-simplex in $\mathbb{R}^2$ is a triangle, in $\mathbb{R}^3$ it is a tetrahedron. The maximum diameter of these simplices $h := \max_{T\in\mathcal{T}_h} h_T$, where $h_T := \operatorname{diam}(T)$, is called meshsize of the triangulation. In this work we will always consider shape regular triangulations, i.e. there is a constant $\kappa > 0$ such that every simplex $T \in \mathcal{T}_h$ contains a ball with radius ρ_T satisfying $\kappa\rho_T \geq h_T$. We will also consider only conforming triangulations, i.e. the intersection of two simplices is

either empty, a common vertex or a lower dimensional simplex.

The $\lambda_i = \lambda_i(\boldsymbol{x})$ are called barycentric coordinates of $\boldsymbol{x} \in T$. The reference simplex in $\mathbb{R}^d$ is the $d-$simplex $\hat{T}$ with $\hat{\boldsymbol{a}}_0 = \boldsymbol{0}, \hat{\boldsymbol{a}}_{\boldsymbol{1}} = \boldsymbol{e}_1, \ldots \hat{\boldsymbol{a}}_d = \boldsymbol{e}_d$, the $\boldsymbol{e}_i \in \mathbb{R}^d$ denoting the canonical basis vectors. Every $d-$simplex T can be obtained from the reference simplex $\hat{T}$ by a bijective reference mapping $F_T : \hat{T} \to T$ which is completely determined by the relation

$$F_T(\hat{\boldsymbol{a}}_i) \;=\; \boldsymbol{a}_0 + \boldsymbol{F}_T \hat{\boldsymbol{a}}_i \;=\; \boldsymbol{a}_i \;,$$

$\boldsymbol{F}_T \in \mathbb{R}^{d\times d}$ being a regular matrix. The following transformation formula holds for functions $v \in H^m(T)$:

$$|v \circ F_T|_{m;\hat{T}} \;\leq\; c\, \det(\boldsymbol{F}_T)^{-\frac{1}{2}}\, \|\boldsymbol{F}_T\|^m\, |v|_{m;T} \;.$$

Now, the approximation subspace $\mathcal{X}_h := \mathcal{X}^N$ will be constructed locally on the simplices by the use of piecewise polynomials of degree k,

$$\mathcal{X}_h \;:=\; \{\; v \in L^2(\Omega) \,|\;\; v|_T \in \mathbb{P}_k(T) \;, \quad \forall T \in \mathcal{T}_h \;\} \;.$$

On a simplex with vertices $\boldsymbol{a}_0, \ldots \boldsymbol{a}_d$ these functions are uniquely determined by the function values on the set of nodal points

$$L_k(T) \;=\; \left\{ \boldsymbol{x} = \sum_{i=0}^{d} \lambda_i \boldsymbol{a}_i \;,\; \lambda_i \in \{0, \frac{1}{k}, \ldots \frac{k-1}{k}, 1\} \;,\; \sum_{i=0}^{d} \lambda_i = 1 \right\} \;=:\; \{\boldsymbol{x}_i\}_{i=1}^N \;.$$

For $k \geq 1$, if we assume continuity at these points, i.e. $\mathcal{X}_h \subset C(\Omega)$, then there also holds $\mathcal{X}_h \subset H^1(\Omega)$. A nodal basis $\mathcal{N}_h = \{\varphi_i\}_{i=1}^N$ for the finite element space $\mathcal{X}_h$ can be constructed by fixing

$$\varphi_i|_T \;\in\; \mathbb{P}_k(T) \,, \quad \forall T \in \mathcal{T}_h \,, \qquad \text{and} \qquad \varphi_i(\boldsymbol{x}_j) \;=\; \delta_{ij} \,, \quad \forall \boldsymbol{x}_j \in L_k(T) \,,$$

Moreover, for a function $u \in H^2(\Omega) \subset C(\Omega)$ we are able to define a Lagrangian interpolant $\mathcal{I}u \in \mathcal{X}_h$ at the nodal points by

$$(\mathcal{I}u)|_T(\boldsymbol{x}) \;=\; u(\boldsymbol{x}) \;, \qquad \forall \boldsymbol{x} \in L_k(T) \;,$$

yielding the following approximation result for $u \in H^{k+1}$:

$$\|u - \mathcal{I}u\|_{m;\Omega} \;\leq\; ch^{k+1-m}|u|_{k+1;\Omega} \;, \qquad 0 \leq m \leq k+1 \;.$$

Thus, in both variants of Ceá's lemma $(4.1.4)$ and $(4.1.6)$, we can use the interpolation property of finite element spaces:

$$\inf_{v \in \mathcal{X}_h} \|u - v\|_{1;\Omega} \;\leq\; \|u - \mathcal{I}u\|_{1;\Omega} \;\leq\; ch^k|u|_{k+1;\Omega} \;. \tag{4.1.8}$$

4.2 Finite Element Methods for the Saddle Point Problem

In this section, we consider variational problems in saddle point form, i.e., we are searching for a solution $(u, \Phi) \in \mathcal{V} \times \mathcal{W}$ satisfying

$$\begin{aligned} a(u,v) \;+\; b(v,\Phi) \quad &=\; (f,v)_{\mathcal{V}} \;, \qquad && \forall v \in \mathcal{V} \;, \\ b(u,\varphi) \;-\; c(\Phi,\varphi) \quad &=\; (g,\varphi)_{\mathcal{W}} \;, \qquad && \forall \varphi \in \mathcal{W} \;, \end{aligned} \tag{4.2.1}$$

where $a(\cdot,\cdot) : \mathcal{V} \times \mathcal{V} \longrightarrow \mathbb{R}$, $b(\cdot,\cdot) : \mathcal{V} \times \mathcal{W} \longrightarrow \mathbb{R}$ and $c(\cdot,\cdot) : \mathcal{W} \times \mathcal{W} \longrightarrow \mathbb{R}$ are bilinear forms and $a(\cdot,\cdot)$ and $c(\cdot,\cdot)$ are additionally symmetric and elliptic. Moreover, the spaces $\mathcal{V}$ and $\mathcal{W}$ are real Hilbert spaces with inner products $(\cdot,\cdot)_{\mathcal{V}}$ and $(\cdot,\cdot)_{\mathcal{W}}$, respectively. For the sake of simplicity, we consider here the real case, but the approach directly generalizes to the complex situation.
Sometimes, whenever it proves to be useful, we consider the equivalent problem in the product space $\mathcal{X} := \mathcal{V} \times \mathcal{W}$,

$$z(U,V) \;=\; \ell(V) \;, \qquad \forall V \in \mathcal{X} \;, \tag{4.2.2}$$

where $\ell = \begin{pmatrix} f \\ g \end{pmatrix} \in \mathcal{X}'$, and for $\begin{pmatrix} v \\ \varphi \end{pmatrix}, \begin{pmatrix} w \\ \psi \end{pmatrix} \in \mathcal{X}$ the form $z(\cdot,\cdot)$ is given by

$$z\left(\begin{pmatrix} v \\ \varphi \end{pmatrix}, \begin{pmatrix} w \\ \psi \end{pmatrix}\right) \;:=\; a(v,w) \;+\; b(\varphi,w) \;+\; b(\psi,v) \;-\; c(\varphi,\psi) \;.$$

The bilinear form $z(\cdot,\cdot)$ is obviously symmetric but indefinite (inherited from the corresponding properties of $a(\cdot,\cdot)$ and $c(\cdot,\cdot)$).

We are interested in solutions to the equations arising from the modeling of piezoelectric SAW devices. Saddle point problems with $c(\cdot,\cdot) \equiv 0$ have been extensively studied, e.g., in [10, 22, 23, 31, 52]. In this work our interest will be on the case where $c(\cdot,\cdot)$ is not identically zero and the saddle point problem no longer can be viewed as a minimization problem on u alone. However, many results transfer to the new situation. Problems with $c(\cdot,\cdot) \not\equiv 0$ frequently arise in the context of stabilized mixed finite element methods when the finite element spaces are constructed in a way that they do not satisfy the inf-sup condition originally (see e.g. [17, 23, 31, 101]). Systems of the form $(4.2.1)$ also arise in the finite element modeling of slightly compressible fluids and solids [18, 65] and from certain interior point methods in optimization [108, 109]. In most cases, the bilinear form $c(\cdot,\cdot)$ has small norm compared to the other blocks.

The case where both forms $a(\cdot,\cdot)$ and $c(\cdot,\cdot)$ are symmetric positive definite is referred to as the quasidefinite case. Properties of quasidefinite matrices have been studied in [50, 51, 99].

4.2.1 Preliminaries

We assume that the bilinear forms are bounded, i.e., there exist positive constants $\|a\|, \|b\|$ and $\|c\|$ such that

$$|a(v,w)| \leq \|a\|\|v\|_{\mathcal{V}}\|w\|_{\mathcal{V}} , \qquad \forall v,w \in \mathcal{V} , \tag{4.2.3}$$

$$|b(v,\varphi)| \leq \|b\|\|v\|_{\mathcal{V}}\|\varphi\|_{\mathcal{W}} , \qquad \forall v \in \mathcal{V}, \varphi \in \mathcal{W} , \tag{4.2.4}$$

$$|c(\varphi,\psi)| \leq \|c\|\|\varphi\|_{\mathcal{W}}\|\psi\|_{\mathcal{W}} , \qquad \forall \varphi,\psi \in \mathcal{W} . \tag{4.2.5}$$

Then, the bilinear form $z(\cdot,\cdot)$ is also bounded by a constant $\|z\|$ which satisfies

$$\|z\| \leq \|a\| + 2\|b\| + \|c\| .$$

The ellipticity of $a(\cdot,\cdot)$ and $c(\cdot,\cdot)$ yields constants $\mathfrak{a} > 0$ and $\mathfrak{c} > 0$ such that

$$a(v,v) \;\geq\; \mathfrak{a}\,\|v\|_{\mathcal{V}}^2\,, \qquad \forall v \in \mathcal{V}\,, \tag{4.2.6}$$

$$c(\varphi,\varphi) \;\geq\; \mathfrak{c}\,\|\varphi\|_{\mathcal{W}}^2\,, \qquad \forall \varphi \in \mathcal{W}\,. \tag{4.2.7}$$

Then, the energy norm $\|v\|_{\mathcal{A}} := (a(v,v))^{\frac{1}{2}}$ is equivalent to the Hilbert space norm $\|v\|_{\mathcal{V}}$ by

$$\mathfrak{a}\,\|v\|_{\mathcal{V}}^2 \;\leq\; a(v,v) \;\leq\; \|a\|\|v\|_{\mathcal{V}}^2\,, \tag{4.2.8}$$

and the same holds accordingly for $c(\cdot,\cdot)$. Whenever a two-sided inequality in the form $(4.2.8)$ holds, we simply write $\|v\|_{\mathcal{A}} \approx \|v\|_{\mathcal{V}}$ instead.

The notion saddle point stems from the fact that equations $(4.2.1)$ are indeed optimality conditions for the following problem:

$$\inf_{v\in\mathcal{V}} \sup_{\varphi\in\mathcal{W}} \;\frac{1}{2}a(v,v) \;+\; b(v,\varphi) \;-\; \frac{1}{2}c(\varphi,\varphi) \;-\; (f,v)_{\mathcal{V}} \;+\; (g,\varphi)_{\mathcal{W}}\,.$$

In a standard Riesz fashion, operators are associated with the above bilinear forms:

$$\begin{aligned}
&\mathcal{A} : \mathcal{V} \to \mathcal{V}'\,, && \langle \mathcal{A}v, w\rangle_{\mathcal{V}} \;:=\; a(v,w)\,, && \forall w \in \mathcal{V}\,,\\
&\mathcal{B}' : \mathcal{V} \to \mathcal{W}'\,, && \langle \mathcal{B}'v, \varphi\rangle_{\mathcal{W}} \;:=\; b(\varphi,v)\,, && \forall \varphi \in \mathcal{W}\,,\\
&\mathcal{B} : \mathcal{W} \to \mathcal{V}'\,, && \langle \mathcal{B}\varphi, v\rangle_{\mathcal{V}} \;:=\; b(\varphi,v)\,, && \forall v \in \mathcal{V}\,,\\
&\mathcal{C} : \mathcal{W} \to \mathcal{W}'\,, && \langle \mathcal{C}\varphi, \psi\rangle_{\mathcal{W}} \;:=\; c(\varphi,\psi)\,, && \forall \psi \in \mathcal{W}\,,
\end{aligned}$$

where $\langle\cdot,\cdot\rangle_{\mathcal{V}}$ and $\langle\cdot,\cdot\rangle_{\mathcal{W}}$ denote dual pairings in $\mathcal{V}' \times \mathcal{V}$ and $\mathcal{W}' \times \mathcal{W}$, respectively. Then, the constants in $(4.2.3)$-$(4.2.5)$ can be chosen as

$$\|a\| \;=\; \|\mathcal{A}\|_{\mathcal{V}\to\mathcal{V}'}\,, \qquad \|b\| \;=\; \|\mathcal{B}\|_{\mathcal{W}\to\mathcal{V}'} \;=\; \|\mathcal{B}'\|_{\mathcal{V}\to\mathcal{W}'}\,, \qquad \|c\| \;=\; \|\mathcal{C}\|_{\mathcal{W}\to\mathcal{W}'}\,.$$

For symmetric operators $\mathcal{O}_1$ and $\mathcal{O}_2$ defined on a common Hilbert space, we write $\mathcal{O}_1 > \mathcal{O}_2$ whenever $\mathcal{O}_1 - \mathcal{O}_2$ is a positive definite operator in the according dual pairing. In terms of the above defined operators, $(4.2.1)$ can be written as

$$\begin{pmatrix} \mathcal{A} & \mathcal{B} \\ \mathcal{B}' & -\mathcal{C} \end{pmatrix} \begin{pmatrix} u \\ \Phi \end{pmatrix} \;=\; \begin{pmatrix} f \\ g \end{pmatrix}\,, \qquad \text{or} \qquad \mathcal{Z}U \;=\; \ell\,. \tag{4.2.9}$$

The operator $\mathcal{C}$ is symmetric, bounded and $\mathcal{W}$-elliptic. Thus it yields an inverse operator $\mathcal{C}^{-1} : \mathcal{W}' \to \mathcal{W}$ by the Lax-Milgram theorem. Then, we define the Schur complement operator $\mathcal{S}$ by

$$\mathcal{S} \ := \ \mathcal{A} + \mathcal{B}\mathcal{C}^{-1}\mathcal{B}' \ , \tag{4.2.10}$$

and consider sometimes instead of $(4.2.9)$ the equivalent Schur complement system

$$\begin{aligned} \mathcal{S}u \ &= \ F \ := \ f + \mathcal{B}\mathcal{C}^{-1}g \ , \\ \mathcal{C}\Phi \ &= \ \mathcal{B}'u - g \ , \end{aligned} \tag{4.2.11}$$

where $\mathcal{S}$ is obviously symmetric and $\mathcal{V}$-elliptic by the symmetry and ellipticity properties of $\mathcal{A}$ and $\mathcal{C}^{-1}$,

$$\langle \mathcal{S}v, v\rangle_{\mathcal{V}} \ = \ \langle \mathcal{A}v, v\rangle_{\mathcal{V}} \ + \ \langle \mathcal{C}^{-1}\mathcal{B}'v, \mathcal{B}'v\rangle_{\mathcal{W}} \ > \ \mathfrak{a}\|v\|^2_{\mathcal{V}} \ . \tag{4.2.12}$$

Note, the Schur complement operator could surely be defined the other way around as

$$\tilde{\mathcal{S}} \ := \ \mathcal{C} \ + \ \mathcal{B}'\mathcal{A}^{-1}\mathcal{B} \ .$$

These approaches seem to be equivalent since both operators are symmetric, continuous and elliptic. We have chosen the definition of the Schur complement as in $(4.2.10)$ for computational reasons because the discretized operator corresponding to $\mathcal{C}$ can be inverted with less computational effort. Moreover, considering the time dependency of our PDE problem, the symmetry of the two approaches is broken. This is an issue that will be frequently addressed in the sequel.

4.2.2 Finite Element Discretization

For our approximate method, we construct finite dimensional subspaces

$$\mathcal{V}_h \ \subset \ \mathcal{V} \ , \qquad \text{and} \qquad \mathcal{W}_h \subset \mathcal{W} \ ,$$

by the finite element method described in Section 4.1.2. We recall that the parameter h denotes the meshsize of the triangulation $\mathcal{T}_h$ used for the construction of the finite element spaces. As above, we associate operators with the forms $a(\cdot,\cdot)$, $b(\cdot,\cdot)$ and $c(\cdot,\cdot)$

$$\begin{aligned}
&\mathcal{A}_h : \mathcal{V}_h \to \mathcal{V}_h' , && \langle \mathcal{A}_h v, w\rangle_{\mathcal{V}} &:=\ a(v,w) , && \forall w \in \mathcal{V}_h ,\\
&\mathcal{B}_h' : \mathcal{V}_h \to \mathcal{W}_h' , && \langle \mathcal{B}_h' v, \varphi\rangle_{\mathcal{W}} &:=\ b(\varphi,v) , && \forall \varphi \in \mathcal{W}_h ,\\
&\mathcal{B}_h : \mathcal{W}_h \to \mathcal{V}_h' , && \langle \mathcal{B}_h \varphi, v\rangle_{\mathcal{V}} &:=\ b(\varphi,v) , && \forall v \in \mathcal{V}_h ,\\
&\mathcal{C}_h : \mathcal{W}_h \to \mathcal{W}_h' , && \langle \mathcal{C}_h \varphi, \psi\rangle_{\mathcal{W}} &:=\ c(\varphi,\psi) , && \forall \psi \in \mathcal{W}_h .
\end{aligned}$$

Certainly, one has $\|\mathcal{A}_h\|_{\mathcal{V}_h\to\mathcal{V}_h'} \ \leq\ \|a\|$, and the same applies accordingly for $\mathcal{B}_h$ and $\mathcal{C}_h$. Moreover, by the ellipticity of $a(\cdot,\cdot)$ and $c(\cdot,\cdot)$ we have

$$\mathcal{A}_h \ >\ \mathfrak{a} \ >\ 0 , \qquad \text{and} \qquad \mathcal{C}_h \ >\ \mathfrak{c} \ >\ 0 . \tag{4.2.13}$$

Note that in the discrete case the spaces $\mathcal{V}_h$ and $\mathcal{V}_h'$ are indeed the same, but in general they are equipped with different inner products and norms.

In terms of these operators, the discretized saddle point problem then reads

$$\begin{pmatrix} \mathcal{A}_h & \mathcal{B}_h \\ \mathcal{B}_h' & -\mathcal{C}_h \end{pmatrix} \begin{pmatrix} u_h \\ \Phi_h \end{pmatrix} \ =\ \begin{pmatrix} f_h \\ g_h \end{pmatrix} \qquad \text{or} \qquad \mathcal{Z}_h U_h \ =\ \ell_h . \tag{4.2.14}$$

Again, from the ellipticity and boundedness of $\mathcal{C}_h$, a discrete version of the Schur complement operator can formally defined by

$$\mathcal{S}_h \ :=\ \mathcal{A}_h \ +\ \mathcal{B}_h \mathcal{C}_h^{-1} \mathcal{B}_h' . \tag{4.2.15}$$

Hence, instead of $(4.2.14)$ we may consider the equivalent Schur complement system

$$\begin{aligned}
\mathcal{S}_h u_h \ &=\ F_h \ :=\ f_h + \mathcal{B}_h \mathcal{C}_h^{-1} g_h ,\\
\mathcal{C}_h \Phi_h \ &=\ \mathcal{B}_h^T u_h - g_h ,
\end{aligned} \tag{4.2.16}$$

where $\mathcal{S}_h$ is obviously symmetric and elliptic by the symmetry and positive definiteness of $\mathcal{A}_h$ and $\mathcal{C}_h^{-1}$ using the same arguments as in the continuous case. Caution should be paid to the fact that it is not clear immediately that $\mathcal{S}_h$ is a direct discretization of the Schur complement operator $\mathcal{S}$:

Theorem 4.2.1 *The finite element discretization of $\mathcal{S}$ is given by $\mathcal{S}_h$, i.e.*

$$\langle \mathcal{S}_h v, w\rangle_{\mathcal{V}} \;=\; \langle \mathcal{S} v, w\rangle_{\mathcal{V}} \;, \qquad \forall v, w \in \mathcal{V}_h \;.$$

Proof. A direct computation yields

$$\begin{aligned}\langle \mathcal{S}_h v, w\rangle_{\mathcal{V}} &= \langle \mathcal{A}_h v, w\rangle_{\mathcal{V}} + \langle \mathcal{B}_h' w, \mathcal{C}_h^{-1}\mathcal{B}_h' v\rangle_{\mathcal{W}} \\ &= a(v,w) + b(\mathcal{C}_h^{-1}\mathcal{B}_h' v, w) \\ &= \langle \mathcal{A} v, w\rangle_{\mathcal{V}} + \langle \mathcal{B}' w, \mathcal{C}_h^{-1}\mathcal{B}_h' v\rangle_{\mathcal{W}} \;.\end{aligned}$$

Moreover, by the symmetry of $c(\cdot,\cdot)$,

$$\langle \mathcal{C}\varphi, \mathcal{C}_h^{-1}\psi\rangle_{\mathcal{W}} \;=\; c(\varphi, \mathcal{C}_h^{-1}\psi) \;=\; c(\mathcal{C}_h^{-1}\psi, \varphi) \;=\; \langle \psi, \varphi\rangle_{\mathcal{W}} \;,$$

for arbitrary $\varphi \in \mathcal{W}, \psi \in \mathcal{W}'$, and the proof is finished by

$$\begin{aligned}\langle \mathcal{B}' w, \mathcal{C}_h^{-1}\mathcal{B}_h' v\rangle_{\mathcal{W}} &= \langle \mathcal{C}\mathcal{C}^{-1}\mathcal{B}' w, \mathcal{C}_h^{-1}\mathcal{B}_h' v\rangle_{\mathcal{W}} \\ &= \langle \mathcal{B}_h' v, \mathcal{C}^{-1}\mathcal{B}' w\rangle_{\mathcal{W}} \\ &= \langle \mathcal{B}' v, \mathcal{C}^{-1}\mathcal{B}' w\rangle_{\mathcal{W}} \;.\end{aligned}$$

□

4.2.3 Saddle Points with $\mathcal{C} = 0$

In this section, we shortly review results in the limiting case $\mathcal{C} = 0$, i.e., we are looking for solutions to the system

$$\begin{pmatrix} \mathcal{A} & \mathcal{B} \\ \mathcal{B}' & 0 \end{pmatrix} \begin{pmatrix} u \\ \Phi \end{pmatrix} \;=\; \begin{pmatrix} f \\ g \end{pmatrix} \;, \qquad \text{or} \qquad \mathcal{Z}U \;=\; \ell \;, \tag{4.2.17}$$

where $\mathcal{A}$ is a symmetric, continuous and elliptic operator and $\mathcal{B}$, f and g are bounded. It can be easily seen that $\mathcal{Z}$ fulfills the conditions of Babuška's theorem 4.1.1, if $b(\cdot,\cdot)$ satisfies the inf-sup condition, i.e., there exists a positive constant β such that

$$\inf_{\varphi\in\mathcal{W}} \sup_{v\in\mathcal{V}} \frac{|b(v,\varphi)|}{\|v\|_{\mathcal{V}}\|\varphi\|_{\mathcal{W}}} \;\geq\; \beta \;>\; 0 \;. \tag{4.2.18}$$

The inf-sup condition is satisfied, if $\mathcal{B}$ is a closed operator, i.e. $\mathcal{B}(\mathcal{W})$ is closed. In principle, the inf-sup condition guarantees that the Schur complement is positive definite:

$$\begin{aligned} \langle \mathcal{B}'\mathcal{A}^{-1}\mathcal{B}\varphi, \varphi\rangle_{\mathcal{W}} &= \langle \mathcal{A}\mathcal{A}^{-1}\mathcal{B}\varphi, \mathcal{A}^{-1}\mathcal{B}\varphi\rangle_{\mathcal{V}} \\ &= \sup_{v\in\mathcal{V}} \frac{\langle \mathcal{A}\mathcal{A}^{-1}\mathcal{B}\varphi, v\rangle_{\mathcal{V}}^2}{\langle \mathcal{A}v, v\rangle_{\mathcal{V}}} \\ &= \sup_{v\in\mathcal{V}} \frac{\langle \mathcal{B}\varphi, v\rangle_{\mathcal{V}}^2}{\|v\|_{\mathcal{A}}^2} \\ &\geq \frac{\beta^2}{\|a\|}\|\varphi\|_{\mathcal{W}}^2 \;>\; 0 \;. \end{aligned} \tag{4.2.19}$$

Problems arise with the finite element discretization of the linear system: In finite dimensions with $\mathcal{V}_h = \mathbb{R}^n$ and $\mathcal{W}_h = \mathbb{R}^m$, where $m \leq n$, the inf-sup condition simply states that $\mathcal{B}_h$ is a full rank matrix, since

$$\sup_{\varphi\in\mathbb{R}^m} \frac{|b(v,\varphi)|}{\|\varphi\|_2} \;=\; \sup_{\varphi\in\mathbb{R}^m} \frac{|(\mathcal{B}_h' v, \varphi)|}{\|\varphi\|_2} \;=\; \|\mathcal{B}_h' v\|_2 \;.$$

Note that an elliptic bilinear form retains its ellipticity, if it is restricted to a finite dimensional subspace with an ellipticity constant bounded from below by the original one. This is not true for the inf-sup condition. Hence, the finite element element spaces $\mathcal{V}_h \subset \mathcal{V}$ and $\mathcal{W}_h \subset \mathcal{W}$ have to be constructed such that $b(\cdot,\cdot)$ satisfies the inf-sup condition with inf-sup constants β_h that are uniformly bounded from below by a positive constant

$$\beta_h \;\geq\; \beta_{\min} \;>\; 0 \;, \qquad \text{as} \;\; h \to 0 \;. \tag{4.2.20}$$

Otherwise, the positive definiteness of the Schur complement will asymptotically be lost by $(4.2.19)$. Also, in view of $(4.1.6)$, the error estimate will blow up. Finite element spaces satisfying the inf-sup condition with β_h as in $(4.2.20)$ are called LBB-stable. Moreover, by the bounds in Babuška's theorem we get

$$\langle \mathcal{B}_h'\mathcal{A}_h^{-1}\mathcal{B}_h\varphi, \varphi\rangle_{\mathcal{W}} \;=\; \langle \mathcal{B}_h\varphi, \mathcal{A}_h^{-1}\mathcal{B}_h\varphi\rangle_{\mathcal{V}} \;\leq\; \frac{\|b\|^2}{\mathfrak{a}}\|\varphi\|_{\mathcal{W}}^2 \;,$$

and thus, together with the discrete version of $(4.2.19)$ we obtain

$$\frac{\beta_{\min}^2}{\|a\|} \;\leq\; \frac{\langle \mathcal{B}_h' \mathcal{A}_h^{-1} \mathcal{B}_h \varphi, \varphi \rangle_{\mathcal{W}}}{\|\varphi\|_{\mathcal{W}}^2} \;\leq\; \frac{\|b\|^2}{\mathfrak{a}} \;. \tag{4.2.21}$$

This means that the Schur complement has a spectral condition number independent of the meshsize h (with respect to the energy norm $\|\cdot\|_{\mathcal{C}} \approx \|\cdot\|_{\mathcal{W}}$).

4.2.4 Quasi-Definite Saddle Point Problems

We now return to the original problem where $\mathcal{C}$ is a symmetric, continuous and $\mathcal{W}$-elliptic operator, i.e., we are looking for a solution $(u, \Phi) \in \mathcal{V} \times \mathcal{W}$ satisfying

$$\begin{pmatrix} \mathcal{A} & \mathcal{B} \\ \mathcal{B}' & -\mathcal{C} \end{pmatrix} \begin{pmatrix} u \\ \Phi \end{pmatrix} \;=\; \begin{pmatrix} f \\ g \end{pmatrix} \;, \qquad \text{or} \qquad \mathcal{Z} U \;=\; \ell \;.$$

We recall that here the Schur complement operator is chosen as $\mathcal{S} = \mathcal{A} + \mathcal{B}\mathcal{C}^{-1}\mathcal{B}'$, and a simple estimate yields the positive definiteness of $\mathcal{S}$ in $(4.2.12)$. In order to get a better bound, we relax the inf-sup condition in $(4.2.18)$ to

$$\inf_{v \in \mathcal{V}} \sup_{\varphi \in \mathcal{W}} \frac{|b(v,\varphi)|}{\|v\|_{\mathcal{V}} \|\varphi\|_{\mathcal{W}}} \;\geq\; \beta \;\geq\; 0 \;, \tag{4.2.22}$$

i.e., we allow for the case $\beta = 0$ and there might be a non-trivial kernel for the operator $\mathcal{B}$. In case of a finite element approximation this estimate should hold with some $\beta_h \geq \beta_{\min} \geq 0$ (compare $(4.2.20)$). A simple estimate yields

$$\begin{aligned}
\langle \mathcal{S} v, v \rangle_{\mathcal{V}} \;&=\; \langle \mathcal{A} v, v \rangle_{\mathcal{V}} \;+\; \langle \mathcal{B}' v, \mathcal{C}^{-1} \mathcal{B}' v \rangle_{\mathcal{W}} \\
&=\; \langle \mathcal{A} v, v \rangle_{\mathcal{V}} \;+\; \langle \mathcal{C}\mathcal{C}^{-1} \mathcal{B}' v, \mathcal{C}^{-1} \mathcal{B}' v \rangle_{\mathcal{W}} \\
&\geq\; \langle \mathcal{A} v, v \rangle_{\mathcal{V}} \;+\; \sup_{\varphi \in \mathcal{W}} \frac{\langle \mathcal{C}\mathcal{C}^{-1} \mathcal{B}' v, \varphi \rangle_{\mathcal{W}}^2}{\langle \mathcal{C}\varphi, \varphi \rangle_{\mathcal{W}}} \\
&=\; \langle \mathcal{A} v, v \rangle_{\mathcal{V}} \;+\; \sup_{\varphi \in \mathcal{W}} \frac{\langle \mathcal{B}' v, \varphi \rangle_{\mathcal{W}}^2}{\|\varphi\|_{\mathcal{C}}^2} \\
&\geq\; \left(\mathfrak{a} \;+\; \frac{\beta^2}{\|c\|} \right) \|v\|_{\mathcal{V}}^2 \;.
\end{aligned}$$

An upper bound can be obtained by

$$\begin{aligned}\langle \mathcal{S}v, v\rangle_{\mathcal{V}} &= \langle \mathcal{A}v, v\rangle_{\mathcal{V}} + \langle \mathcal{C}^{-1}\mathcal{B}'v, \mathcal{B}'v\rangle_{\mathcal{W}} \\ &\leq \left(\|a\| + \frac{\|b\|^2}{\mathfrak{c}}\right)\|v\|_{\mathcal{V}}^2 .\end{aligned}$$

The condition number estimate in the quasi-definite case is then given by

$$\mathfrak{a} + \frac{\beta^2}{\|c\|} \leq \frac{\langle \mathcal{S}v, v\rangle_{\mathcal{V}}}{\|v\|_{\mathcal{V}}^2} \leq \|a\| + \frac{\|b\|^2}{\mathfrak{c}} , \qquad \forall v \in \mathcal{V} . \tag{4.2.23}$$

Since by $(4.2.13)$, all bounds used above are also satisfied for the discrete operators $\mathcal{A}_h$, $\mathcal{B}_h$ and $\mathcal{C}_h$, the condition number estimates also hold for the discrete Schur complement operator $\mathcal{S}_h$, i.e.,

$$\mathfrak{a} + \frac{\beta_{\min}^2}{\|c\|} \leq \frac{\langle \mathcal{S}_h v, v\rangle_{\mathcal{V}}}{\|v\|_{\mathcal{V}}^2} \leq \|a\| + \frac{\|b\|^2}{\mathfrak{c}} , \qquad \forall v \in \mathcal{V}_h . \tag{4.2.24}$$

Hence, the spectral condition number of the Schur complement operator is bounded in the energy norm $\|\cdot\|_{\mathcal{A}}$ by a constant independent of h. We note that this h-independency does not hold true for the matrix representation $\boldsymbol{v}^T\boldsymbol{S}\boldsymbol{w} = \langle \mathcal{S}_h v, w\rangle_{\mathcal{V}}$ as in $(4.1.3)$. In our case, choosing $\mathcal{V}_h$ as some subspace of the Sobolev space $H^1(\Omega)$, from $\|v\|_0 \leq \|v\|_1 \leq \frac{C}{h}\|v\|_0$ we obtain an upper bound in the condition number estimate that depends on the meshsize h.

Remark 4.2.2 *Note that the somewhat different approach of choosing the Schur complement according to $\tilde{\mathcal{S}} = \mathcal{C} + \mathcal{B}'\mathcal{A}^{-1}\mathcal{B}$ would result in*

$$\mathfrak{c} + \frac{\tilde{\beta}^2}{\|a\|} \leq \frac{\langle \tilde{\mathcal{S}}\varphi, \varphi\rangle_{\mathcal{W}}}{\|\varphi\|_{\mathcal{W}}^2} \leq \|c\| + \frac{\|b\|^2}{\mathfrak{a}} , \qquad \forall \varphi \in \mathcal{W} ,$$

where $\tilde{\beta}$ is the inf-sup constant of an adapted condition like $(4.2.22)$. Since in our case $\mathcal{V}$ and $\mathcal{W}$ are both spaces including generalized derivatives, there is no advantage in choosing the Schur complement this way. In principle, both approaches are well suited for a numerical discretization.

4.3 Finite Element Discretization for the Time Harmonic Equations

In this section, we consider the finite element discretization of the time harmonic equation

$$(\boldsymbol{\mathcal{S}} - \omega^2 \boldsymbol{I})\boldsymbol{u} \;=\; \boldsymbol{F} \;, \qquad \text{in } \boldsymbol{\mathcal{V}}' \;,$$

where $\boldsymbol{\mathcal{S}}$ is the $\boldsymbol{\mathcal{V}}$-elliptic Schur complement operator and $\boldsymbol{I}$ is the compact embedding $\boldsymbol{I} : \boldsymbol{\mathcal{V}} \to \boldsymbol{\mathcal{V}}'$. We introduce sesquilinear forms as in Section 3.2.3,

$$\begin{aligned} s(\boldsymbol{v},\boldsymbol{w}) \;&:=\; (\boldsymbol{\mathcal{S}}\boldsymbol{v},\boldsymbol{w}) \;, && \forall \boldsymbol{v},\boldsymbol{w} \in \boldsymbol{\mathcal{V}} \;, \\ s_\omega(\boldsymbol{v},\boldsymbol{w}) \;&:=\; ((\boldsymbol{\mathcal{S}} - \omega^2\boldsymbol{I})\boldsymbol{v},\boldsymbol{w}) \;, && \forall \boldsymbol{v},\boldsymbol{w} \in \boldsymbol{\mathcal{V}} \;. \end{aligned}$$

Here, we assume that the continuous problem is solvable. According to Babuška's theorem, there exists some constant β such that

$$0 \;<\; \beta \;:=\; \inf_{0\neq \boldsymbol{v}\in\boldsymbol{\mathcal{V}}} \sup_{0\neq \boldsymbol{w}\in\boldsymbol{\mathcal{V}}} \frac{s_\omega(\boldsymbol{v},\boldsymbol{w})}{\|\boldsymbol{v}\|_{1;\Omega}\|\boldsymbol{w}\|_{1;\Omega}} \;.$$

The finite element discretization involves finite dimensional subspaces $\boldsymbol{\mathcal{V}}_h \subset \boldsymbol{\mathcal{V}}$ where the inf-sup condition does not hold true in general. We set

$$0 \;\leq\; \beta_h \;:=\; \inf_{0\neq \boldsymbol{v}\in\boldsymbol{\mathcal{V}}_h} \sup_{0\neq \boldsymbol{w}\in\boldsymbol{\mathcal{V}}_h} \frac{s_\omega(\boldsymbol{v},\boldsymbol{w})}{\|\boldsymbol{v}\|_{1;\Omega}\|\boldsymbol{w}\|_{1;\Omega}} \;,$$

temporarily allowing for $\beta_h = 0$. Of course, according to the previous sections, we require $\beta_h \geq \beta_{\min} \geq 0$.

For the bilinear form $s_0(\cdot,\cdot) = s(\cdot,\cdot)$, the ellipticity and continuity immediately transfer from $\boldsymbol{\mathcal{V}}$ to $\boldsymbol{\mathcal{V}}_h$. Consequently, there are constants $\mathfrak{s}, \|s\|$ such that for all $\boldsymbol{v} \in \boldsymbol{\mathcal{V}}$ (and for all $\boldsymbol{v} \in \boldsymbol{\mathcal{V}}_h$),

$$\mathfrak{s}\|\boldsymbol{v}\|_{1;\Omega}^2 \;\leq\; s(\boldsymbol{v},\boldsymbol{v}) \;\leq\; \|s\|\,\|\boldsymbol{v}\|_{1;\Omega}^2 \;.$$

We only consider the case $\omega \neq 0$. Then, by a first application of the Lax-Milgram lemma there exist linear operators $\boldsymbol{s}^{-1}\!:\boldsymbol{\mathcal{V}} \to \boldsymbol{\mathcal{V}}$ and $\boldsymbol{s}_h^{-1} : \boldsymbol{\mathcal{V}}_h \to \boldsymbol{\mathcal{V}}_h$, inverse in some special sense to $\boldsymbol{\mathcal{S}}$, i.e., satisfying

$$\begin{aligned} s(\boldsymbol{s}^{-1}\boldsymbol{v}, \boldsymbol{w}) \;&=\; (\boldsymbol{I}\boldsymbol{v}, \boldsymbol{w}) \;, \qquad \forall \boldsymbol{v}, \boldsymbol{w} \in \boldsymbol{\mathcal{V}} \;, \\ s(\boldsymbol{s}_h^{-1}\boldsymbol{v}, \boldsymbol{w}) \;&=\; (\boldsymbol{I}\boldsymbol{v}, \boldsymbol{w}) \;, \qquad \forall \boldsymbol{v}, \boldsymbol{w} \in \boldsymbol{\mathcal{V}}_h \;, \end{aligned}$$

whence

$$s(\boldsymbol{s}^{-1}\boldsymbol{v} - \boldsymbol{s}_h^{-1}\boldsymbol{v}, \boldsymbol{w}) \;=\; 0 \;, \qquad \forall \boldsymbol{v}, \boldsymbol{w} \in \boldsymbol{\mathcal{V}}_h \;.$$

The operators are bounded by

$$\mathfrak{s}\|\boldsymbol{s}^{-1}\boldsymbol{v}\|_{1;\Omega} \;\leq\; \frac{s(\boldsymbol{s}^{-1}\boldsymbol{v}, \boldsymbol{s}^{-1}\boldsymbol{v})}{\|\boldsymbol{s}^{-1}v\|_{1;\Omega}} \;=\; \frac{(\boldsymbol{I}\boldsymbol{v}, \boldsymbol{s}^{-1}\boldsymbol{v})}{\|\boldsymbol{s}^{-1}v\|_{1;\Omega}} \;\leq\; \|\boldsymbol{I}\boldsymbol{v}\|_{-1;\Omega} \;=\; \|\boldsymbol{v}\|_{1;\Omega} \;,$$

and also $\mathfrak{s}\|\boldsymbol{s}_h^{-1}\boldsymbol{v}\|_{1;\Omega} \leq \|\boldsymbol{v}\|_{1;\Omega}$. Thus, the proper choice of the finite element approximation yields

$$\|\boldsymbol{s}^{-1} - \boldsymbol{s}_h^{-1}\| \;\longrightarrow\; 0 \;, \qquad \text{as} \qquad h \to 0 \;.$$

By continuity and the inf-sup condition, we have for $\boldsymbol{v} \in \boldsymbol{\mathcal{V}}$

$$\begin{aligned} \beta\|\boldsymbol{v}\|_{1;\Omega} \;&\leq\; \sup_{0\neq\boldsymbol{w}\in\boldsymbol{\mathcal{V}}} \frac{|s_\omega(\boldsymbol{v}, \boldsymbol{w})|}{\|\boldsymbol{w}\|_{1;\Omega}} \\ &=\; \sup_{0\neq\boldsymbol{w}\in\boldsymbol{\mathcal{V}}} \frac{|s(\boldsymbol{v} - \omega^2\boldsymbol{s}^{-1}\boldsymbol{v}, \boldsymbol{w})|}{\|\boldsymbol{w}\|_{1;\Omega}} \\ &\leq\; \|s\|\,\|\boldsymbol{v} - \omega^2\boldsymbol{s}^{-1}\boldsymbol{v}\|_{1;\Omega} \;. \end{aligned}$$

From this result and by the $\boldsymbol{\mathcal{V}}$-ellipticity of $s(\cdot,\cdot)$, we get for $\boldsymbol{v} \in \boldsymbol{\mathcal{V}}_h$

$$\begin{aligned}
\sup_{0\neq\boldsymbol{w}\in\boldsymbol{\mathcal{V}}_h} \frac{|s_\omega(\boldsymbol{v},\boldsymbol{w})|}{\|\boldsymbol{w}\|_{1;\Omega}} &= \sup_{0\neq\boldsymbol{w}\in\boldsymbol{\mathcal{V}}_h} \frac{|s(\boldsymbol{v}-\omega^2\boldsymbol{s}_h^{-1}\boldsymbol{v},\boldsymbol{w})|}{\|\boldsymbol{w}\|_{1;\Omega}} \\
&\geq \frac{|s(\boldsymbol{v}-\omega^2\boldsymbol{s}_h^{-1}\boldsymbol{v},\boldsymbol{v}-\omega^2\boldsymbol{s}_h^{-1}\boldsymbol{v})|}{\|\boldsymbol{v}-\omega^2\boldsymbol{s}_h^{-1}\boldsymbol{v}\|_{1;\Omega}} \\
&\geq \mathfrak{s}\|\boldsymbol{v}-\omega^2\boldsymbol{s}_h^{-1}\boldsymbol{v}\|_{1;\Omega} \\
&\geq \mathfrak{s}\|\boldsymbol{v}-\omega^2\boldsymbol{s}^{-1}\boldsymbol{v}\|_{1;\Omega} \;-\; \omega^2\mathfrak{s}\|(\boldsymbol{s}_h^{-1}-\boldsymbol{s}^{-1})\boldsymbol{v}\|_{1;\Omega} \\
&\geq \left(\frac{\beta\mathfrak{s}}{\|s\|} \;-\; \omega^2\mathfrak{s}\|\boldsymbol{s}_h^{-1}-\boldsymbol{s}^{-1}\|\right)\|\boldsymbol{v}\|_{1;\Omega}
\end{aligned}$$

whence

$$\beta_h \;\geq\; \frac{\beta\mathfrak{s}}{\|s\|} \;-\; \omega^2\mathfrak{s}\|\boldsymbol{s}_h^{-1}-\boldsymbol{s}^{-1}\| \;.$$

This inequality can be used for estimating the size of the meshsize h needed to yield an appropriate approximation. We obtain the following result (cf. Theorem 4.1.2):

Theorem 4.3.1 *For $\omega^2 \in \mathbb{R}$ and a $\boldsymbol{\mathcal{V}}$-elliptic sesquilinear form $s : \boldsymbol{\mathcal{V}} \times \boldsymbol{\mathcal{V}} \to \mathbb{C}$, let the inf-sup condition*

$$0 \;<\; \beta \;\leq\; \inf_{0\neq\boldsymbol{v}\in\boldsymbol{\mathcal{V}}} \sup_{0\neq\boldsymbol{w}\in\boldsymbol{\mathcal{V}}} \frac{|s(\boldsymbol{v},\boldsymbol{w})-\omega^2(\boldsymbol{v},\boldsymbol{w})|}{\|\boldsymbol{v}\|_{1;\Omega}\|\boldsymbol{w}\|_{1;\Omega}} \;,$$

hold true. Then, for sufficiently small h_0 there exists a constant $\beta_{\min}$ such that for all $h < h_0$

$$0 \;<\; \beta_{\min} \;\leq\; \beta_h \;\leq\; \inf_{0\neq\boldsymbol{v}\in\boldsymbol{\mathcal{V}}_h} \sup_{0\neq\boldsymbol{w}\in\boldsymbol{\mathcal{V}}_h} \frac{|s(\boldsymbol{v},\boldsymbol{w})-\omega^2(\boldsymbol{v},\boldsymbol{w})|}{\|\boldsymbol{v}\|_{1;\Omega}\|\boldsymbol{w}\|_{1;\Omega}} \;.$$

5 Efficient Iterative Solution Of The Discretized Problem

Resulting from the finite element discretization of the piezoelectric equations we are looking for a discrete solution by solving a linear system of the form

$$\boldsymbol{Z}\boldsymbol{U} \;=\; \boldsymbol{\ell}\,, \tag{5.0.1}$$

where $\boldsymbol{Z} \in \mathbb{R}^{N\times N}$ (or $\boldsymbol{Z} \in \mathbb{C}^{N\times N}$) is a regular matrix and $\boldsymbol{\ell} \in \mathbb{R}^{N}$ (or $\boldsymbol{\ell} \in \mathbb{C}^{N}$). Direct methods for sparse linear systems have been developed, e.g., in [38, 86]. However, direct methods scale poorly with problem size in terms of operations counts and memory requirements, especially on problems arising from the discretization of partial differential equations. Here, iterative methods are more suitable.

5.1 Iterative Methods for Indefinite Systems

There exist many classical iterative methods to solve problem $(5.0.1)$, such as the Richardson, Gauss-Seidel and Jacobi iteration. Each of these methods converge for positive definite symmetric problems. Some of the classical methods might even converge for non-symmetric problems, but then usually some spectral information is required to assure convergence, see [54, 76]. However, it can be easily shown that Richardson's method fails to converge for all complex damping parameters, if $\boldsymbol{Z}$ has both positive and negative real eigenvalues, as is the case for symmetric indefinite problems.

As seen from above, spectral information about the matrices is required for the analysis of iterative methods. For a matrix $\boldsymbol{Z}$, we denote by $\sigma(\boldsymbol{Z}) = \{\lambda_i\}$ the

spectrum (containing the eigenvalues λ_i) of this matrix and its spectral radius and extremal eigenvalues by

$$\rho(\boldsymbol{Z}) \;:=\; \max\{\,|\lambda|\;|\;\lambda\in\sigma(\boldsymbol{Z})\,\}\;, \qquad \lambda_{\max}(\boldsymbol{Z}) \;:=\; \max\{\,\lambda\;|\;\lambda\in\sigma(\boldsymbol{Z})\,\}\;,$$

where $\lambda_{\min}(\boldsymbol{Z})$ is defined as $\lambda_{\max}(\boldsymbol{Z})$ but taking the minimum. A good measure for the stability of the obtained solution usually is the condition number $\kappa(\boldsymbol{Z})$, given by

$$\kappa(\boldsymbol{Z}) \;:=\; \rho(\boldsymbol{Z})\,\rho(\boldsymbol{Z}^{-1}) \;=\; \frac{\rho(\boldsymbol{Z})}{\min\{\,|\lambda|\;|\;\lambda\in\sigma(\boldsymbol{Z})\,\}}\;.$$

We will make use of a class of iterative methods where there will be no need for any a priori spectral information: The Krylov space methods are a class of iterative procedures especially designed for indefinite and also nonsymmetric problems.

5.1.1 Krylov Space Methods

What makes Krylov space methods interesting for the solution of linear systems $\boldsymbol{ZU} = \boldsymbol{\ell}$ is the fact that in practical relevant applications the appearing matrix-vector products are often quite cheap in terms of computational costs. Especially, in the finite element framework the appearing coefficient matrix $\boldsymbol{Z}$ is often sparse. The name refers to a method introduced by Krylov [69] in 1931 with the purpose to determine divisors of the minimal polynomial of an operator. For a detailed introduction to Krylov space methods see [24, 102, 76].

Krylov space methods are iterations taking the form

$$\boldsymbol{U}_{m+1} \;:=\; \boldsymbol{U}_0 \;+\; p_m(\boldsymbol{Z})\boldsymbol{R}_0 \;=\; \boldsymbol{U}_m \;+\; \alpha_m\boldsymbol{D}_m, \tag{5.1.1}$$

where $p_m \in \mathbb{P}_m$ is a polynomial of degree at most m, $\boldsymbol{U}_0$ is an initial guess and $\boldsymbol{R}_m := \boldsymbol{\ell} - \boldsymbol{Z}\boldsymbol{x}_m$ is the residual associated with the iterate $\boldsymbol{U}_m$. Then, $\boldsymbol{D}_m$ is a search direction for the update from $\boldsymbol{U}_{m-1}$ to $\boldsymbol{U}_m$. From $(5.1.1)$ it gets clear that the new iterate $\boldsymbol{U}_m$ is sought in an affine subspace $\boldsymbol{U}_0 + \mathcal{K}_m(\boldsymbol{Z}, \boldsymbol{R}_0)$, i.e.

$$\boldsymbol{U}_m \;\in\; \boldsymbol{U}_0 \;+\; \mathcal{K}_m(\boldsymbol{Z}, \boldsymbol{R}_0)\;, \tag{5.1.2}$$

where

$$\mathcal{K}_m \;=\; \mathcal{K}_m(\boldsymbol{Z}, \boldsymbol{R}_0) \;=\; \mathrm{span}\{\boldsymbol{R}_0, \boldsymbol{Z}\boldsymbol{R}_0, \ldots, \boldsymbol{Z}^{m-1}\boldsymbol{R}_0\} \;, \tag{5.1.3}$$

is the Krylov space of dimension m. The search directions $\boldsymbol{D}_m$ are then chosen as a basis of these spaces satisfying

$$\boldsymbol{D}_m \;\in\; \mathcal{K}_m / \mathcal{K}_{m-1} \;.$$

Note, the Cayley-Hamilton theorem guarantees for non-singular matrices that the inverse matrix can be written as a polynomial in $\boldsymbol{Z}$, at most of degree $N-1$. Thus, the proper choice of the polynomials p_m in $(5.1.1)$ will yield a solution after at most N steps. Moreover, depending on the initial guess $\boldsymbol{U}_0$ and the minimal polynomial of $\boldsymbol{Z}$, the solution might be reached in considerably less than N steps. Of course, here we assume that all arithmetic operations are exact, i.e. no rounding errors occur.

There are in general two reasonable ways to choose the iterate $\boldsymbol{U}_m$:

Definition 5.1.1 (Krylov Subspace Methods) *A Krylov subspace method is an iterative method where, starting from an initial guess $\boldsymbol{U}_0$, the new iterate $\boldsymbol{U}_m$ is chosen such that*

(i) it satisfies $\boldsymbol{U}_m \;\in\; \boldsymbol{U}_0 + \mathcal{K}_m \;,$ *where $\mathcal{K}_m = \mathcal{K}_m(\boldsymbol{Z}, \boldsymbol{R}_0)$ is the Krylov space as in $(5.1.3)$, and*

(ii) one of the following conditions:

- *Projective Method:* $(\boldsymbol{\ell} - \boldsymbol{Z}\boldsymbol{U}_m, \boldsymbol{V}) \;=\; 0 \;, \qquad \forall \boldsymbol{V} \in \mathcal{L}_m \;,$ *with a suitable chosen $m-$dimensional space $\mathcal{L}_m$.*
- *Residual Method:* $\boldsymbol{U}_m \;=\; \arg \min_{\boldsymbol{U} \in \boldsymbol{U}_0 + \mathcal{K}_m} \|\boldsymbol{\ell} - \boldsymbol{Z}\boldsymbol{U}\| \;.$

In the case where we choose $\mathcal{L}_m = \mathcal{K}_m$, the orthogonality condition in the projective Krylov method is a standard Galerkin orthogonality relation. Examples for algorithms

that minimize the residual are the methods of conjugate residuals (CR) and generalized minimized residuals (GMRES). On the other hand, the stabilized biconjugate gradient method (BI-CGSTAB) is a method based on a combination of a local minimization property and a global orthogonality relation. The BI-CGSTAB method requires twice as many matrix-vector products per iteration step as the GMRES method, but is based on a three-term recurrence and thus requires less memory. Comparative studies of different Krylov space methods can be found in [92].

As is immediately clear from $(5.1.1)$, the construction of the iterates $\boldsymbol{U}_m$ will get quite expensive with higher iteration number m considering computational costs and memory requirements. However, for the symmetric problems we consider inside this thesis, the update of the Krylov spaces can be done by a three-term recurrence. The question if this is possible also for non-symmetric coefficient matrices $\boldsymbol{Z}$ was solved essentially to the negative [44]: Short recurrences are only possible if the spectrum of the matrix lies on a straight line in the complex plane.
In practice, the unbounded storage needs e.g. for the GMRES method are a problem. The most common solution is to fix the maximum dimension m of the Krylov space $\mathcal{K}_m$ in advance. Then, if the prescribed accuracy is not obtained after m iterations, the method is restarted with the initial guess being the last iterate of the last cycle.

Recursion formulas for the residual $\boldsymbol{R}_m := \boldsymbol{\ell} - \boldsymbol{Z}\boldsymbol{U}_m$ and the error $\boldsymbol{E}_m = \boldsymbol{U} - \boldsymbol{U}_m$ are easily obtained considering $(5.1.1)$:

$$\boldsymbol{R}_{m+1} = (\boldsymbol{I} - p_m(\boldsymbol{Z})\boldsymbol{Z})\boldsymbol{R}_0 =: q_{m+1}(\boldsymbol{Z})\boldsymbol{R}_0 \,, \tag{5.1.4}$$

$$\boldsymbol{E}_{m+1} = (\boldsymbol{I} - p_m(\boldsymbol{Z})\boldsymbol{Z})\boldsymbol{E}_0 =: q_{m+1}(\boldsymbol{Z})\boldsymbol{E}_0 = \boldsymbol{Z}\boldsymbol{R}_{m+1} \,. \tag{5.1.5}$$

5.1.2 The GMRES Method

The generalized minimal residual (GMRES) method is a Krylov space method for general nonsymmetric matrices. The main concern in these methods is the minimization of the residual. Since typically no special structure of the matrix $\boldsymbol{Z}$ can be exhibited, the GMRES method in most cases needs to make use of long term recurrences. Thus,

computational work and storage requirements grow linearly with the number of iterations. A common solution for this problem is to fix the maximum dimension m of the Krylov space $\mathcal{K}_m$ in advance. Then, if the prescribed accuracy is not obtained after m iterations, the method is restarted with the initial guess being the last iterate of the last cycle. The method presented here is mainly due to [91]; see also [24].

Algorithm 5.1.2 (GMRES Method) *Let $\boldsymbol{U}_0$ be an initial guess, $\epsilon > 0$ a relative tolerance and $\boldsymbol{P}_l$ and $\boldsymbol{P}_r$ left and right preconditioners, respectively, for the linear system*

$$\boldsymbol{Z}\boldsymbol{U} \;=\; \boldsymbol{\ell}\;.$$

Let $\boldsymbol{e}_i$ be the standard basis vector along the x_i-axis. Fix the dimension m of the Krylov space $\mathcal{K}_m$. For the GMRES *method calculate*

(i) *Initialization:*
$$\boldsymbol{R}_0 \;=\; \boldsymbol{\ell} - \boldsymbol{Z}\boldsymbol{U}_0\;, \quad \boldsymbol{s}_0 \;=\; \boldsymbol{P}_l\boldsymbol{R}_0\;, \quad \boldsymbol{v}_1 \;=\; \frac{\boldsymbol{s}_0}{\|\boldsymbol{s}_0\|}\;,$$

(ii) *Loop:*
$$\begin{aligned}
&\textbf{for}\;\; (i = 1, 2, \ldots m)\{\\
&\qquad \textbf{for}\;\; (j = 1, 2, \ldots i)\{\;\; h_{j,i} = (\boldsymbol{P}_l\boldsymbol{Z}\boldsymbol{P}_r\boldsymbol{v}_i, \boldsymbol{v}_j)\;\;\}\;,\\
&\qquad \boldsymbol{w} = \boldsymbol{P}_l\boldsymbol{Z}\boldsymbol{P}_r\boldsymbol{v}_i - \sum_{j=1}^{i} h_{j,i}\boldsymbol{v}_j\;, \qquad h_{i+1,i} = \|\boldsymbol{w}\|\;,\\
&\qquad \boldsymbol{v}_{i+1} = \frac{\boldsymbol{w}}{h_{i+1,i}}\;,\\
&\}
\end{aligned}$$

(iii) *Evaluate:*
$$\begin{aligned}
&\boldsymbol{V}_m = (\boldsymbol{v}_1, \boldsymbol{v}_2, \ldots, \boldsymbol{v}_m)\;, \quad \bar{\boldsymbol{H}}_m = \begin{pmatrix} \boldsymbol{V}_m^T\boldsymbol{Z}\boldsymbol{P}_r\boldsymbol{V}_m \\ h_{m+1,m}\boldsymbol{e}_m^T \end{pmatrix}\;,\\
&\boldsymbol{y} = \operatorname{argmin}_{\boldsymbol{z}\in\mathbb{R}^m}\left\|\|\boldsymbol{s}_0\|\boldsymbol{e}_1 - \bar{\boldsymbol{H}}_m\boldsymbol{z}\right\|\;,\\
&\boldsymbol{U}_m = \boldsymbol{U}_0 + \boldsymbol{P}_r\boldsymbol{V}_m\boldsymbol{y}\;.
\end{aligned}$$

Restart steps $(i)-(iii)$ with $\boldsymbol{U}_0 = \boldsymbol{U}_m$ until convergence. The minimization problem in (iii) is usually solved by a QR-factorization.

It can easily be seen that this method requires one matrix-vector product with each the matrix $\boldsymbol{Z}$ and the preconditioners $\boldsymbol{P}_l$ and $\boldsymbol{P}_r$. Usually, right preconditioning is used since GMRES is a residual minimization procedure, and in this case the residual of the original system is minimized according to $(6.1.2)$.

Convergence results can be derived from the representation $(5.1.4)$ for the residual, which was given as $\boldsymbol{R}_{m+1} = q_{m+1}(\boldsymbol{Z})\boldsymbol{R}_0$, for the polynomial $q_{m+1} \in \mathbb{P}_{m+1}$ satisfying $q_{m+1}(0) = 1$. By reducing $\boldsymbol{Z}$ to its Jordan canonical form by a transformation $\boldsymbol{T}$, i.e. $\boldsymbol{J} = \boldsymbol{T}^{-1}\boldsymbol{Z}\boldsymbol{T}$, we get

$$\|\boldsymbol{R}_m\| \;\leq\; \|q_m(\boldsymbol{Z})\|\,\|\boldsymbol{R}_0\| \;\leq\; \kappa(\boldsymbol{T})\|q_m(\boldsymbol{J})\|\,\|\boldsymbol{R}_0\| \;. \tag{5.1.6}$$

By using residual minimization properties of the GMRES method the bounds can be further refined, e.g. for diagonalizable matrices, i.e. for matrices with diagonal Jordan canonical form $\boldsymbol{J} = \mathrm{diag}\{\lambda_i\}$, a bound was derived in the original work [91] on GMRES methods:

$$\|\boldsymbol{R}_m\|_2 \;\leq\; \kappa(\boldsymbol{T})\|\boldsymbol{R}_0\|_2 \min_{p\in\mathbb{P}_m, p(0)=1} \max_{\lambda\in\sigma(\boldsymbol{Z})} |p(\lambda)| \;.$$

For normal matrices, i.e. $\boldsymbol{Z}^T\boldsymbol{Z} = \boldsymbol{Z}\boldsymbol{Z}^T$, it is well known that the transformation $\boldsymbol{T}$ can be chosen orthogonal, and thus we can forget about the transformation $\boldsymbol{T}$ since $\kappa(\boldsymbol{T}) = 1$, a result that can also be found in [80].

5.2 Iterative Methods for the Saddle Point Problem

In this section, we consider iterative methods for the solution of algebraic saddle point problems resulting from the finite element discretization of the saddle point problem as given in $(4.2.14)$. Here, we restrict ourselves to the real case with the Euclidian inner product and norm and choose alternative inner products where necessary. The approach at once generalizes to the complex situation.

For $\boldsymbol{A} \in \mathbb{R}^{n\times n}$, $\boldsymbol{B} \in \mathbb{R}^{n\times m}$, $\boldsymbol{C} \in \mathbb{R}^{m\times m}$, $\boldsymbol{f} \in \mathbb{R}^n$ and $\boldsymbol{g} \in \mathbb{R}^m$, find $(\boldsymbol{u}, \Phi) \in \mathbb{R}^{n+m}$ such that

$$\begin{pmatrix} \boldsymbol{A} & \boldsymbol{B} \\ \boldsymbol{B}^T & -\boldsymbol{C} \end{pmatrix} \begin{pmatrix} \mathbf{u} \\ \boldsymbol{\Phi} \end{pmatrix} \;=\; \begin{pmatrix} \mathbf{f} \\ \mathbf{g} \end{pmatrix} \;, \qquad \text{or} \qquad \boldsymbol{Z}\boldsymbol{U} \;=\; \boldsymbol{\ell}\;, \tag{5.2.1}$$

where $\boldsymbol{A}$ and $\boldsymbol{C}$ are symmetric and positive definite matrices, thus yielding symmetric and positive definite inverse matrices $\boldsymbol{A}^{-1}$ and $\boldsymbol{C}^{-1}$, respectively. Altogether, the

matrix $\boldsymbol{Z}$ is symmetric and indefinite and the methods developed in Section 5.1 can be applied.

The case where both of the matrices $\boldsymbol{A}$ and $\boldsymbol{C}$ are symmetric positive definite is referred to as the quasi-definite case. Properties of quasi definite matrices were studied in [99, 51, 50], among them the existence of a stable Cholesky factorization. However, direct methods seem not to be well suited for the systems of equations occurring here due to their huge computational effort in high-dimensional systems.
Saddle point problems in the context of finite element methods occur in a variety of applications, both with $\boldsymbol{C} = \boldsymbol{0}$ and $\boldsymbol{C} \neq \boldsymbol{0}$. Here, references can be taken from the beginning of Section 4.2. More general saddle point problems have been considered allowing for nonsymmetric coefficient matrices $\boldsymbol{K}$ in $(5.2.1)$ stemming either from a non-symmetric matrix $\boldsymbol{A}$ or from non-corresponding off-diagonal blocks $\boldsymbol{B}_1 \neq \boldsymbol{B}_2^T$, cf. [15, 26, 32, 82].

5.2.1 Properties of Matrices in Saddle Point Form

As in the continuous setting, we define the Schur complement matrix $\boldsymbol{S}$ by

$$\boldsymbol{S} \;:=\; \boldsymbol{A} + \boldsymbol{B}\boldsymbol{C}^{-1}\boldsymbol{B}^T \;, \tag{5.2.2}$$

and consider sometimes instead of $(5.2.1)$ the equivalent Schur complement system

$$\boldsymbol{S}\boldsymbol{u} \;=\; \boldsymbol{F} \;:=\; \boldsymbol{f} + \boldsymbol{B}\boldsymbol{C}^{-1}\boldsymbol{g} \;, \qquad\qquad \boldsymbol{C}\boldsymbol{\Phi} \;=\; \boldsymbol{B}^T\boldsymbol{u} - \boldsymbol{g} \;, \tag{5.2.3}$$

where $\boldsymbol{S}$ is obviously symmetric and positive definite by the symmetry and positive definiteness of $\boldsymbol{A}$ and $\boldsymbol{C}^{-1}$,

$$\boldsymbol{v}^T\boldsymbol{S}\boldsymbol{v} \;=\; \boldsymbol{v}^T\boldsymbol{A}\boldsymbol{v} + (\boldsymbol{B}^T\boldsymbol{v})^T\boldsymbol{C}^{-1}(\boldsymbol{B}^T\boldsymbol{v}) \;>\; 0 \;.$$

Note, the Schur complement operator surely could be defined the other way around as $\boldsymbol{C} + \boldsymbol{B}^T\boldsymbol{A}^{-1}\boldsymbol{B}$. Then, with the use of iterative schemes on the Schur complement system $(5.2.3)$ we would have to solve a linear system with coefficient matrix $\boldsymbol{A}$ in each iteration step. In our case, in terms of computational costs, the matrix $\boldsymbol{C}$ can be inverted very easily in comparison to $\boldsymbol{A}$. Thus, the Schur complement is chosen

as above.

The coefficient matrix $\boldsymbol{Z}$ in $(5.2.1)$ admits the following congruent transformation,

$$\begin{pmatrix} \boldsymbol{A} & \boldsymbol{B} \\ \boldsymbol{B}^T & -\boldsymbol{C} \end{pmatrix} = \begin{pmatrix} \boldsymbol{I}_n & -\boldsymbol{B}\boldsymbol{C}^{-1} \\ \boldsymbol{0} & \boldsymbol{I}_m \end{pmatrix} \begin{pmatrix} \boldsymbol{S} & \boldsymbol{0} \\ \boldsymbol{0} & -\boldsymbol{C} \end{pmatrix} \begin{pmatrix} \boldsymbol{I}_n & \boldsymbol{0} \\ -\boldsymbol{C}^{-1}\boldsymbol{B}^T & \boldsymbol{I}_m \end{pmatrix} , \qquad (5.2.4)$$

thus fixing the number of positive and negative eigenvalues to n and m, respectively, by Sylvester's theorem. Also useful are the equivalent factorizations

$$\boldsymbol{Z} = \begin{pmatrix} \boldsymbol{I}_n & -\boldsymbol{B}\boldsymbol{C}^{-1} \\ \boldsymbol{0} & \boldsymbol{I}_m \end{pmatrix} \begin{pmatrix} \boldsymbol{S} & \boldsymbol{0} \\ \boldsymbol{B}^T & -\boldsymbol{C} \end{pmatrix} = \begin{pmatrix} \boldsymbol{S} & \boldsymbol{B} \\ \boldsymbol{0} & -\boldsymbol{C} \end{pmatrix} \begin{pmatrix} \boldsymbol{I}_n & \boldsymbol{0} \\ -\boldsymbol{C}^{-1}\boldsymbol{B}^T & \boldsymbol{I}_m \end{pmatrix} . \qquad (5.2.5)$$

This shows that $\boldsymbol{Z}$ is invertible since the matrices $\boldsymbol{C}$ and $\boldsymbol{S}$ are positive definite and thus invertible. The inverse operator then is given by

$$\boldsymbol{Z}^{-1} = \begin{pmatrix} \boldsymbol{S}^{-1} & \boldsymbol{S}^{-1}\boldsymbol{B}\boldsymbol{C}^{-1} \\ \boldsymbol{C}^{-1}\boldsymbol{B}^T\boldsymbol{S}^{-1} & \boldsymbol{C}^{-1}\boldsymbol{B}^T\boldsymbol{S}^{-1}\boldsymbol{B}\boldsymbol{C}^{-1} - \boldsymbol{C}^{-1} \end{pmatrix} . \qquad (5.2.6)$$

However, the explicit representation of $\boldsymbol{Z}^{-1}$ is of limited practical use. In the framework of linear systems arising from a finite element modeling this is not sufficient to ensure meaningful computed solutions. In order to ensure well-posedness for the discrete problem it is essential that the saddle point matrix remains uniformly invertible as the mesh size h goes to zero, see also Section 4.2.4.

5.2.2 The Uzawa Algorithm

We consider a fixed parameter first-order Richardson iteration applied to the Schur complement system $(5.2.3)$, i.e.

$$\boldsymbol{u}^{k+1} = \boldsymbol{u}^k + \alpha(\boldsymbol{F} - \boldsymbol{S}\boldsymbol{u}^k) = \boldsymbol{u}^k + \alpha(\boldsymbol{f} - \boldsymbol{A}\boldsymbol{u}^k - \boldsymbol{B}\boldsymbol{\Phi}^k) , \qquad (5.2.7)$$

which is the basis for the Uzawa algorithm first introduced in [6]:

Algorithm 5.2.1 (Uzawa Algorithm) *Given $\boldsymbol{u}^0 \in \mathbb{R}^n$, calculate $\boldsymbol{u}^k$ and $\boldsymbol{\Phi}^k$ from*

$$\begin{aligned} \boldsymbol{C}\boldsymbol{\Phi}^{k+1} &= \boldsymbol{B}^T\boldsymbol{u}^k - \boldsymbol{g} , \\ \mathbf{u}^{k+1} &= \boldsymbol{u}^k + \alpha(\boldsymbol{f} - \boldsymbol{A}\boldsymbol{u}^k - \boldsymbol{B}\Phi^{k+1}) . \end{aligned}$$

Introducing the residual $\boldsymbol{r}^{k+1} := \boldsymbol{A}\boldsymbol{u}^k + \boldsymbol{B}\Phi^{k+1} - \boldsymbol{f}$ yields

$$\boldsymbol{u}^k - \boldsymbol{u}^{k-1} \;=\; -\alpha \boldsymbol{r}^k \;=\; \alpha \boldsymbol{S}(\boldsymbol{u}^{k-1} - \boldsymbol{u}) \;, \tag{5.2.8}$$

and hence,

$$\boldsymbol{u} - \boldsymbol{u}^k = (\boldsymbol{I} - \alpha \boldsymbol{S})^k (\boldsymbol{u} - \boldsymbol{u}^0) \;. \tag{5.2.9}$$

Then, the method converges e.g. for $\alpha < \frac{2}{\|\boldsymbol{S}\|}$. For a better estimate, we interpret the Uzawa algorithm from $(5.2.8)$ as gradient method applied to the quadratic functional $q(\boldsymbol{u}) = \frac{1}{2}\boldsymbol{u}^T \boldsymbol{S}\boldsymbol{u} - \boldsymbol{F}^T\boldsymbol{u}$, and the optimal step size is given by $\alpha_k \;=\; \frac{\langle \boldsymbol{r}^k, \boldsymbol{r}^k \rangle}{\langle \boldsymbol{r}^k, \boldsymbol{S}\boldsymbol{r}^k \rangle}$. Now, as in the conjugate gradient method, the search directions can be chosen to be orthogonal in the inner product induced by $\boldsymbol{S}$, cf. [18], yielding a more efficient variant of the Uzawa algorithm.

Certainly, in the case we are dealing with here, the dimension of the matrix $\boldsymbol{C}$ will also be large and thus we will not compute $\boldsymbol{C}^{-1}$ exactly. However, because of the symmetry and positive definiteness of $\boldsymbol{C}$ iterative methods like the conjugate gradient algorithm can be applied. This results in an inexact Uzawa method with inner and outer iteration and we will be confronted with the question of the accuracy we have to obtain in the inner iteration to conserve the convergence of the overall method. Inexact Uzawa methods were studied e.g. in [11, 40, 19].

Algorithm 5.2.2 (Inexact Uzawa Algorithm) *Given $\boldsymbol{u}^0 \in \mathbb{R}^n$, calculate $\boldsymbol{u}^k$ and $\boldsymbol{\Phi}^k$ from*

$$\begin{aligned} \boldsymbol{C}\boldsymbol{\Phi}^{k+1} \;&=\; \boldsymbol{B}^T\boldsymbol{u}^k - \boldsymbol{g} \;+\; \boldsymbol{r}_\Phi^k, \\ \mathbf{u}^{k+1} \;&=\; \boldsymbol{u}^k \;+\; \alpha(\boldsymbol{f} - \boldsymbol{A}\boldsymbol{u}^k - \boldsymbol{B}\Phi^{k+1}) \;. \end{aligned}$$

The question of how small $\|\boldsymbol{r}_\Phi^k\|_2$ should get was answered in [40] essentially by

$$\|\boldsymbol{r}_\Phi^k\|_2 \;\leq\; \tau \|\boldsymbol{r}^k\|_2 \;,$$

where $\tau > 0$ is a parameter satisfying certain conditions. Numerical computations show that even large values for τ, e.g. $\tau \approx 0.1$, work very well.

5.2.3 Non-Symmetric Saddle Point Formulation

For certain distributions of the eigenvalues with positive and negative real parts, the Krylov space method tends to converge poorly. In this section, we analyze a variant of the methods considered in the previous section. Instead of dealing with the indefinite system

$$\begin{pmatrix} \boldsymbol{A} & \boldsymbol{B} \\ \boldsymbol{B}^T & -\boldsymbol{C} \end{pmatrix} \begin{pmatrix} \mathbf{u} \\ \boldsymbol{\Phi} \end{pmatrix} \;=\; \begin{pmatrix} \mathbf{f} \\ \mathbf{g} \end{pmatrix} \;, \qquad \text{or} \qquad \boldsymbol{Z}\boldsymbol{U} \;=\; \boldsymbol{\ell} \;,$$

we multiply the second equation with -1 and obtain the equivalent form

$$\begin{pmatrix} \boldsymbol{A} & \boldsymbol{B} \\ -\boldsymbol{B}^T & \boldsymbol{C} \end{pmatrix} \begin{pmatrix} \boldsymbol{u} \\ \boldsymbol{\Phi} \end{pmatrix} \;=\; \begin{pmatrix} \boldsymbol{f} \\ -\boldsymbol{g} \end{pmatrix} \;, \qquad \text{or} \qquad \hat{\boldsymbol{Z}}\boldsymbol{U} \;=\; \hat{\boldsymbol{\ell}} \;, \tag{5.2.10}$$

where again $\boldsymbol{A} \in \mathbb{R}^{n\times n}$ and $\boldsymbol{C} \in \mathbb{R}^{m\times m}$ are assumed to be symmetric and positive definite matrices as in $(5.2.1)$. Then, the matrix $\hat{\boldsymbol{Z}}$ is a positive definite matrix according to

$$\boldsymbol{x}^T \hat{\boldsymbol{Z}} \boldsymbol{x} \;=\; \boldsymbol{x}_1^T \boldsymbol{A} \boldsymbol{x}_1 \,+\, \boldsymbol{x}_2^T \boldsymbol{C} \boldsymbol{x}_2 \;>\; 0 \quad , \qquad \text{for } \boldsymbol{x} \neq 0 \;.$$

More precisely, if λ is an eigenvalue of $\hat{\boldsymbol{Z}}$, then

$$\min\{\lambda_{\min}(\boldsymbol{A}), \lambda_{\min}(\boldsymbol{C})\} \;\leq\; \lambda \;\leq\; \lambda_{\max}(\boldsymbol{A}) + \lambda_{\max}(\boldsymbol{C}) \;. \tag{5.2.11}$$

6 Preconditioners For Saddle Point Problems

The innermost computational kernel of many large-scale scientific applications and industrial numerical simulations is often a large sparse matrix problem,

$$\boldsymbol{Z}\boldsymbol{U} \;=\; \boldsymbol{\ell}\,, \tag{6.0.1}$$

which typically consumes a significant portion of the overall computational time required by the simulation. As already pointed out, direct methods are not well suited for the solution of this type of equation. Iterative techniques are the only viable alternative (see also Chapter 5).

Unfortunately, iterative methods lack the robustness of direct methods. They often fail when the matrix is very ill-conditioned. The performance of these methods is eventually related to the condition number of the coefficient matrix of the system. Thus, the aim should be to construct either a left or right preconditioner such that the transformed system has a considerably better condition number. A survey on preconditioning techniques can be found, e.g., in [14]. For multilevel preconditioners, used in this work, we refer to [96].

6.1 Principles of Preconditioning

Preconditioning functions act as a transformation of the linear system either in the definition or the image space. The aim of using preconditioners is to improve the performance of the iterative method. Suppose $\boldsymbol{P}_l$ and $\boldsymbol{P}_r$ are given nonsingular

matrices. Then, the preconditioned iterative method is the original algorithm applied to the transformed system

$$\boldsymbol{P}_l\boldsymbol{Z}\boldsymbol{P}_r\tilde{\boldsymbol{U}} \;=\; \boldsymbol{P}_l\boldsymbol{\ell}\;, \qquad \boldsymbol{P}_r\tilde{\boldsymbol{U}} \;=\; \boldsymbol{U}\;,$$

or

$$\tilde{\boldsymbol{Z}}\tilde{\boldsymbol{U}} \;=\; \tilde{\boldsymbol{\ell}}\;. \tag{6.1.1}$$

The Krylov space for this problem is $\mathcal{K}_m(\tilde{\boldsymbol{Z}}, \tilde{\boldsymbol{R}}_0) = \mathcal{K}_m(\boldsymbol{P}_l\boldsymbol{Z}\boldsymbol{P}_r, \boldsymbol{P}_l\boldsymbol{R}_0)$. The common case is left preconditioning, i.e. $\boldsymbol{P}_r = \boldsymbol{I}$, since the right preconditioner often may be incorporated into the left preconditioner and the bilinear form. However, for residual methods the choice of left or right preconditioning can make a difference: In the case of right preconditioning we minimize the residual in the m-th step

$$\|\boldsymbol{\ell} - (\boldsymbol{Z}\boldsymbol{P}_r)\tilde{\boldsymbol{U}}\| \;=\; \|\boldsymbol{\ell} - \boldsymbol{Z}\boldsymbol{U}_m\| \;=\; \|\boldsymbol{R}_m\|\;, \tag{6.1.2}$$

i.e. we minimize the residual of the non preconditioned linear system. On the other hand, for left preconditioning, the residual of the preconditioned system is a good approximation for the error $\boldsymbol{E}_m$ of the non preconditioned system only if $\boldsymbol{P}_l\boldsymbol{Z} \approx \boldsymbol{I}$:

$$\|\boldsymbol{P}_l\boldsymbol{\ell} - (\boldsymbol{P}_l\boldsymbol{Z})\boldsymbol{U}_m\| \;=\; \|\boldsymbol{P}_l\boldsymbol{Z}(\boldsymbol{U} - \boldsymbol{U}_m)\| \;\approx\; \|\boldsymbol{U} - \boldsymbol{U}_m\|\;.$$

In principle, a good preconditioner should meet the following requirements: First, the preconditioned system should be easy to solve, meaning that the preconditioned iterative method should converge rapidly. Second, constructing and applying the preconditioner should be cheap, i.e. each step of the iteration is not too expensive. In practice, we have to balance between these requirements. Altogether, with a good preconditioner the computing time for the preconditioned iteration should be significantly less than that for the original one.

For the construction of preconditioners a wide variety of approaches is available. We review the abstract framework of general additive Schwarz methods that provides a powerful tool for the construction of positive definite preconditioners, cf. [37, 87, 96].

6.2 Additive Schwarz Methods

Again, the starting point will be the variational formulation of our problem. Here, we search for solutions $U \in \mathcal{X}_h$ satisfying

$$z(U,V) \;=\; \ell(V)\;, \qquad \forall V \in \mathcal{X}_h\;, \tag{6.2.1}$$

where we assume $z : \mathcal{X}_h \times \mathcal{X}_h \to \mathbb{R}$ to be a symmetric and positive definite bilinear form and $\mathcal{X}_h$ is a Hilbert space. Then, equation $(6.2.1)$ admits a unique solution $U \in \mathcal{X}_h$.

The ingredients of an additive Schwarz method (ASM) are conceivably simple: First, we need a decomposition of $\mathcal{X}_h$ into suitable subspaces

$$\mathcal{X}_h \;=\; \mathcal{X}^{(0)} + \mathcal{X}^{(1)} + \ldots + \mathcal{X}^{(L)}, \tag{6.2.2}$$

where there is no need for choosing an orthogonal sum. Second, we construct projection-like operators $T^{(l)}, 0 \le l \le L$, mapping $\mathcal{X}_h$ onto the subspaces $\mathcal{X}^{(l)}$. In the context of abstract Schwarz methods these operators are defined by additional symmetric and positive definite bilinear forms $b^{(l)}(\cdot,\cdot) : \mathcal{X}^{(l)} \times \mathcal{X}^{(l)} \longrightarrow \mathbb{R}$, and

$$b^{(l)}(T^{(l)}V, W) \;=\; z(V,W)\;, \qquad \forall W \in \mathcal{X}^{(l)}\;. \tag{6.2.3}$$

$T^{(l)}$ is well posed since the subspaces $\mathcal{X}^{(l)}$ are finite dimensional Hilbert spaces. If we choose $b^{(l)}(\cdot,\cdot) = z(\cdot,\cdot)$, the operators $T^{(l)}$ simply are the orthogonal projection operators onto the subspaces $\mathcal{X}^{(l)}$ in the $z(\cdot,\cdot)$-inner product.

We set $T := \sum_{l=0}^{L} T^{(l)}$, and note, given the solution U to $(6.2.1)$, that

$$b^{(l)}(T^{(l)}U, V) \;=\; z(U,V) \;=\; (\ell, V)\;, \qquad \forall V \in \mathcal{X}^{(l)}\;.$$

This implies that U is also solution to

$$TU \;=\; G\;, \tag{6.2.4}$$

where $G := \sum_{l=0}^{L} G^{(l)} := \sum_{l=0}^{L} T^{(l)}u$. We remark that $G^{(l)}$ can be computed without knowledge of $T^{(l)}$ by using the identity

$$b^{(l)}(G^{(l)}, V) \;=\; (\ell, V)\;, \qquad \forall V \in \mathcal{X}^{(l)}.$$

If T is invertible, problem $(6.2.1)$ and $(6.2.4)$ are equivalent. Additive Schwarz methods thus provide a new operator equation which usually is much better conditioned than the original problem. We will see that these methods provide a positive definite operator equation that can be solved by iterations like the conjugate gradient method. Then, the number of iterations required to decrease an appropriate norm of the error by a fixed factor depends on the condition number $\kappa(T)$.

We cite [96, 114] an abstract result on the condition number of T. The framework given by this result is sufficiently general to analyze several domain decomposition and multilevel methods.

Theorem 6.2.1 *Let the following assumptions hold:*

a) There exists a constant C_0^2 such that every $V \in \mathcal{X}_h$ can be decomposed into a sum $V = \sum_{l=0}^{L} V^{(l)}$ with $V^{(l)} \in \mathcal{X}^{(l)}$, which satisfies

$$\sum_{l=1}^{L} b^{(l)}(V^{(l)}, V^{(l)}) \;\leq\; C_0^2 z(V,V) \;.$$

b) There exists a constant $\omega > 0$ such that

$$z(V,V) \;\leq\; \omega\, b^{(l)}(V,V) \;, \qquad \forall V \in \mathcal{X}^{(l)} \;,\; l = 0, \ldots L \;.$$

c) There exist constants $\epsilon_{ij},\ i,j = 1, \ldots L$, such that

$$z(V,W) \;\leq\; \epsilon_{ij}\, z(V,V)^{\frac{1}{2}}\, z(W,W)^{\frac{1}{2}} \;, \qquad \forall V \in \mathcal{X}^{(i)},\; W \in \mathcal{X}^{(j)} \;.$$

The first hypothesis a) is strong enough to guarantee that the operator T is invertible. If assumptions a)-c) hold, we get an estimate for the condition number of T:

$$C_0^2 z(V,V) \leq z(TV,V) \leq (\rho(\epsilon) + 1)\, \omega z(V,V) \qquad \forall V \in \mathcal{X}_h. \tag{6.2.5}$$

Here, $\rho(\epsilon)$ is the spectral radius of the matrix $\epsilon = (\epsilon_{ij})_{i=1,j=1}^{L\ \ L}$.

We remark that $\epsilon_{ij} \leq 1$ and thus $\rho(\epsilon) \leq L$. However, often an upper bound for $\rho(\epsilon)$ can be given independently of the number of subspaces L. Subspace splittings satisfying a)-c) are often called stable, cf. [87].

6.2.1 Multilevel Additive Schwarz Methods

In this section, we give an example for the construction of an additive Schwarz method as introduced in the previous section. For simplicity of presentation, we restrict ourselves to the $2D$ case. Thus, let $\Omega \subset \mathbb{R}^2$ be a polygonal domain on which an initial triangulation $\mathcal{T}^{(0)}$ with mesh size $H := h^{(0)}$ is posed. We get a finer triangulation $\mathcal{T}^{(1)}$ by subdividing each triangle of $\mathcal{T}^{(0)}$ into four equal triangles. Proceeding this way, we get a triangulation $\mathcal{T}^{(l+1)}$ recursively by subdividing each triangle of $\mathcal{T}^{(l)}$ into four equal triangles (see Figure 6.1). Then, the mesh size at level l is given by

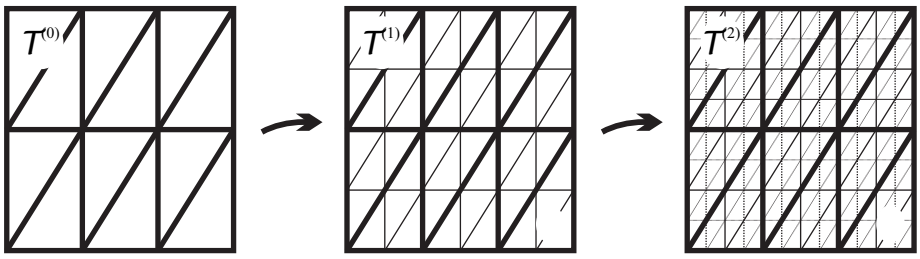

Figure 6.1: Nested triangulations on Ω

$h^{(l)} = 2^{-l}H$. By fixing a maximum level L we get a sequence of nested triangulations

$$\mathcal{T}^{(0)} \subset \mathcal{T}^{(1)} \subset \cdots \subset \mathcal{T}^{(L)}.$$

Of course, other refinement methods are conceivable. E.g., the finite element package `ALBERTA` used for the numerical computations inside this thesis incorporates refinement techniques relying on bisection.

One can think of the different meshes as triangulations of overlapping subdomains $\Omega = \bigcup_{l=1}^{L} \Omega^{(l)}$. Thus, such methods are often referred to as overlapping domain decomposition methods. For general domain decomposition methods we refer for instance to [37, 96, 89]. Non-overlapping domain decomposition methods can also be considered within the additive Schwarz framework, an approach that is not adapted here. See e.g. [28, 29], and my recent contribution [36].

Let $\mathcal{N}^{(l)} = \{\varphi_j^{(l)}\}_{j=1}^{N_l}$ be a basis for the finite element spaces $\mathcal{X}^{(l)}$ associated to the triangulations $\mathcal{T}^{(l)}$. These spaces are nested, i.e.

$$\mathcal{X}^{(0)} \subset \mathcal{X}^{(1)} \subset \cdots \subset \mathcal{X}^{(L)}.$$

Now, the idea of multilevel methods is to get a better solution to problem $(6.2.1)$ in the space $\mathcal{X}^{(L)}$ of the finest discretization level by making use of some easy-to-gain properties on the coarser triangulations. Here, the well-known BPX method shall serve as an example, see e.g. [20, 37, 96].

The BPX Method

Let $\boldsymbol{V}^{(l)} = (V_i)_{i=1}^{N_l} \in \mathbb{R}^{N_l}$ denote the vector representation of a finite element function $V = \sum_{i=1}^{N_l} V_i \in \mathcal{X}^{(l)}$. However, by $\mathcal{X}^{(l)} \subset \mathcal{X}^{(l+k)}$, the function V is also in $\mathcal{X}^{(l+k)}$ and the corresponding vector $\boldsymbol{V}^{(l+k)} \in \mathbb{R}^{N_{l+k}}$ can easily be obtained by a matrix transformation

$$\boldsymbol{V}^{(l+k)} \;=\; \boldsymbol{R}_l^{l+k} \boldsymbol{V}^{(l)} \;,$$

where $\boldsymbol{R}_l^{l+k} \in \mathbb{R}^{N_{l+k} \times N_l}$. Moreover, for $z(\cdot,\cdot) : \mathcal{X}_h \times \mathcal{X}_h \longrightarrow \mathbb{R}$ we associate matrices $\boldsymbol{Z}^{(l)} \in \mathbb{R}^{N_l \times N_l}$ such that

$$z(V,W) \;=\; \left(\boldsymbol{Z}^{(l)} \boldsymbol{W}^{(l)}\right)^T \boldsymbol{V}^{(l)} \;, \qquad \forall V, W \in \mathcal{X}^{(l)}.$$

We set $\boldsymbol{Z} := \boldsymbol{Z}^{(L)}$, $\boldsymbol{V} := \boldsymbol{V}^{(L)}$ and $\boldsymbol{R}^{(l)} := \boldsymbol{R}_l^L$.

In addition to the decomposition $\mathcal{X}_h = \sum_{l=0}^{L} \mathcal{X}^{(l)}$, we introduce the bilinear forms $b^{(l)}(\cdot,\cdot) : \mathcal{X}^{(l)} \times \mathcal{X}^{(l)} \longrightarrow \mathbb{R}$ by

$$b^{(0)}(V,W) \;:=\; z(V,W) \;, \qquad V, W \in \mathcal{X}_h^{(0)} \;,$$

and for $l = 1, \ldots L$ by

$$b^{(l)}(V,W) \;:=\; (\boldsymbol{W}^{(l)})^T \boldsymbol{V}^{(l)} \;, \qquad V, W \in \mathcal{X}_h^{(l)}.$$

The operator $T^{(l)} : \mathcal{X}_h \longrightarrow \mathcal{X}^{(l)}$ is then given through

$$b^{(l)}(T^{(l)}V, W) = z(V,W) \;, \qquad \forall W \in \mathcal{X}_h^{(l)} \;.$$

We obtain a matrix representation $\boldsymbol{T}^{(l)} \in \mathbb{R}^{N_l \times N}$ of $T^{(l)}$ by noticing

$$\left(\boldsymbol{R}^{(l)} \boldsymbol{W}^{(l)}\right)^T \boldsymbol{T}^{(l)} \boldsymbol{V} \;=\; b^{(l)}(T^{(l)}V, W) \;=\; z(V,W) \;=\; \left(\boldsymbol{R}^{(l)} \boldsymbol{W}^{(l)}\right)^T \boldsymbol{Z} \boldsymbol{V},$$

for all functions $V \in \mathcal{X}_h, W \in \mathcal{X}_h^{(l)}$, and levels $l = 1, \ldots L$; similar for functions at level 0. The global matrix representation $\mathbf{T} := \sum_{l=0}^{L} \boldsymbol{T}^{(l)} \in \mathbb{R}^{N \times N}$ is hence given by

$$\mathbf{T} \;=\; \boldsymbol{R}^{(0)} \left(\boldsymbol{Z}^{(0)} \right)^{-1} \left(\boldsymbol{R}^{(0)} \right)^{T} \boldsymbol{Z} \;+\; \sum_{l=1}^{L} \boldsymbol{R}^{(l)} \left(\boldsymbol{R}^{(l)} \right)^{T} \boldsymbol{Z} \;. \tag{6.2.6}$$

Thus, solving the linear system of equations $\boldsymbol{TU} = \boldsymbol{G}$, can be interpreted as applying a preconditioner $\boldsymbol{P}$ to the original linear system $\boldsymbol{ZU} = \boldsymbol{\ell}$, where

$$\boldsymbol{P} \;:=\; \boldsymbol{R}^{(0)} \left(\boldsymbol{Z}^{(0)} \right)^{-1} \left(\boldsymbol{R}^{(0)} \right)^{T} + \sum_{l=1}^{L} \boldsymbol{R}^{(l)} \left(\boldsymbol{R}^{(l)} \right)^{T} \;. \tag{6.2.7}$$

It can be shown [96] that the condition number of the preconditioned system can be bounded independently of the number of refinement levels:

$$c_0 \boldsymbol{Z} \;\leq\; \boldsymbol{PZ} \;\leq\; c_1 \boldsymbol{Z} \;, \tag{6.2.8}$$

where c_0 and c_1 are constants independent of the level number L. This means that for instance with the conjugate gradient method the number of iterations required to achieve a fixed tolerance is bounded independently of the number of unknowns. Moreover, the effort in applying the preconditioner $\boldsymbol{P}$ to a vector $\boldsymbol{V} \in \mathbb{R}^N$ is of order $\mathcal{O}(N)$ if a recursive formulation of interpolation and restriction as in the original work [20] is used.

The Hierarchical Basis Method

Various other multilevel ASMs have been established. Here, we only mention the hierarchical basis method [110, 111, 96] for comparison. It is based on a different splitting of the space $\mathcal{X}_h$, namely

$$\tilde{\mathcal{X}}^{(0)} \;:=\; \mathcal{X}^{(0)} \;, \qquad \tilde{\mathcal{X}}^{(l)} \;:=\; \mathcal{X}^{(l)} \setminus \mathcal{X}^{(l-1)} \;, \quad 1 \leq l \leq L \;,$$

and, as a consequence, different bilinear forms

$$\tilde{b}^{(0)} \;:= b^{(0)} \;, \qquad \tilde{b}^{(l)} \;:= b^{(l)} - b^{(l-1)} \;, \quad 1 \leq l \leq L \;.$$

This method yields a preconditioner $\tilde{\boldsymbol{P}}$ which satisfies [96]

$$c_0 \boldsymbol{Z} \;\leq\; \tilde{\boldsymbol{P}} \boldsymbol{Z} \;\leq\; c_1 (1 + L^2) \boldsymbol{Z} \;, \tag{6.2.9}$$

i.e. the condition number grows like $1 + L^2$ with increasing level numbers L. The effort in applying the preconditioner is of the same order as for the BPX method. But the number of iterations required e.g. within the conjugate gradient method to achieve a fixed tolerance still grows with the number of unknowns. However, the memory requirements are considerably less than for the BPX method.

6.3 Preconditioners for Systems where Babuška's Theorem is Applicable

In this section, we want to establish the construction principles for an efficient preconditioner for systems of equations

$$\boldsymbol{Z}\boldsymbol{U} \;=\; \boldsymbol{\ell} \;,$$

where $\boldsymbol{U}, \boldsymbol{\ell} \in \mathbb{R}^N$ and $\boldsymbol{Z} \in \mathbb{R}^{N \times N}$. We assume that the system stems from a finite element discretization of a variational equation on a Hilbert space $\mathcal{X}_h \subset \mathcal{X}$ as described in Section $(4.1.3)$,

$$z(U, V) \;=\; \ell(V) \;, \qquad \forall V \in \mathcal{X}_h \;,$$

where the bilinear form $z : \mathcal{X}_h \times \mathcal{X}_h \to \mathbb{R}$ satisfies the conditions of Babuška's Theorem 4.1.1, i.e., there exist constants $\mathfrak{z}$ and $\|z\|$ such that

$$\begin{aligned} z(U, V) \;&\leq\; \|z\| \|U\|_{\mathcal{X}} \|V\|_{\mathcal{X}} \;, \qquad \forall U, V \in \mathcal{X}_h \\ \mathfrak{z} \;&\leq\; \inf_{0 \neq U \in \mathcal{X}_h} \sup_{0 \neq V \in \mathcal{X}_h} \frac{|z(U, V)|}{\|U\|_{\mathcal{X}} \|V\|_{\mathcal{X}}} \;. \end{aligned}$$

Moreover, for every $0 \neq V \in \mathcal{X}_h$ there is a $U \in \mathcal{X}_h$ such that $z(U, V) \neq 0$. The second condition above should hold with a constant independent of h, cf. Chapter 4. By the Galerkin approximation, every function $V \in \mathcal{X}_h$ can be uniquely represented as a vector $\boldsymbol{V} \in \mathbb{R}^N$ and vice versa.

Now, we consider a preconditioner $\boldsymbol{P} \in \mathbb{R}^{N\times N}$. What is of interest is the condition number of the preconditioned system given by

$$\kappa(\boldsymbol{PZ}) \;:=\; \rho(\boldsymbol{PZ})\,\rho((\boldsymbol{PZ})^{-1}) \;.$$

We will require $\boldsymbol{P}$ to be symmetric and positive definite in a special sense, i.e. there are constants $\mathfrak{p}$ and $\|p\|$ satisfying

$$\frac{1}{\|p\|} \;\leq\; \frac{\boldsymbol{V}^T\boldsymbol{P}^{-1}\boldsymbol{V}}{\|V\|_{\mathcal{X}}^2} \;\leq\; \frac{1}{\mathfrak{p}} \;, \qquad \forall \boldsymbol{V} \in \mathbb{R}^N \;. \tag{6.3.1}$$

Then, $\boldsymbol{P}$ is also symmetric and positive definite and there exists a symmetric and positive definite matrix $\boldsymbol{P}^{\frac{1}{2}}$ such that $\boldsymbol{P} = \boldsymbol{P}^{\frac{1}{2}}\boldsymbol{P}^{\frac{1}{2}}$. Note, the eigenvalue problem $\boldsymbol{PZV} = \lambda \boldsymbol{V}$ can be reformulated as

$$\boldsymbol{P}^{\frac{1}{2}}\boldsymbol{Z}\boldsymbol{P}^{\frac{1}{2}}\tilde{\boldsymbol{V}} \;=\; \lambda\tilde{\boldsymbol{V}} \;, \qquad\qquad \tilde{\boldsymbol{V}} \;=\; \boldsymbol{P}^{-\frac{1}{2}}\boldsymbol{V} \;. \tag{6.3.2}$$

Thus, the spectrum of $\boldsymbol{PZ}$ is identical to the spectrum of $\boldsymbol{P}^{\frac{1}{2}}\boldsymbol{Z}\boldsymbol{P}^{\frac{1}{2}}$, and the condition number estimate for $\boldsymbol{PZ}$ can be obtained from estimating the condition number of $\boldsymbol{P}^{\frac{1}{2}}\boldsymbol{Z}\boldsymbol{P}^{\frac{1}{2}}$.

Lemma 6.3.1 *The condition number of $\boldsymbol{PZ}$ is bounded independently of h by*

$$\mathfrak{p}_{\mathfrak{Z}} \;\leq\; \frac{\boldsymbol{V}^T\boldsymbol{P}^{\frac{1}{2}}\boldsymbol{Z}\boldsymbol{P}^{\frac{1}{2}}\boldsymbol{V}}{\|\boldsymbol{V}\|_2^2} \;\leq\; \|z\|\|p\| \;, \qquad \forall \boldsymbol{V} \in \mathbb{R}^N \;.$$

Proof. From the inf-sup condition and the positive definiteness of $\boldsymbol{P}^{-1}$ we obtain

$$\begin{aligned}
\inf_{\boldsymbol{W}\neq 0}\sup_{\boldsymbol{V}\neq 0}\frac{\boldsymbol{V}^T\boldsymbol{P}^{\frac{1}{2}}\boldsymbol{Z}\boldsymbol{P}^{\frac{1}{2}}\boldsymbol{W}}{\|\boldsymbol{V}\|_2\|\boldsymbol{W}\|_2} \;&=\; \inf_{\tilde{\boldsymbol{W}}\neq 0}\sup_{\tilde{\boldsymbol{V}}\neq 0}\frac{\tilde{\boldsymbol{V}}^T\boldsymbol{Z}\tilde{\boldsymbol{W}}}{(\tilde{\boldsymbol{V}}^T\boldsymbol{P}^{-1}\tilde{\boldsymbol{V}})^{\frac{1}{2}}(\tilde{\boldsymbol{W}}^T\boldsymbol{P}^{-1}\tilde{\boldsymbol{W}})^{\frac{1}{2}}} \\
&\geq\; \mathfrak{p}\inf_{\tilde{\boldsymbol{W}}\neq 0}\sup_{\tilde{\boldsymbol{V}}\neq 0}\frac{\tilde{\boldsymbol{V}}^T\boldsymbol{Z}\tilde{\boldsymbol{W}}}{\|\tilde{V}\|_{\mathcal{X}}\|\tilde{W}\|_{\mathcal{X}}} \\
&\geq\; \mathfrak{p}_{\mathfrak{Z}} \;.
\end{aligned}$$

Similar arguments using the boundedness of z and again the positive definiteness of $\boldsymbol{P}^{-1}$ show

$$\sup_{\boldsymbol{W}\neq 0}\sup_{\boldsymbol{V}\neq 0}\frac{\boldsymbol{V}^T\boldsymbol{P}^{\frac{1}{2}}\boldsymbol{Z}\boldsymbol{P}^{\frac{1}{2}}\boldsymbol{W}}{\|\boldsymbol{V}\|_2\|\boldsymbol{W}\|_2} \;\leq\; \|z\|\|p\| \;.$$

□

Thus, the special definiteness of $\boldsymbol{P}$ is enough to guarantee that the condition number remains bounded as $h \to 0$.

6.4 Blockdiagonal Preconditioners for the Saddle Point Problem

In this section, we want to establish the construction principles for an efficient preconditioner for the saddle point problem in matrix form

$$\begin{pmatrix} \boldsymbol{A} & \boldsymbol{B} \\ \boldsymbol{B}^T & -\boldsymbol{C} \end{pmatrix}\begin{pmatrix} \boldsymbol{u} \\ \boldsymbol{\Phi} \end{pmatrix} \;=\; \begin{pmatrix} \boldsymbol{f} \\ \boldsymbol{g} \end{pmatrix} \;, \qquad \text{or} \qquad \boldsymbol{Z}\boldsymbol{U} \;=\; \boldsymbol{\ell} \;, \tag{6.4.1}$$

where $\boldsymbol{A} \in \mathbb{R}^{n\times n}$ and $\boldsymbol{C} \in \mathbb{R}^{m\times m}$ are symmetric and positive definite matrices, $\boldsymbol{B} \in \mathbb{R}^{n\times m}$, $\boldsymbol{f} \in \mathbb{R}^n$ and $\boldsymbol{g} \in \mathbb{R}^m$. The approach chosen here is similar e.g. to [67, 94].

We assume that this problem stems from a finite element discretization of the saddle point problem as in $(4.2.1)$, i.e. we search for a solution $(u, \Phi) \in \mathcal{X}_h = \mathcal{V}_h \times \mathcal{W}_h$ satisfying

$$\begin{aligned} a(u,v) \;+\; b(v,\Phi) \quad &=\; (f,v)_{\mathcal{V}} \;, \qquad && \forall v \in \mathcal{V}_h \;, \\ b(u,\varphi) \;-\; c(\Phi,\varphi) \quad &=\; (g,\varphi)_{\mathcal{W}} \;, \qquad && \forall \varphi \in \mathcal{W}_h \;, \end{aligned} \tag{6.4.2}$$

where all occurring bilinear forms are bounded and $a(\cdot,\cdot)$ and $c(\cdot,\cdot)$ are symmetric and elliptic on the Hilbert spaces $\mathcal{V}$ and $\mathcal{W}$, respectively. Moreover, $\mathcal{V}_h \subset \mathcal{V}$ and $\mathcal{W}_h \subset \mathcal{W}$ are approximating subspaces constructed by the finite element method. Then, every element $v \in \mathcal{V}_h$ can be uniquely represented as $\boldsymbol{v} \in \mathbb{R}^n$ and vice versa. The same holds accordingly for $\varphi \in \mathcal{W}_h$ and $\boldsymbol{\varphi} \in \mathbb{R}^m$ as well as for $V \in \mathcal{X}_h$ and

$\boldsymbol{V} \in \mathbb{R}^N$.

The continuity and ellipticity of $a(\cdot,\cdot)$ and $c(\cdot,\cdot)$ yields constants $\mathfrak{a}, \|a\|$ and $\mathfrak{c}, \|c\|$ such that

$$\begin{aligned} \mathfrak{a} \;&\leq\; \frac{\boldsymbol{v}^T \boldsymbol{A} \boldsymbol{v}}{\|v\|_{\mathcal{V}}^2} \;\leq\; \|a\| \;, \qquad \forall v \in \mathcal{V}_h \;, \\ \mathfrak{c} \;&\leq\; \frac{\boldsymbol{\varphi}^T \boldsymbol{C} \boldsymbol{\varphi}}{\|\varphi\|_{\mathcal{W}}^2} \;\leq\; \|c\| \;, \qquad \forall \varphi \in \mathcal{W}_h \;. \end{aligned}$$

The boundedness of $b(\cdot,\cdot)$ yields a constant $\|b\|$ such that

$$b(\varphi, v) \;\leq\; \|b\| \, \|\varphi\|_{\mathcal{W}} \|v\|_{\mathcal{V}} \;.$$

We consider preconditioners $\boldsymbol{P}$ of blockdiagonal form, i.e.

$$\boldsymbol{P}^{-1} \;:=\; \begin{pmatrix} \tilde{\boldsymbol{A}} & 0 \\ 0 & \tilde{\boldsymbol{C}} \end{pmatrix} \;,$$

where $\tilde{\boldsymbol{A}} \in \mathbb{R}^{n \times n}$ and $\tilde{\boldsymbol{C}} \in \mathbb{R}^{m \times m}$ are symmetric matrices being positive definite in a certain sense, i.e. they yield positive constants $\tilde{\mathfrak{a}}, \|\tilde{a}\|$ and $\tilde{\mathfrak{c}}, \|\tilde{c}\|$, respectively, such that

$$\begin{aligned} \tilde{\mathfrak{a}} \;&\leq\; \frac{\boldsymbol{v}^T \tilde{\boldsymbol{A}} \boldsymbol{v}}{\|v\|_{\mathcal{V}}^2} \;\leq\; \|\tilde{a}\| \;, \qquad \forall v \in \mathcal{V}_h \;, \\ \tilde{\mathfrak{c}} \;&\leq\; \frac{\boldsymbol{\varphi}^T \tilde{\boldsymbol{C}} \boldsymbol{\varphi}}{\|\varphi\|_{\mathcal{W}}^2} \;\leq\; \|\tilde{c}\| \;, \qquad \forall \varphi \in \mathcal{W}_h \;. \end{aligned} \tag{6.4.3}$$

Note, preconditioners satisfying the above conditions can be constructed by the techniques developed in Section 6.2.

Now, according to Lemma 6.3.1 it is desirable to show a special definiteness of $\boldsymbol{P}^{-1}$ as in $(6.3.1)$. Here, the following result is immediately clear:

Lemma 6.4.1 *$\boldsymbol{P}^{-1}$ is positive definite with constants $\mathfrak{p}$ and $\|p\|$ satisfying*

$$\frac{1}{\|p\|} \;:=\; \frac{1}{\min\{\tilde{\mathfrak{a}}, \tilde{\mathfrak{c}}\}} \;\leq\; \frac{\boldsymbol{V}^T \boldsymbol{P}^{-1} \boldsymbol{V}}{\|V\|_{\mathcal{X}}^2} \;\leq\; \max\{\|\tilde{a}\|, \|\tilde{c}\|\} \;:=\; \frac{1}{\mathfrak{p}} \;, \qquad \forall \boldsymbol{V} \in \mathbb{R}^N \;,$$

Proof.

$$\begin{aligned}\mathbf{V}^T\boldsymbol{P}^{-1}\boldsymbol{V} &= \boldsymbol{v}^T\tilde{\boldsymbol{A}}\boldsymbol{v} + \boldsymbol{\varphi}^T\tilde{\boldsymbol{C}}\boldsymbol{\varphi} \le \|\tilde{a}\|\,\|v\|_{\mathcal{V}}^2 + \|\tilde{c}\|\,\|\varphi\|_{\mathcal{W}}^2 \\ &\le \max\{\|\tilde{a}\|,\|\tilde{c}\|\}\left(\|v\|_{\mathcal{V}}^2 + \|\varphi\|_{\mathcal{W}}^2\right) = \max\{\|\tilde{a}\|,\|\tilde{c}\|\}\,\|V\|_{\mathcal{X}}^2 .\end{aligned}$$

This is the first bound. The second is obtained by

$$\|V\|_{\mathcal{X}}^2 = \|v\|_{\mathcal{V}}^2 + \|\varphi\|_{\mathcal{W}}^2 \le \frac{1}{\tilde{\mathfrak{a}}}\boldsymbol{v}^T\tilde{\boldsymbol{A}}\boldsymbol{v} + \frac{1}{\tilde{\mathfrak{c}}}\boldsymbol{\varphi}^T\tilde{\boldsymbol{C}}\boldsymbol{\varphi} \le \frac{1}{\min\{\tilde{\mathfrak{a}},\tilde{\mathfrak{c}}\}}\boldsymbol{V}^T\boldsymbol{P}^{-1}\boldsymbol{V} .$$

□

Thus, the condition number of the preconditioned system is bounded uniformly by a constant independent of h, cf. Lemma 6.3.1, as long as $\boldsymbol{Z}$ satisfies the conditions of Babuška's theorem.

Remark 6.4.2 *The above blockdiagonal preconditioner is not restricted to systems in the special saddle point form* $(6.4.1)$*, but can be applied (after a possible partitioning) to all systems where the coefficient matrix satisfies the conditions of Babuška's theorem, i.e. in particular to the linear systems* $\hat{\boldsymbol{Z}}\boldsymbol{U} = \hat{\boldsymbol{\ell}}$ *considered in Section 5.2.3.*

As in $(4.2.22)$, we relax the inf-sup condition in $(4.2.18)$ to

$$\inf_{v\in\mathcal{V}_h}\sup_{\varphi\in\mathcal{W}_h}\frac{|b(v,\varphi)|}{\|v\|_{\mathcal{V}}\|\varphi\|_{\mathcal{W}}} \ge \beta_h \ge \beta_{\min} \ge 0 , \tag{6.4.4}$$

again allowing for $\beta_{\min} = 0$. In this case, $\boldsymbol{B}$ may have a non-trivial kernel, and we get the following

Lemma 6.4.3

$$\frac{\beta_{\min}^2}{\|c\|} \le \frac{\boldsymbol{v}^T\boldsymbol{B}\boldsymbol{C}^{-1}\boldsymbol{B}^T\boldsymbol{v}}{\|v\|_{\mathcal{V}}^2} \le \frac{\|b\|^2}{\mathfrak{c}} .$$

Proof.

$$\begin{aligned}\mathbf{v}^T\boldsymbol{B}\boldsymbol{C}^{-1}\boldsymbol{B}^T\boldsymbol{v} &= (\boldsymbol{C}\boldsymbol{C}^{-1}\boldsymbol{B}^T\boldsymbol{v}, \boldsymbol{C}^{-1}\boldsymbol{B}^T\boldsymbol{v}) = \sup_{\varphi\in\mathcal{W}_h}\frac{(\boldsymbol{C}\boldsymbol{C}^{-1}\boldsymbol{B}^T\boldsymbol{v},\varphi)^2}{(\boldsymbol{C}\varphi,\varphi)} , \\ &\ge \frac{1}{\|c\|}\frac{b(\varphi,\boldsymbol{v})^2}{\|\varphi\|_{\mathcal{W}}^2} \ge \frac{\beta_{\min}^2}{\|c\|}\|v\|_{\mathcal{V}}^2 .\end{aligned}$$

$$\mathbf{v}^T \boldsymbol{B}\boldsymbol{C}^{-1}\boldsymbol{B}^T\boldsymbol{v} \;\leq\; (\boldsymbol{C}^{-1}\boldsymbol{B}^T\boldsymbol{v}, \boldsymbol{B}^T\boldsymbol{v}) \;\leq\; \frac{1}{\mathfrak{c}}\|\boldsymbol{B}^T\boldsymbol{v}\|^2 \;\leq\; \frac{\|b\|^2}{\mathfrak{c}}\|v\|_{\mathcal{V}}^2 \,.$$

□

The preconditioned saddle point system now is given by

$$\begin{pmatrix} \tilde{\boldsymbol{A}}^{-1}\boldsymbol{A} & \tilde{\boldsymbol{A}}^{-1}\boldsymbol{B} \\ \tilde{\boldsymbol{C}}^{-1}\boldsymbol{B}^T & -\tilde{\boldsymbol{C}}^{-1}\boldsymbol{C} \end{pmatrix} \begin{pmatrix} \boldsymbol{u} \\ \boldsymbol{\Phi} \end{pmatrix} \;=\; \begin{pmatrix} \tilde{\boldsymbol{A}}^{-1}\boldsymbol{f} \\ \tilde{\boldsymbol{C}}^{-1}\boldsymbol{g} \end{pmatrix} \,, \qquad \text{or} \qquad \tilde{\boldsymbol{Z}}\boldsymbol{U} \;=\; \tilde{\boldsymbol{\ell}} \,.$$

A simple computation shows that the Schur complement matrix of the preconditioned system is given by

$$\tilde{\boldsymbol{S}} \;=\; \tilde{\boldsymbol{A}}^{-1}\boldsymbol{S} \,,$$

thus completely neglecting the dependence on the preconditioner part $\tilde{\boldsymbol{C}}^{-1}$. This gets immediately clear since this preconditioner only speeds up the inner iteration when solving systems with coefficient matrix $\boldsymbol{C}$. By a reformulation as in $(6.3.2)$, the spectrum of $\tilde{\boldsymbol{A}}^{-1}\boldsymbol{S}$ can be determined from the eigenvalues of $\tilde{\boldsymbol{A}}^{-\frac{1}{2}}\boldsymbol{S}\tilde{\boldsymbol{A}}^{-\frac{1}{2}}$. Then, the condition number of $\tilde{\boldsymbol{S}}$ can be estimated easily:

Theorem 6.4.4 *The condition number of $\tilde{\boldsymbol{S}}$ is bounded independently of h by*

$$\frac{1}{\|\tilde{a}\|}\left(\mathfrak{a} + \frac{\beta_{\min}^2}{\|c\|}\right) \;\leq\; \frac{\boldsymbol{v}^T\tilde{\boldsymbol{S}}\boldsymbol{v}}{\|\boldsymbol{v}\|_2^2} \;\leq\; \frac{1}{\tilde{\mathfrak{a}}}\left(\|a\| + \frac{\|b\|^2}{\mathfrak{c}}\right) \,.$$

Proof. By a basic computation, setting $\boldsymbol{w} := \tilde{\boldsymbol{A}}^{-\frac{1}{2}}\boldsymbol{v}$,

$$\begin{aligned} \frac{\boldsymbol{v}^T\tilde{\boldsymbol{A}}^{-\frac{1}{2}}\boldsymbol{S}\tilde{\boldsymbol{A}}^{-\frac{1}{2}}\boldsymbol{v}}{\boldsymbol{v}^T\boldsymbol{v}} \;&=\; \left(\frac{\boldsymbol{v}^T\tilde{\boldsymbol{A}}^{-\frac{1}{2}}\boldsymbol{A}\tilde{\boldsymbol{A}}^{-\frac{1}{2}}\boldsymbol{v}}{\boldsymbol{v}^T\boldsymbol{v}} + \frac{\boldsymbol{v}^T\tilde{\boldsymbol{A}}^{-\frac{1}{2}}\boldsymbol{B}\boldsymbol{C}^{-1}\boldsymbol{B}^T\tilde{\boldsymbol{A}}^{-\frac{1}{2}}\boldsymbol{v}}{\boldsymbol{v}^T\boldsymbol{v}}\right) \,, \\ &= \left(\frac{\boldsymbol{w}^T\boldsymbol{A}\boldsymbol{w}}{\boldsymbol{w}^T\tilde{\boldsymbol{A}}\boldsymbol{w}} + \frac{\boldsymbol{w}^T\boldsymbol{B}\boldsymbol{C}^{-1}\boldsymbol{B}^T\boldsymbol{w}}{\boldsymbol{w}^T\tilde{\boldsymbol{A}}\boldsymbol{w}}\right) \,. \end{aligned}$$

The first term can be estimated by the ellipticity properties of $\boldsymbol{A}$ and $\tilde{\boldsymbol{A}}$,

$$\frac{\mathfrak{a}}{\|\tilde{a}\|} \;\leq\; \frac{\boldsymbol{w}^T\boldsymbol{A}\boldsymbol{w}}{\boldsymbol{w}^T\tilde{\boldsymbol{A}}\boldsymbol{w}} \;\leq\; \frac{\|a\|}{\tilde{\mathfrak{a}}} \,.$$

By Lemma 6.4.3 and the ellipticity properties of $\tilde{\boldsymbol{A}}$, the second term can be estimated by

$$\frac{\beta_{\min}^2}{\|\tilde{a}\|\,\|c\|} \;\leq\; \frac{\boldsymbol{w}^T\boldsymbol{B}\boldsymbol{C}^{-1}\boldsymbol{B}^T\boldsymbol{w}}{\boldsymbol{w}^T\tilde{\boldsymbol{A}}\boldsymbol{w}} \;\leq\; \frac{\|b\|^2}{\tilde{\mathfrak{a}}\,\mathfrak{c}} \,.$$

□

7 Numerical Results

We solve the linear equations of piezoelectricity with generalized right-hand side given according to Chapter 2 by

$$\begin{aligned} \rho\, u_{i,tt} - \quad c_{ijkl}\, u_{k,lj} - \; e_{kij}\, \Phi_{,kj} \quad &= \; b_i \;, \\ e_{ikl}\, u_{k,li} \; - \; \epsilon_{ij}\, \Phi_{,ji} \quad &= \; \beta_i \;. \end{aligned} \tag{7.0.1}$$

Since in piezoelectric substrates the magnitudes of the material coefficients differ in several magnitudes (see Appendix A), there is no way of solving the above equations without proper scaling.

For piezoelectric computations it is sufficient to introduce a characteristic displacement U_0 and set $U := U_0 u$, resulting for the time-harmonic situation in

$$\begin{aligned} -\left(\rho\omega^2 U_0\right) U_i \; - \left(U_0 c_{ijkl}\right) U_{k,lj} \; - \; e_{kij}\, \Phi_{,kj} \quad &= \; b_i \;, \\ e_{ikl}\, U_{k,li} \; - \; \frac{\epsilon_{ij}}{U_0}\, \Phi_{,ji} \quad &= \; \frac{\beta_i}{U_0} \;. \end{aligned} \tag{7.0.2}$$

All computations were carried out on a standard Linux workstation with 512 MB memory and a Pentium IV 1.8 GHz processor, using the finite element package ALBERTA developed by Alfred Schmidt and Kunibert Siebert [3, 93]. Saddle point problems are not included in ALBERTA originally, so we had to implement new data structures and solution methods.

7.1 An Academic Test Example

In order to guarantee that our computer implementation for the solution of the piezoelectric equations is working correctly, we first consider an academic test example with a known solution for the mechanical displacement $\boldsymbol{u}$ and the electric potential Φ. Here, we also illustrate the performance of our preconditioner developed in Chapter 6.

7.1.1 Problem Statement

We assume the solutions to take the form

$$\boldsymbol{u}(\boldsymbol{x}) \;=\; \boldsymbol{x}^T\boldsymbol{x}\begin{pmatrix}1\\2\\3\end{pmatrix}\;, \qquad \Phi(\boldsymbol{x}) \;=\; \sum_{i=1}^{3}\sin(\pi x_i)\;,$$

The elastic moduli in Voigt notation (see Section 2.1.3) and the dielectric tensor are given by

$$\boldsymbol{c} \;=\; (c_{IK}) \;=\; \begin{pmatrix} 20 & 5 & 7 & 1 & 0 & 0\\ 5 & 20 & 7 & -1 & 0 & 0\\ 7 & 7 & 25 & 0 & 0 & 0\\ -1 & -1 & 0 & 5 & 0 & 0\\ 0 & 0 & 0 & 0 & 6 & 1\\ 0 & 0 & 0 & 0 & 1 & 7 \end{pmatrix}\;, \quad \boldsymbol{\epsilon} \;=\; (\epsilon_{ij}) \;=\; \begin{pmatrix} 10 & & \\ & 10 & \\ & & 5 \end{pmatrix}\;,$$

whereas the piezoelectric coupling (also in Voigt notation) is chosen as follows

$$\boldsymbol{e} \;=\; (e_{iK}) \;=\; \begin{pmatrix} -4 & 1 & 1 & 0 & 0 & 0\\ 0 & -4 & 1 & 0 & 0 & 0\\ 1 & 1 & 1 & 1 & 1 & 1 \end{pmatrix}\;.$$

We remark that the computer code has been tested on several other problems. Here, the material moduli have been chosen in order to resemble the elastic properties of a typical piezoelectric material like quartz.

We use standard $\mathbb{P}_k$-conforming Lagrangian type finite elements of degree k. Then, starting from an initial triangulation of the domain $\Omega \subset \mathbb{R}^d$, refinement is realized by breaking up each triangle/tetraeder into 2^d triangles/tetraeders of the same shape and size, respectively.

We solve the saddle point problem formulated as

$$\begin{pmatrix} \boldsymbol{A} & \boldsymbol{B}\\ \boldsymbol{B}^T & -\boldsymbol{C}\end{pmatrix}\begin{pmatrix}\boldsymbol{u}\\ \boldsymbol{\Phi}\end{pmatrix} \;=\; \begin{pmatrix}\boldsymbol{f}\\ \boldsymbol{g}\end{pmatrix}\;, \qquad \text{or} \qquad \boldsymbol{ZU} \;=\; \boldsymbol{\ell}\;, \tag{7.1.1}$$

or alternatively,

$$\begin{pmatrix} \boldsymbol{A} & \boldsymbol{B} \\ -\boldsymbol{B}^T & \boldsymbol{C} \end{pmatrix} \begin{pmatrix} \boldsymbol{u} \\ \boldsymbol{\Phi} \end{pmatrix} = \begin{pmatrix} \boldsymbol{f} \\ -\boldsymbol{g} \end{pmatrix} , \qquad \text{or} \qquad \hat{\boldsymbol{Z}}\boldsymbol{U} = \hat{\boldsymbol{\ell}} , \tag{7.1.2}$$

by both the GMRES and the BI-CGSTAB method using the blockdiagonal preconditioner developed in Chapter 6. An experimental comparison of different Krylov space methods can be found in [92]. Moreover, the positive definite Schur complement system

$$\boldsymbol{S}\boldsymbol{u} = \boldsymbol{F} , \tag{7.1.3}$$

is solved by a preconditioned conjugate gradient method. For any of these Krylov space methods the number of iterations required to obtain a fixed accuracy depends on the condition number κ of the coefficient matrices $\boldsymbol{Z}$, $\hat{\boldsymbol{Z}}$ and $\boldsymbol{S}$, respectively.

7.1.2 2D Simulations

In $\mathbb{R}^2$, we choose $\Omega = [-1, 1]^2$, and assume that all physical magnitudes do not depend on x_3. One of the main difficulties in the implementation into existing finite element packages is the treatment of mixed boundary conditions whenever the Dirichlet boundaries Γ_u and Γ_Φ do not coincide. The boundary types are chosen as in Figure 7.1.

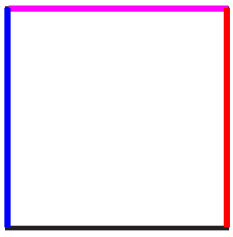

Figure 7.1: Boundary types: $\boldsymbol{u}$ Neumann/Φ Dirichlet, $\boldsymbol{u}$ Neumann/Φ Neumann, $\boldsymbol{u}$ Dirichlet/Φ Neumann, $\boldsymbol{u}$ Dirichlet/Φ Dirichlet

Since the solutions are sufficiently smooth, Ceá's lemma (4.1.6) and the approximation property (4.1.8) for finite element methods of polynomial degree k yield constants c and C such that

$$\begin{aligned} \|\boldsymbol{u} - \boldsymbol{u}_h\|_{1;\Omega} &\leq Ch^k |\boldsymbol{u}|_{k+1;\Omega} \ , \\ \|\Phi - \Phi_h\|_{1;\Omega} &\leq ch^k |\Phi|_{k+1;\Omega} \ . \end{aligned} \tag{7.1.4}$$

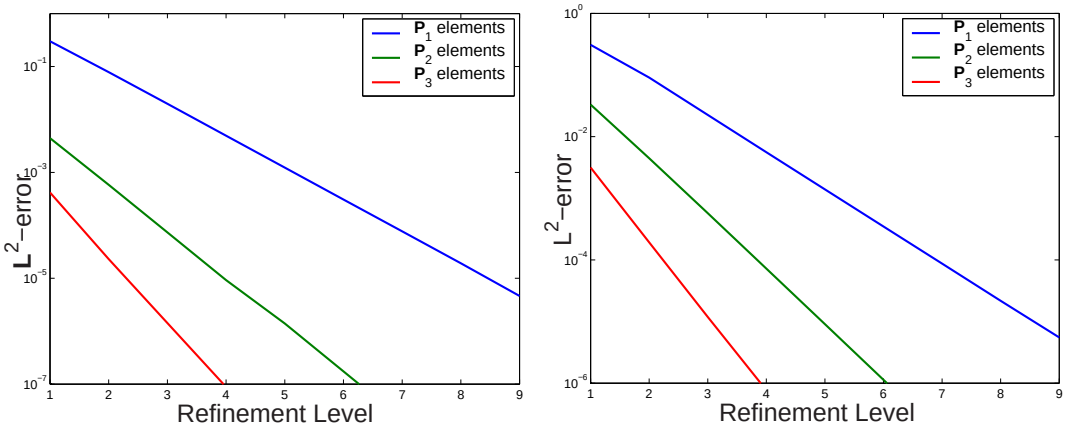

(a) $\boldsymbol{L}^2$-error for $\boldsymbol{u}$ component (b) L^2-error for Φ component

Figure 7.2: L^2–errors for different polynomial degrees

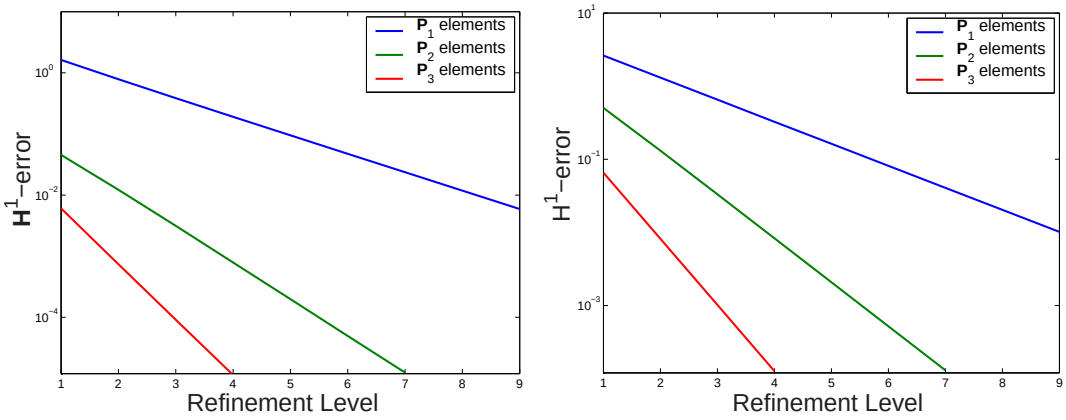

(a) $\boldsymbol{H}^1$-error for $\boldsymbol{u}$ component (b) H^1-error for Φ component

Figure 7.3: H^1-errors for different polynomial degrees

The results of our numerical computations show the correctness of the computer implementation: Figures 7.2 and 7.3 illustrate the L^2- and H^1-errors for different polynomial degrees of the used finite element methods. The straight lines have slopes in the logarithmic scale that correspond to the theoretical prediction given by (7.1.4).

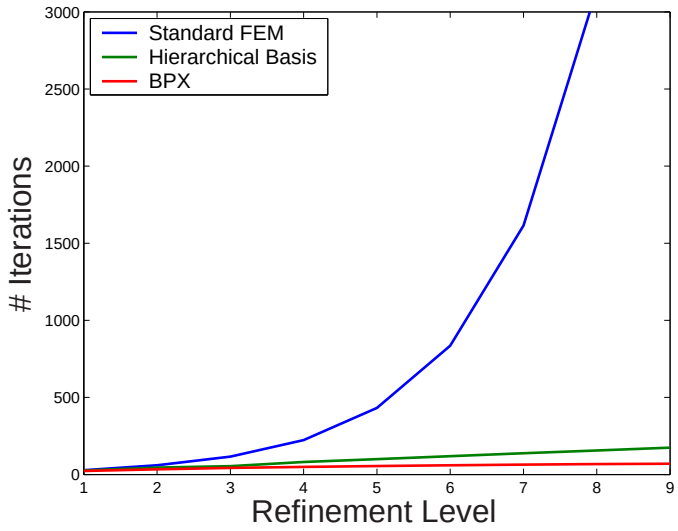

Figure 7.4: Number of iterations required to reach a fixed tolerance $1.0e-6$

For the preconditioned conjugate gradient (PCG) method, the number of iterations required to obtain a fixed accuracy is directly proportional to $\sqrt{\kappa}$, where κ is the condition number of the preconditioned coefficient matrix. We solve the equation $\boldsymbol{\mathcal{S}u} = \boldsymbol{F}$ by a PCG method. Figure 7.4 shows that for a blockdiagonal BPX-preconditioner the condition number is indeed independent of the refinement level L whereas without preconditioner the condition number grows exponentially with L. For comparison, the green line in Figure 7.4 indicates the number of iterations in the case where a blockdiagonal HB-preconditioner is used.

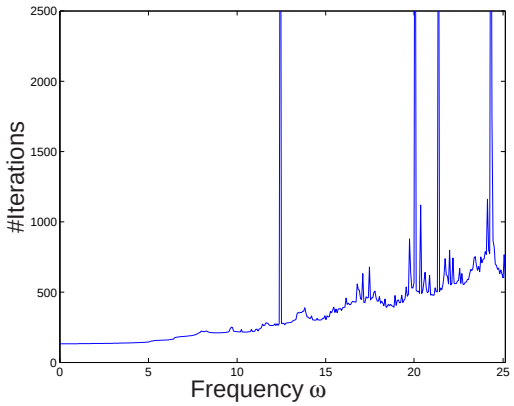

Figure 7.5: Number of iterations required to reach a fixed tolerance $1.0e-6$

Another interesting problem is the solution of the time harmonic equations

$$(\boldsymbol{S} - \omega^2)\,\boldsymbol{u} \;=\; \boldsymbol{F}\;.$$

We investigate the behavior of the solution method when the angular frequency ω varies between 0 and 25. According to the eigenvalue considerations above, we would expect that the number of iterations required to obtain a fixed accuracy will grow with increasing frequency, since ω^2 controls the number of negative eigenvalues in the saddle point problem. Moreover, the solution behavior drastically deteriorates when an eigenvalue of $\boldsymbol{S}$ is reached.

7.1.3 3D Simulations

In $\mathbb{R}^3$, we choose $\Omega = [-1,1]^3$. Again, one of the main concerns is the correct treatment of the mixed boundary conditions whenever the Dirichlet boundaries Γ_u and Γ_Φ do not coincide. The boundary types for our test calculations are chosen as indicated in Figure 7.6.

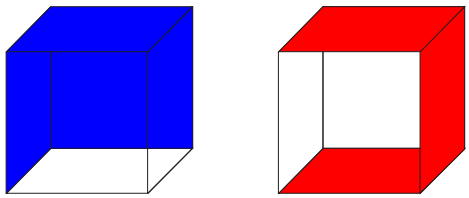

Figure 7.6: Neumann boundaries for $\boldsymbol{u}$ and Φ, respectively.

Ceá's lemma now yields the same estimate as in the 2D setting (7.1.4), which is again confirmed by the numerical results in Figures 7.7 and 7.8.

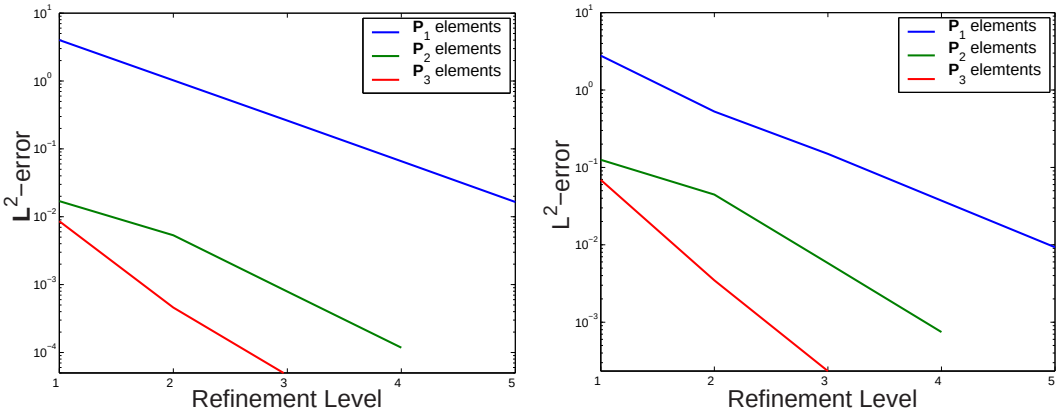

(a) $\boldsymbol{L}^2$-error for $\boldsymbol{u}$ component (b) L^2-error for Φ component

Figure 7.7: L^2–errors for different polynomial degrees

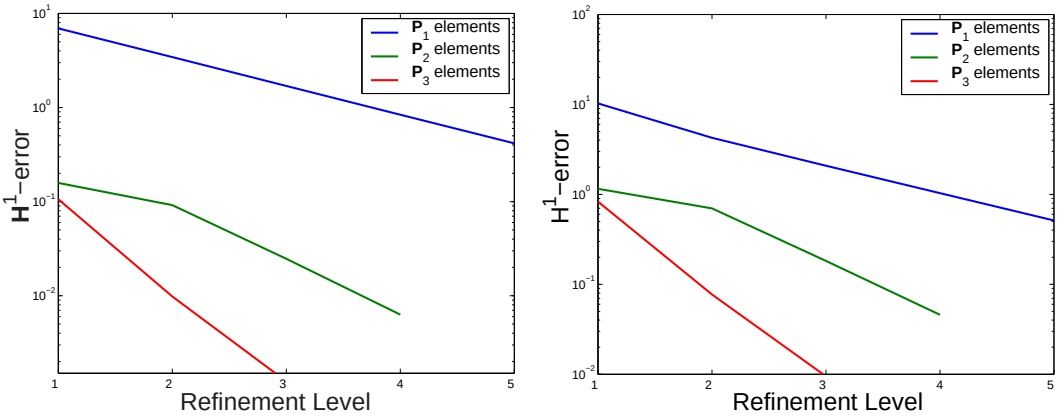

(a) $\boldsymbol{H}^1$-error for $\boldsymbol{u}$ component (b) H^1-error for Φ component

Figure 7.8: H^1-errors for different polynomial degrees

For the preconditioned conjugate gradient method, the number of iterations required to obtain a fixed accuracy is directly proportional to $\sqrt{\kappa}$, where κ is the condition number of the preconditioned coefficient matrix. Figure 7.9 shows the performance increase by the use of a block-BPX preconditioner. From Figure 7.9 it can also be seen that the use of a block-HB preconditioner does not make too much sense in 3D, cf. [96].

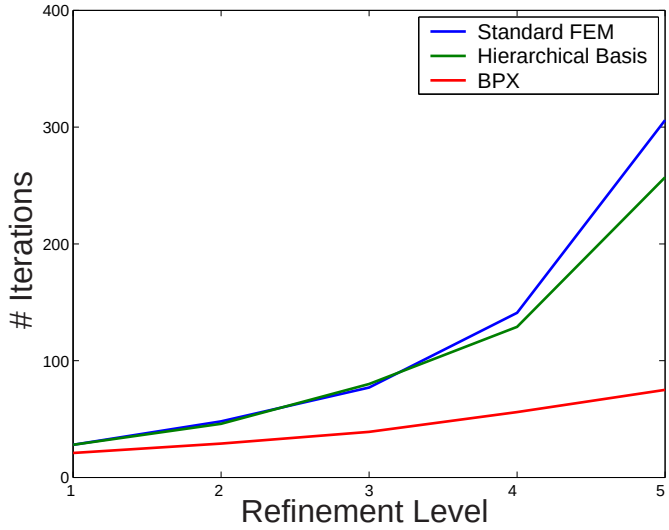

Figure 7.9: Number of iterations required to reach a fixed tolerance $1.0e-4$

7.1.4 Comparison of Solvers and Solution Methods

In this section, we want to compare different methods and strategies to obtain a solution for the piezoelectric equations $(7.0.1)$. First, we solve the Schur complement system $(7.1.3)$ by a conjugate gradient method (`SC-CG`). Then, the `BI-CGSTAB` and `GMRES` methods are applied to both the symmetric and non-symmetric saddle-point

formulations $(7.1.1)$ and $(7.1.2)$, respectively.

We start with the 2D calculations, where the stopping criterion is chosen such that the residual gets smaller than $1.0e-6$. We give the number of iterations needed for convergence. However, since the effort for one iteration step is not comparable at once (e.g., there is an inner iteration in the application of the Schur complement), we also measured the used CPU-time (in seconds) needed for convergence. The resulting L^2- and H^1-errors for all methods are essentially the same. So they are not listed here. In order to demonstrate the performance of our preconditioner, we first give results for the system solution without preconditioner:

Level	SC-CG		BI-CGSTAB				GMRES			
			non-symm.		symm.		non-symm.		symm.	
	time	iter	time	iter	time	iter	time	iter	time	iter
3	0.15	74	0.10	65	0.59	662	0.14	17	19	3745
4	1.4	148	0.75	137	17	3170	1.7	56	520	STOP
5	29	311	7.6	324	390	STOP	32	206		
6	440	872	75	678			530	758		

The best performance without preconditioner was achieved by the BI-CGSTAB method when applied to the non-symmetric system $(7.1.2)$. For this system, the GMRES method shows similar good performance. However, both methods converge poorly when applied to the symmetric saddle point problem $(7.1.1)$. We remark that the Schur complement system for both saddle point formulations are equivalent. The performance of the SC-CG method lies somewhere in between the BI-CGSTAB/GMRES solvers applied to both saddle point variants $(7.1.1)$ and $(7.1.2)$.

Now, the same test runs have been executed with the used blockdiagonal BPX-preconditioners. The numerical results show that we are able to treat problems thereupon that previously were too costly to solve:

Level	SC-CG		BI-CGSTAB				GMRES			
			non-symm.		symm.		non-symm.		symm.	
	time	iter	time	iter	time	iter	time	iter	time	iter
5	2.5	48	1.1	33	8.0	289	1.2	6	9.6	60
6	12	52	5.2	39	40	338	5.9	7	56	77
7	70	55	23	41	190	384	25	7	320	101
8	290	57	92	44	910	438	100	8	1140	88

7.2 SAW Device Simulation

It is well-known that the finite element error grows for time-harmonic waves with increasing angular frequency $\omega = \frac{2\pi v}{\lambda}$, even if we account for a condition on the meshsize like $h \lesssim c_1 \lambda$. A common choice is $h \lesssim \frac{\lambda}{2}$ (i.e. two elements per wavelength), an estimate that guarantees an interpolation property for the used finite element spaces. However, an intrinsic analysis shows that an additional condition like $h \lesssim c_2 \sqrt{\lambda^3}$ (with a small constant c_2) is needed if we want to control the finite element error, cf. [61]. For realistic 3D SAW devices this condition cannot be fulfilled for the computer systems at our disposal. Thus, our simulations were performed for reduced 2D models. However, this is no restriction on the developed models and methods but on the available computing power. Moreover, we should keep in mind that the meshsize restrictions should be satisfied for multilevel methods on the coarsest refinement level.

We start our simulations of SAW devices with a reduced model in the (x_1, x_3)-plane and assume that all variables do not depend on x_2 and have no impact in the x_2-direction. The domain Ω is illustrated in Figure 7.10.

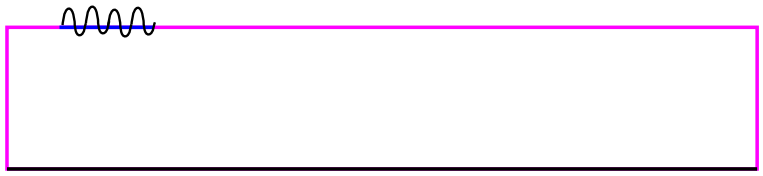

Figure 7.10: Geometry of the SAW device

Zero Neumann conditions for $\boldsymbol{u}$ and Φ are imposed on the pink boundary part (see Figure 7.10), whereas zero Dirichlet conditions are given at $x_3 = 0$. In the blue region, an alternating voltage

$$\Phi_\Gamma(\boldsymbol{x}, t) \;=\; \hat{\Phi} \sin\left(\frac{2\pi}{\lambda_{IDT}}\right) \sin(\omega t) \;,$$

is applied for $k \in \mathbb{N}$.

The piezoelectric material used for the SAW chip in our calculations is lithium niobate ($LiNbO_3$) with density $\rho = 4630 \frac{kg}{m^3}$. This chip is operated at room temperature ($20°C$), and the material moduli can be taken from Appendix A. We remark that the SAW devices can be cooled efficiently. Thus, the assumption of a constant operating temperature is justified. The used crystal cut is `YX1` $128°$ $LiNbO_3$ (see Appendix A), a crystal cut that is commonly utilized in transducer design. The use of rotated crystal cuts leads to a transformation of the components of the material tensors for the elastic stiffness, piezoelectric coupling and dielectric permittivity, see Appendix A.1.

For our computations, we make the realistic choice $\lambda_{IDT} = 40\mu m$ and an operating frequency of $f = \frac{\omega}{2\pi} = 100MHz$. The length of the SAW chip is 1.2mm, its height 0.6mm. Figures 7.11-7.13 show the amplitudes of the electric potential and the

polarized Rayleigh waves, respectively. The amplitudes of the displacement waves are, as expected, in the region of nanometers.

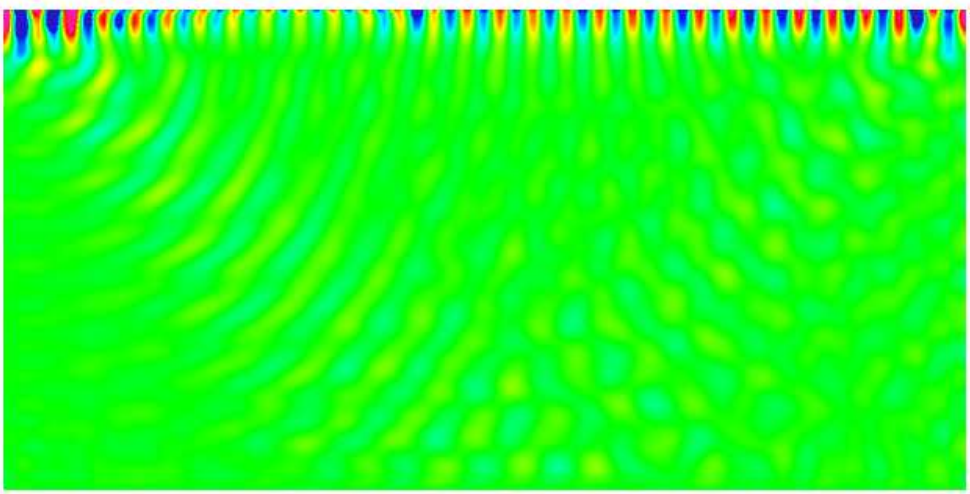

Figure 7.11: Electric potential wave

The SAWs are strictly confined to the surface of the substrate. Their penetration depth into the piezoelectric material is in the range of one wavelength.

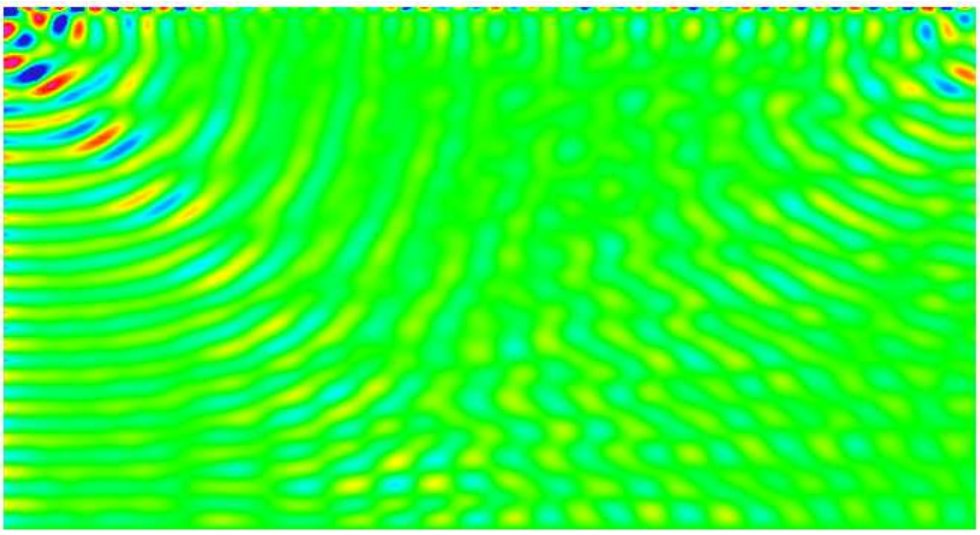

Figure 7.12: Displacement wave amplitudes in x_1-direction

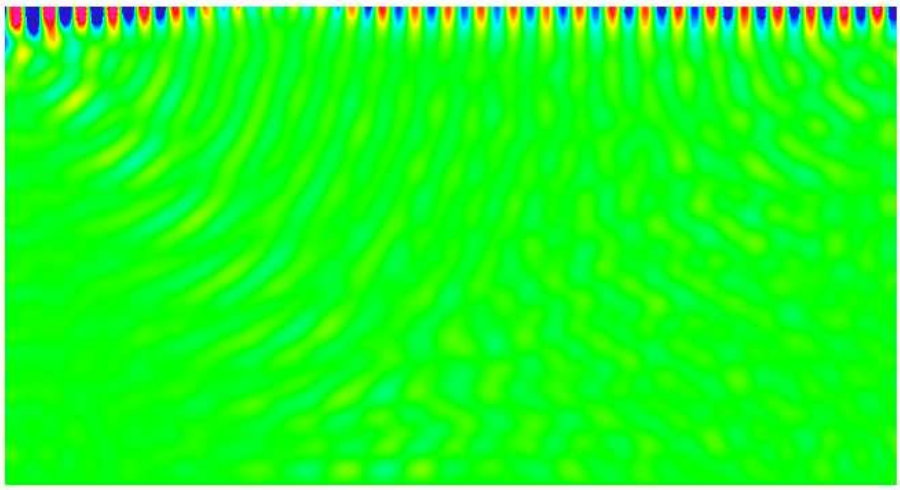

Figure 7.13: Displacement wave amplitudes in x_2-direction

One of the most outstanding properties of surface acoustic wave propagation on piezoelectric materials is that the velocity of the SAW is independent of the applied frequency. In the case of `YXl 128°` $LiNbO_3$ the SAW velocity is given by $v = 3992\frac{m}{s}$, cf. [25]. Thus, for an excitation at the frequency $f = 100\text{MHz}$ the theoretical wavelength of the SAW is given as $\lambda = \frac{v}{f} \approx 40\mu m$. Our calculations show the same wavelength for the SAW. Figure 7.14 also illustrates the piezoelectric wave for $f = 50\text{MHz}$. The wavelength of the SAW for $f = 100\text{MHz}$ is half of that for $f = 50\text{MHz}$.

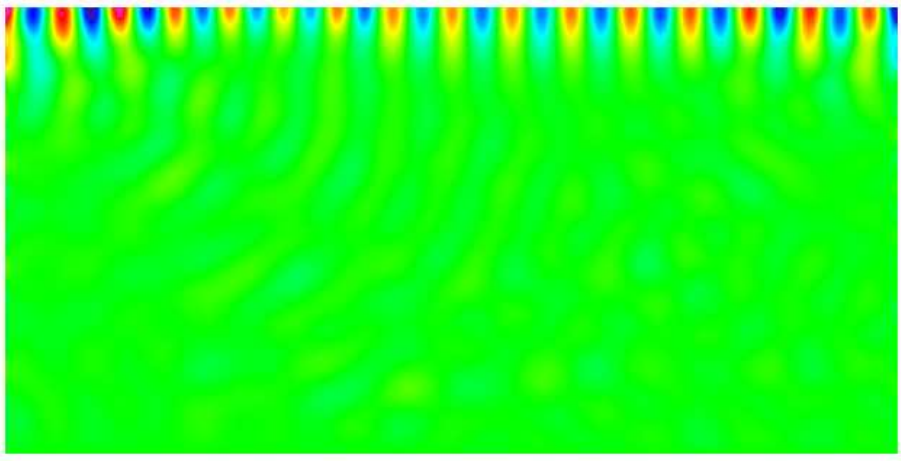

Figure 7.14: Electric potential wave for $f = 50\text{MHz}$

We remark that the wavelength of an occurring electro-magnetical wave is in the region of approximately $0.3m$. Hence, the negligence of this electro-magnetic wave in the modeling of piezoelectric SAW devices is justified.

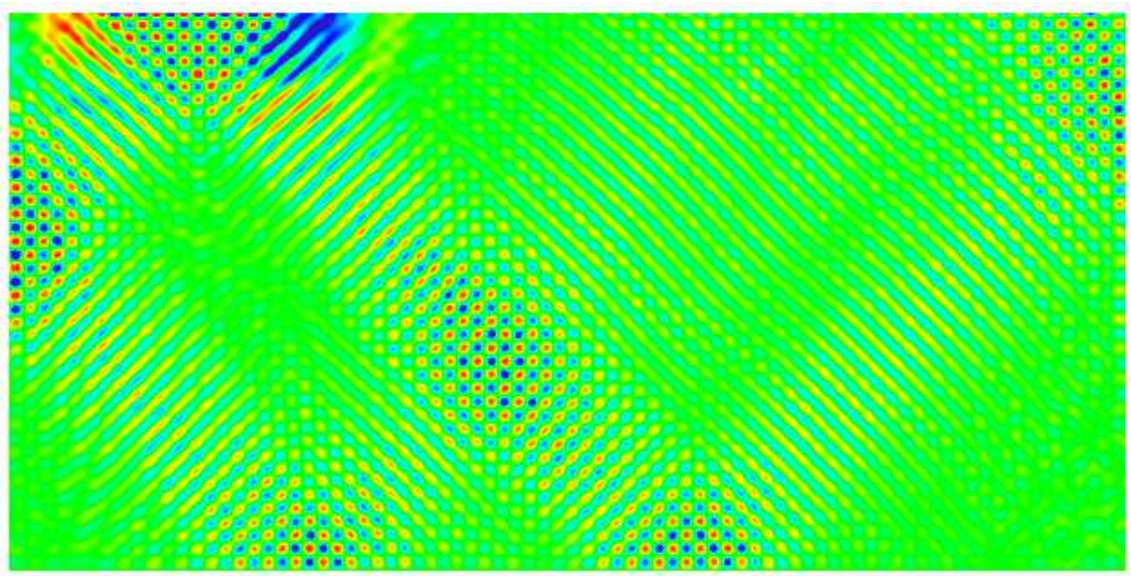

Figure 7.15: Bulkwave Excitation

The excitation of an IDT on the surface of a piezoelectric material leads to the generation of bulk acoustic waves (BAWs) as well as surface acoustic waves. These bulk waves can also be observed in our simulations in Figures 7.11-7.14. Technologically, they are desirably employed in solid-state circuits [25]. However, for SAW devices their presence is unpreferable, since the interference of BAWs with SAWs can lead to a complete loss of functionality of the device. Our approach is sufficiently general to simulate every kind of piezoelectric resonator. In Figure 7.15 we have used an `YXl 38°` cut of $LiNbO_3$ to generate a strong bulk acoustic wave at frequency $f = 200MHz$.

We recall from Chapter 3 that Rayleigh surface waves characteristically show an elliptical displacement, i.e. the displacements in the x_1- and x_2-direction are 90° out of phase with one another. Additionally, the amplitude of the surface displacement in the x_2-direction is larger than that along the SAW propagation axis x_1. These observations are also true in our numerical computations, see Figures 7.16 and 7.17. In Figure 7.16, the displacements in the x_1- and x_2-direction for a certain surface area are depicted. The x_2-displacements are flipped vertically for easier comparability.

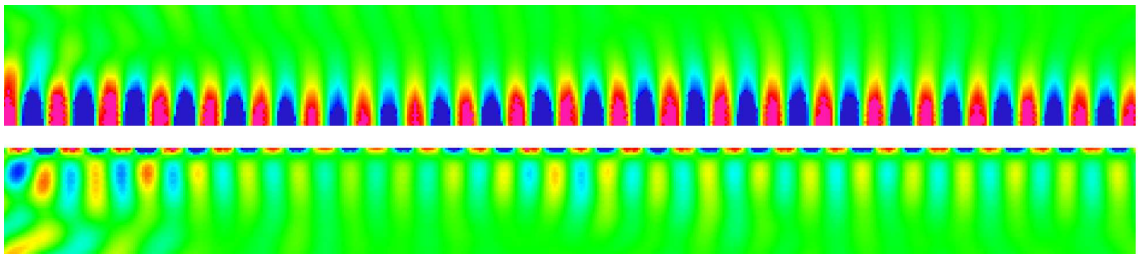

Figure 7.16: Phaseshift of x_1- and x_2- (flipped) displacements

In Figure 7.17 a certain surface area is magnified and the vectors indicate the surface displacements.

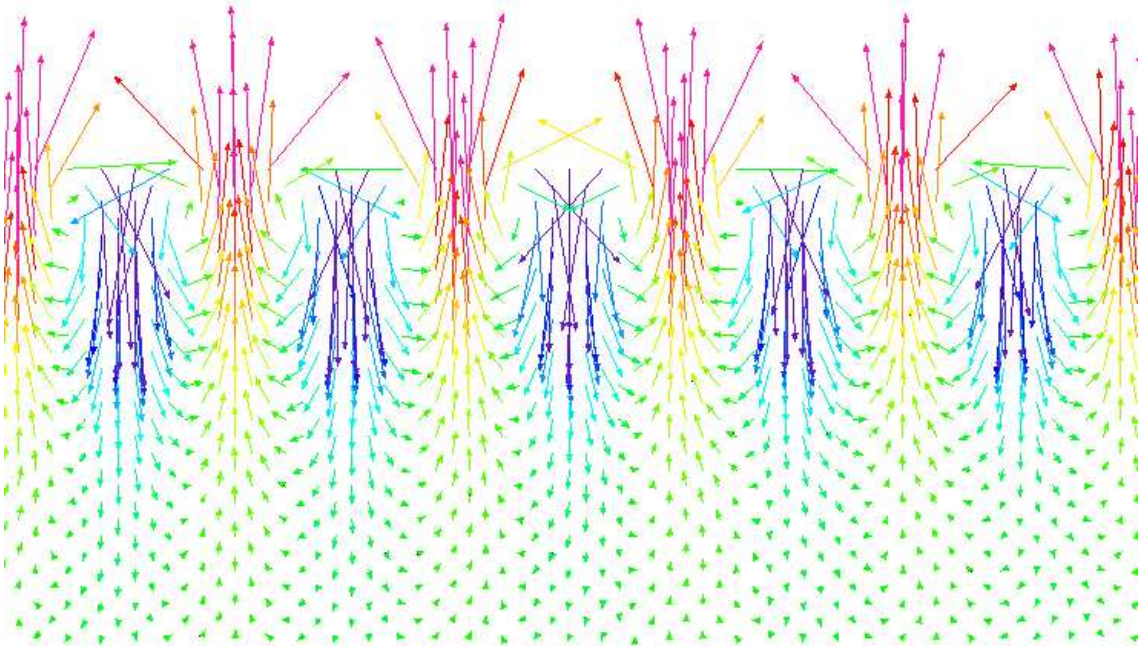

Figure 7.17: Displacement vectors for the SAW

All numerical calculations show relatively strong reflections from the boundaries of the SAW device. In real devices these reflections are usually avoided by attaching some adhesive material to the side boundaries. An easy way to model such a damping is to introduce an additional term (the so-called *gyroscopic* term) into the piezoelectric equations which now become

$$\begin{aligned} \rho\, u_{i,tt} \;-\; \beta_{,j}\, u_{i,jtj} \;-\; & c_{ijkl}\, u_{k,lj} - \; e_{kij}\, \Phi_{,kj} \;\; = \; b_i \;, \\ & e_{ikl}\, u_{k,li} \;-\; \epsilon_{ij}\, \Phi_{,ji} \;\; = \; \beta_i \;, \end{aligned} \tag{7.2.1}$$

cf. e.g. [12, 64]. Introducing such a damping at the boundaries of the bottom and lefthand side we indeed get less reflections and thus less disturbances for the SAW. This gets extraordinaly palpable, if we compare the x_1-displacements in Figure 7.12 (calculations without damping) to the new calculations with damping term in Figure 7.18:

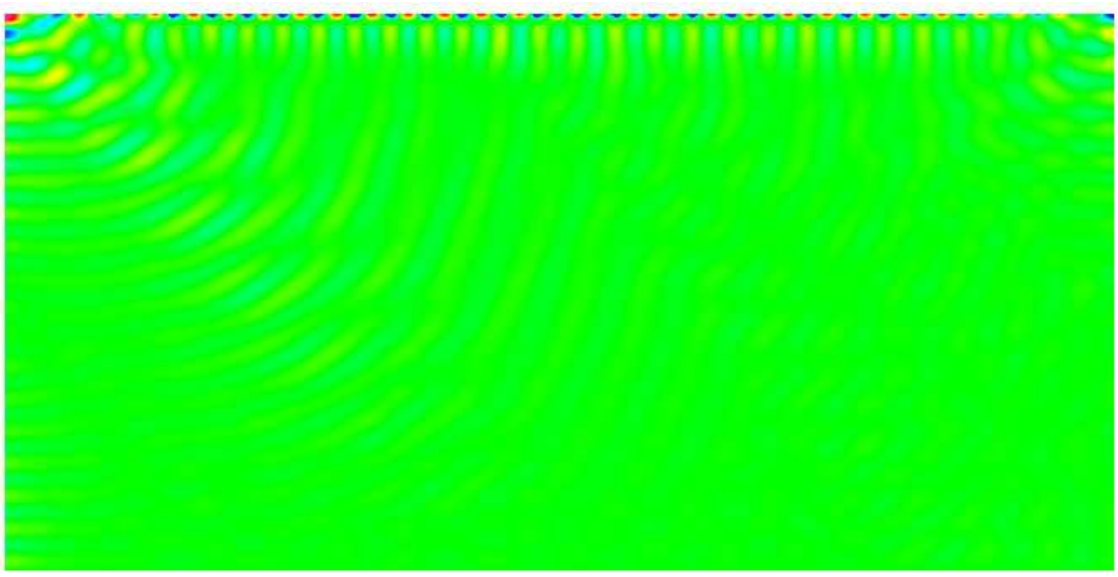

Figure 7.18: x_1-displacements with damping

A Material Moduli

In this section, material moduli and additional information for some commonly used piezoelectric materials are given. Usually, one is interested in very large monocrystals appearing only randomly in nature. However, sophisticated production procedures for all technologically relevant materials are at hand. Depending on the cut used for the special device the monocrystals are sawed. For details concerning production procedures, natural appearances and the material constants stated here we refer to [113] and the references therein.
The material moduli are given here in a way such that the coordinate x_3-axis is identical with the polar axis Z along which rotatory polarization occurs (the crystallographic Z-axis). By convention, the crystallographic axes are denoted by X, Y, Z, while the coordinate axes are denoted x_1, x_2, x_3.

Quartz (SiO_2) in the form of α-quartz is one of the most commonly used materials for the design of piezoelectric devices because of its excellent mechanical properties. The α-quartz is stable up to $573°C$, at higher temperatures β-quartz is made. The density at room temperature ($20°C$) is $\rho = 2649 \frac{kg}{m^3}$, material moduli are given in the following table:

Elastic coeff. $\left[\frac{10^9 N}{m^2}\right]$	$c_{11} = c_{22}$	c_{12}	$c_{13} = c_{23}$	$c_{14} = -c_{24} = c_{56}$	c_{33}	$c_{44} = c_{55}$	c_{66}
	86.74	6.99	11.91	-17.91	107.2	57.94	39.88

Piezoelectric coeff. $\left[\frac{C}{m^2}\right]$	$e_{11} = -e_{12} = -e_{26}$	$e_{14} = -e_{25}$	**Dielectric coeff.** $\left[\frac{10^{-12} F}{m}\right]$	$\epsilon_{11} = \epsilon_{22}$	ϵ_{33}
	0.171	-0.0407		39.97	41.03

Lithium Niobate ($LiNbO_3$) is an extremely versatile crystal material. It possesses a very high Curie temperature and excellent piezoelectric coupling coefficient making

it attractive for ultrasonic device applications. Lithium niobate possesses a number of useful cuts that are extensively used in transducer applications, e.g. YZ $LiNbO_3$ (i.e. Y-axis crystal cut, Z-axis propagation) or 128° rotated YX $LiNbO_3$. Material moduli are given for room temperature ($20°C$) in the following table:

Elastic coeff. $\left[\frac{10^{10}\mathbf{N}}{\mathbf{m}^2}\right]$	$c_{11}=c_{22}$	c_{12}	$c_{13}=c_{23}$	$c_{14}=-c_{24}=c_{56}$	c_{33}	$c_{44}=c_{55}$	c_{66}
	20.3	5.3	7.5	0.9	24.5	6.0	7.5
Piezoelectric coeff. $\left[\frac{\mathbf{C}}{\mathbf{m}^2}\right]$	$e_{15}=e_{24}$		$e_{22}=-e_{21}=-e_{16}$		$e_{31}=e_{32}$	e_{33}	
	3.7		2.5		0.1	1.3	
Dielectric coeff. $\left[\frac{10^{-12}\mathbf{F}}{\mathbf{m}}\right]$	$\epsilon_{11}=\epsilon_{22}$		ϵ_{33}	**Density** $\left[\frac{10^{3}\mathbf{kg}}{\mathbf{m}^3}\right]$	ρ		
	749.0		253.2		4.63		

A.1 Transformation of Material Constants

The constants given here are for crystal geometries coinciding with the coordinate planes. For some technological reasons, different cuts of crystals are preferred in practice, i.e. an coordinate transformation is realized by

$$\bar{\boldsymbol{x}} \;=\; \bar{\boldsymbol{x}}(\boldsymbol{x}) \;,$$

The material moduli in the new coordinate system are then regained by the tensor transformations

$$\bar{c}_{\bar{i}\bar{j}\bar{k}\bar{l}} \;=\; c_{ijkl}\frac{\partial \bar{x}_{\bar{i}}}{\partial x_i}\frac{\partial x_j}{\partial x_{\bar{j}}}\frac{\partial \bar{x}_{\bar{k}}}{\partial x_k}\frac{\partial x_l}{\partial x_{\bar{l}}} \;, \tag{A.1.1}$$

$$\bar{e}_{\bar{i}\bar{j}\bar{k}} \;=\; e_{ijk}\frac{\partial \bar{x}_{\bar{i}}}{\partial x_i}\frac{\partial \bar{x}_{\bar{j}}}{\partial x_j}\frac{\partial x_k}{\partial x_{\bar{k}}} \;, \tag{A.1.2}$$

$$\bar{\epsilon}_{\bar{i}\bar{j}} \;=\epsilon_{ij}\frac{\partial \bar{x}_{\bar{i}}}{\partial x_i}\frac{\partial x_j}{\partial x_{\bar{j}}} \;. \tag{A.1.3}$$

Usually, a simple rigid rotation is undertaken, i.e. the coordinate transformation is linear, $\bar{\boldsymbol{x}} = \boldsymbol{T}\boldsymbol{x}$, and $\frac{\partial \bar{x}_{\bar{i}}}{\partial x_i} = T_{\bar{i}i}$ represent the direction cosines between the two frames of reference.

In this setting, the relationship between the so-called crystallographic fundamental orthogonal system of axes X, Y, Z and the coordinate axes x_1, x_2, x_3 must be known. Note, that there are piezoelectric materials where the orientations of the crystallographic unit cell axes do not align with the fundamental coordinate system, but

usually constants are given for the fundamental coordinate system and we will not consider such materials anyway.

In transducer design, there is a simple standardized [62] way to provide this information: Here, the first two letters (out of `X`, `Y`, `Z`) denote the initial plate orientation, the first indicating the plate thickness, the second the plate length before any rotations. The remaining up to three symbols (out of `t` =thickness, `w` =width, `l` =length) are used to indicate the plate edges used for rotation, followed by a list of corresponding angles, see Figure A.1 a) for a `YZ`-plate and Figure A.1 b) for a rotated `YZw` $-\phi$ - plate.

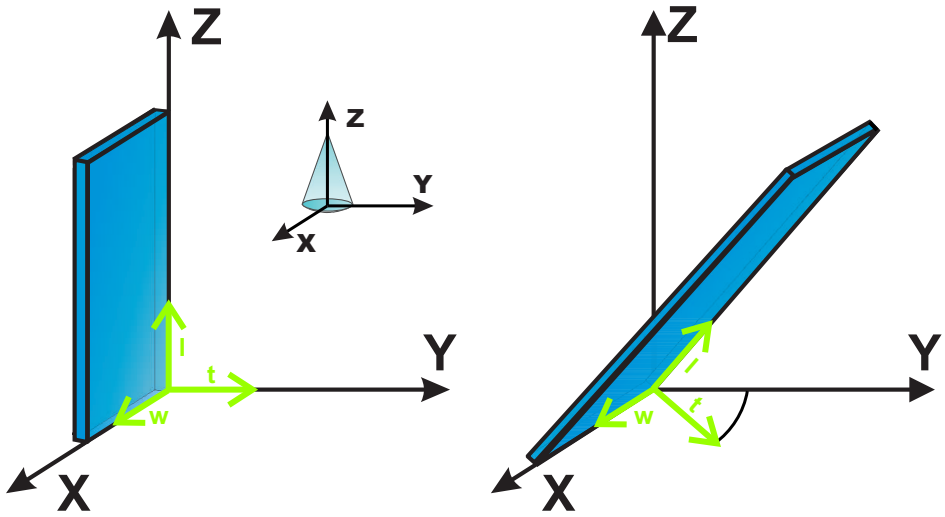

(a) `YZ` - orientation (b) `YZw` $-\phi$ - orientation

Figure A.1: Piezoelectric Plate in Crystallographic `X`, `Y`, `Z`-Coordinate System

In SAW transducer design, speaking of 128°-rotated $LiNbO_3$, usually one considers `YXl` 128° $LiNbO_3$.

Bibliography

[1] R.A. Adams. *Sobolev spaces*, volume 65 of *Pure and Applied Mathematics, a Series of Monographs and Textbooks*. Academic Press, New York - San Francisco - London, 1975.

[2] Advalytix AG, Brunnthal. Homepage: `www.advalytix.de`.

[3] Finite element package ALBERTA. Homepage: `www.alberta-fem.de`.

[4] H. Allik and T.J.R. Hughes. Finite element method for piezoelectric vibration. *Int. J. Numer. Meth. Eng.*, 2:151–157, 1970.

[5] H.W. Alt. *Lineare Funktionalanalysis. Eine anwendungsorientierte Einführung*. Springer-Lehrbuch. Springer, Berlin, 2002. (Linear functional analysis. An application oriented introduction).

[6] K. Arrow, L. Hurwicz, and H. Uzawa. *Studies in Linear and Nonlinear Programming*. Stanford University Press, Stanford, 1958.

[7] B.A. Auld. *Acoustic fields and waves in solids*. Wiley, New York, 1973.

[8] I. Babuška. Error-bounds for finite element method. *Numer. Math.*, 16:322–333, 1971.

[9] I. Babuška. The finite element method with Lagrange multipliers. *Numer. Math.*, 20:179–192, 1973.

[10] I. Babuška and A. Aziz. Survey lectures on the mathematical foundations of the finite element method. In A. Aziz, editor, *The mathematical foundations*

of the finite element method with applications to partial differential equations, New York, 1973. Academic Press.

[11] R.E. Bank, B.D. Welfert, and H. Yserentant. A class of iterative methods for solving saddle point problems. *Numer. Math.*, 56:645–666, 1990.

[12] K.J. Bathe and E. Wilson. *Numerical methods in finite element analysis*. Eaglewood Cliffs, New York, 1976.

[13] A. Bedford and D.S. Drumheller. *Introduction to elastic wave propagation*. J. Wiley, Chichester, 1994.

[14] M. Benzi. Preconditioning techniques for large linear systems: A survey. *J. Comp. Phys.*, 182:418–477, 2002.

[15] M. Benzi and G.H. Golub. A preconditioner for generalized saddle point problems. *SIAM J. Matrix Anal. Appl.*, 26(1):20–41, 2004.

[16] N.D. Botkin and V.L. Turova. Mathematical models of a biosensor. *caesar preprint*, 2002.

[17] D. Braess. Stability of saddle point problems with penalty. M^2AN, 30:731–742, 1996.

[18] D. Braess. *Finite elements: Theory, fast solvers, and applications in solid mechanics*. Cambridge Univ. Press, 2001.

[19] J.H. Bramble, J.E. Pasciak, and A.T. Vassilev. Analysis of the inexact Uzawa algorithm for saddle point problems. *SIAM J. Numer. Anal.*, 34(3):1072–1092, 1997.

[20] J.H. Bramble, J.E. Pasciak, and J. Xu. Parallel multilevel preconditioners. *Math. Comp.*, 55:1–22, 1990.

[21] S.C. Brenner and L.R. Scott. *The mathematical theory of finite element methods*, volume 15 of *Texts in applied mathematics*. Springer, Berlin, 2002.

[22] F. Brezzi. On the existence, uniqueness and approximation of saddle point problems arising from Lagrange multipliers. *RAIRO Math. Model. Numer. Anal.*, 8:129–151, 1974.

[23] F. Brezzi and M. Fortin. *Mixed and hybrid finite element methods*, volume 15 of *Springer Series in Computational Mathematics*. Springer, New York, 1991.

[24] A.M. Bruaset. *A survey of preconditioned iterative methods*. Pitman research notes in mathematics series. Longman, Harlow, 1995.

[25] C. Campbell. *Surface acoustic wave devices and their signal processing applications*. Academic Press, San Diego, 1989.

[26] Z.H. Cao. Fast uzawa algorithm for generalized saddle point problems. *Appl. Numer. Math.*, 46(2):157–171, 2003.

[27] C. Carstensen, S. Funken, W. Hackbusch, R.H.W. Hoppe, and P. Monk, editors. *Computational electromagnetics. Proceedings of the GAMM workshop on computational electromagnetics, Kiel, Germany, January 26–28, 2001*, volume 28 of *Lecture Notes in Computational Science and Engineering*, Berlin, 2003. Springer.

[28] M.A. Casarin and O.B. Widlund. A hierarchical preconditioner for the mortar finite element method. *ETNA, Electron. Trans. Numer. Anal.*, 4:75–88, June 1996.

[29] T.F. Chan and B.F. Smith. Multigrid and domain decomposition on unstructured grids. *Electr. Trans. Numer. Anal.*, 2:171–182, 1994.

[30] P.G. Ciarlet. *The finite element method for elliptic problems*. North-Holland, Amsterdam, 1978.

[31] P.G. Ciarlet and J.L. Lions, editors. *Finite Element Methods (Part 1)*, volume II of *Handbook of Numerical Analysis*. North-Holland, Amsterdam, 1991.

[32] P. Ciarlet, Jr., J. Huang, and J. Zou. Some observations on generalized saddle-point problems. *SIAM J. Matrix Anal. Appl.*, 25(1):224–236, 2003.

[33] J. Curie and P. Curie. Sur l'électricité polaire dans les cristaux hémièdres à faces inclinées. *Comptes Rendus de l'Académie des Sciences*, 91:383–387, 1880.

[34] P. Curie and J. Curie. Development by pressure of polar electricity in hemihedral crystals with inclined faces. *Bull. Soc. Min. de France*, 3:90, 1880.

[35] M. Denda and Y.K. Yong. Two-dimensional boundary element analysis of quartz surface wave resonators. In *IEEE/EIA International Frequence Control Symposium and Exhibition*, 2000.

[36] M. Dryja, A. Gantner, O.B. Widlund, and B.I. Wohlmuth. Multilevel additive Schwarz preconditioner for nonconfroming mortar finite element methods. *J. Numer. Math.*, 12(1):23–38, 2004.

[37] M. Dryja and O.B. Widlund. Multilevel additive methods for elliptic finite element problems. In *Parallel Algorithms for Partial Differential Equations, Proc. 6th GAMM- Semin.*, pages 58–69. Notes Numer. Fluid Mech. 31, 1991.

[38] I.S. Duff, A.M. Erisman, and J.K. Reid. *Direct methods for sparse matrices*. Monographs on numerical analysis. Clarendon, Oxford, 1992.

[39] G. Duvaut and J.L. Lions. *Les inéquations en mécanique et en pysique*. Dunod, Paris, 1972.

[40] H.C. Elman and G.H. Golub. Inexact and preconditioned Uzawa algorithms for saddle point problems. *SIAM J. Numer. Anal.*, 31(6):1645–1661, 1994.

[41] G. Endoh, K. Hashimoto, and M. Yamaguchi. Surface acoustic wave propagation characterization by finite-element method and spectral domain analysis. *Jpn. J. Appl. Phys.*, 34, 1995.

[42] A.C. Eringen and G.A. Maugin. *Electrodynamics of continua I. Foundations and solid media*. Springer, New York, 1990.

[43] L.C. Evans. *Partial differential equations*. American Mathematical Society, Providence, 1998.

[44] V. Faber and T.A. Manteuffel. Orthogonal error methods. *SIAM J. Numer. Anal.*, 24(1):170–187, 1987.

[45] J. Fagerholm. Wave propagation in diffractive optical elements and surface-acoustic wave devices. Technical report, CSC Research Report R07/96, Center for Scientific Computing, Helsinki University of Technology, Espoo, Finland, 1996.

[46] G.W. Farnell. Elastic surface waves. In H. Matthews, editor, *Surface wave filters*. Wiley, New York, 1977.

[47] M. Feldmann and J. Hénaff. *Surface acoutic waves for signal processing*. Artech House, Boston, 1989.

[48] N. Finger, G. Kovacs, J. Schöberl, and U. Langer. Accurate FEM/BEM-simulation of surface acoustic wave filters. In *IEEE Ultrasonics symposium*, 2003.

[49] H. Gajewski, K. Gröger, and K. Zacharias. *Nichtlineare Operatorgleichungen und Operatordifferentialgleichungen*. Akademie-Verlag, Berlin, 1974.

[50] A. George, K. Ikramov, and A.B. Kucherov. Some properties of symmetric quasi-definite matrices. *SIAM J. Matrix Anal. Appl.*, 21(4):1318–1323, 2000.

[51] P.E. Gill, M.A. Saunders, and M.H. Wright. On the stability of Cholesky factorization for symmetric quasidefinite systems. *SIAM J. Matrix Anal. Appl.*, 17(1):35–46, 1996.

[52] V. Girault and P.A. Raviart. *Finite element methods for Navier Stokes equations*, volume 6 of *Springer series in computational mathematics*. Springer, New York, 1986.

[53] P. Grisvard. *Elliptic problems in nonsmooth domains*. Monographs and Studies in Mathematics, 24. Pitman, Boston, 1985.

[54] W. Hackbusch. *Iterative Lösung großer schwachbesetzter Gleichungssysteme. (Iterative solution of large sparse systems of equations)*, volume 69 of *Leitfäden der Angewandten Mathematik und Mechanik*. Teubner, Stuttgart, 1991.

[55] W. Hackbusch. *Elliptic differential equations: theory and numerical treatment*, volume 18 of *Springer Series in Computational Mathematics*. Springer, Berlin, 1992.

[56] E. Hairer, S.P. Nørsett, and G. Wanner. *Solving ordinary differential equations. I: Nonstiff problems. 2*, volume 8 of *Springer Series in Computational Mathematics*. Springer, Berlin, 1993.

[57] K. Hashimoto and M. Yamaguchi. SAW device simulation using boundary element methods. *Jpn. J. Appl. Phys.*, 29, 1990.

[58] R. Hiptmair. Finite elements in computational electromagnetism. *Acta Numer.*, pages 237–339, 2002.

[59] M. Hofer, M. Jungwirth, R. Lerch, and R. Weigel. Accurate and efficient modeling of SAW structures. *Frequenz*, 55(1–2):64–72, 2001.

[60] J. Sanchez Hubert and E. Sanchez Palencia. *Vibration and coupling of continuous systems. Asymptotic methods*. Springer, Berlin, 1989.

[61] F. Ihlenburg. *Finite element analysis of acoustic scattering*, volume 132 of *Applied Mathematical Sciences*. Springer, New York, 1998.

[62] Institute of Electrical and Electronics Engineers, New York. *IEEE Standard on piezoelectricity*, IEEE transactions on sonics and ultrasonics 3 edition, 1978.

[63] J.D. Jackson. *Classical Electrodynamics*. Wiley, New York, 1998.

[64] H. Kardestuncer, editor. *Finite element handbook*. McGraw-Hill, New York, 1987.

[65] R.B. Kellogg and B. Liu. A finite element method for compressible stokes equations. *SIAM J. Numer. Anal.*, 33:780–788, 1996.

[66] G.S. Kino. *Acoustic waves: devices, imaging, and analog signal processing*. Prentice-Hall, Englewood Cliffs, 1987.

[67] A. Klawonn. An optimal preconditioner for a class of saddle point problems with a penalty term. *SIAM J. Sci. Comput.*, 19(2):540–552, 1998.

[68] A. Klawonn and L.F. Pavarino. Overlapping schwarz methods for mixed linear elasticity and stokes problems. *Comput. Methods Appl. Mech. Eng.*, 265:233–45, 1998.

[69] A.N. Krylov. On the numerical solution of the equation by which the frequency of small oscillations is determined in technical problems. *Isz. Akad. Nauk SSSR Ser. Fiz.-Math*, 4:491–539, 1931.

[70] R. Lerch. Simulation of piezoelectric devices by two- and three-dimensional finite elements. *IEEE Trans. Ultrasonics, Ferroelectrics and Frequency Control*, 37(3):233–247, 1990.

[71] M.F. Lewis. On Rayleigh waves and related propagating acoustic waves. In E.A. Ash and E.G.S. Paige, editors, *Rayleigh-Wave Theory and Applications*, volume 2 of *Springer Series on Wave Phenomena*, pages 37–58. Springer, 1985.

[72] J. Lions and E. Magenes. *Non-homogenous boundary value problems and applications*, volume 1. Springer, Berlin, 1972.

[73] J.E. Marsden and T.J.R. Hughes. *Mathematical foundations of elasticity*. Prentice-Hall Civil Engineering and Engineering Mechanics Series. Prentice-Hall, Englewood Cliffs, New Jersey, 1983.

[74] G.A. Maugin. *Continuum mechanics of electromagnetic solids*, volume 33 of *North-Holland series in applied mathematics and mechanics*. North-Holland, 1987.

[75] W. McLean. *Strongly elliptic systems and boundary integral equations*. Cambridge University Press, Cambridge, 2000.

[76] A. Meister. *Numerik linearer Gleichungssysteme. Eine Einführung in moderne Verfahren*. Vieweg, Braunschweig, 1999.

[77] P. Monk. *Finite element methods for Maxwell's equations*. Numerical Mathematics and Scientific Computation. Oxford University Press, Oxford, 2003.

[78] D.P. Morgan. *Surface Wave Devices for Signal Processing*. Elsevier, Amsterdam, 1991.

[79] D.P. Morgan. *Surface-wave devices for signal processing*. Elsevier, Amsterdam, 1991.

[80] N.M. Nachtigal, S.C. Reddy, and L.N. Trefethen. How fast are nonsymmetric matrix iterations? *SIAM J. Matrix Anal.*, 13:778–795, 1992.

[81] J. Nečas. Sur une méthode pour resoudre les équations aux dérivées partielles du type elliptique, voisine de la variationnelle. *Ann. Sc. Norm. Super. Pisa*, 16:305–326, 1962.

[82] R.A. Nicolaides. Existence, uniqueness and approximation for generalized saddle point problems. *SIAM J. Numer. Anal.*, 19:349–357, 1982.

[83] J. Nitsche. On Korn's second inequality. *RAIRO Anal. Numér.*, 15:237–248, 1981.

[84] W. Nolting. *Grundkurs Theoretische Physik. Elektrodynamik*. Springer, Berlin, 2004.

[85] J.A. Ogilvy. An approximate analysis of waves in layered piezoelectric plates from an interdigital source transducer. *J. Phys. D, Applied Physics*, 29:876–884, 1996.

[86] O. Osterby and Z. Zlatev. *Direct methods for sparse matrices*, volume 157 of *Lecture notes in computer science*. Springer, Berlin, 1983.

[87] P. Oswald. *Multilevel Finite Element Approximation: Theory and Applications*. Teubner Skripten zur Numerik. B. G. Teubner, Stuttgart, 1994.

[88] A. Pazy. *Semigroups of linear operators and applications to partial differential equations*. Number 44 in Applied Mathematical Sciences. Springer, Berlin, 1983.

[89] A. Quateroni and A. Valli. *Domain Decomposition Methods for Partial Differential Equations*. Numerical Mathematics and Scientific Computation. Oxford University Press, New York, 1999.

[90] Lord Rayleigh. On waves propagating along the plane surface of an elastic surface. *Proc. London Math. Soc.*, 7:4–11, 1885.

[91] Y. Saad and M.H. Schultz. GMRES: A generalized minimal residual algorithm for solving nonsymmetric linear systems. *SIAM J. Sci. Stat. Comp.*, 7:856–869, 1986.

[92] W. Schmid, M. Paffrath, and R.H.W. Hoppe. Application of iterative methods for solving nonsymmetric linear systems in the simulation of semiconductor processing. *Surv. Math. Industry*, 5:1–26, 1995.

[93] A. Schmidt and K.G. Siebert. *Design of adaptive finite element software. The finite element toolbox ALBERTA*, volume 42 of *Lecture Notes in Computational Science and Engineering*. Springer, 2005.

[94] D. Silvester and A. Wathen. Fast iterative solution of stabilised Stokes systems part II: Using general block preconditioners. *SIAM J. Numer. Anal.*, 31(5):1352–1367, 1994.

[95] W.S. Slaughter. *The linearized theory of elasticity*. Birkhäuser, Boston, 2002.

[96] B.F. Smith, P.E. Bjørstad, and W.D. Gropp. *Domain Decomposition: Parallel Multilevel Methods for Elliptic Partial Differential Equations*. Cambridge University Press, 1996.

[97] H. Tanabe. *Equations of evolution*. Number 6 in Monographs and Studies in Mathematics. Pitman, London, 1979.

[98] H. Uzawa. Iterative methods for concave programming. In *Studies in Linear and Nonlinear Programming* [6].

[99] R.J. Vanderbrei. Symmetric quasidefinite operators. *SIAM J. Optim.*, 5(1), 1995.

[100] P. Ventura, J.M. Hodé J. Desbois, and M. Solal. Combined FEM and Green's function analysis of periodic SAW strucutre, application to the calculation of reflection and scattering parameters. *IEEE Trans. Ultrasonics, Ferroelectrics and Frequency Control*, 48(5), 2001.

[101] A. Wathen and D. Silvester. Fast iterative solution of stabilised Stokes systems part I: Using simple diagonal preconditioners. *SIAM J. Numer. Anal.*, 30(3):630–649, 1993.

[102] R. Weiss. A theoretical overview of Krylov subspace methods. *Applied Numerical Mathematics: Transactions of IMACS*, 19(3):207–233, 1996.

[103] R.M. White and F.W. Voltmer. Direct piezoelectric coupling to surface elastic waves. *Appl. Phys. Lett.*, 17:314–316, 1965.

[104] A. Wixforth, LSt. Experimentalphysik I, Universität Augsburg. Homepage: `http://www.physik.uni-augsburg.de/exp1/wixforth/wixforth.html`.

[105] A. Wixforth. Nano-Beben auf dem Chip: Akustische Oberflächenwellen als Photonen-Förderband. *Physikalische Blätter*, 54, 1998.

[106] A. Wixforth, C. Gauer, J. Scriba, M. Wassermeier, and R. Kirchner. Flat fluidics: A new route toward programmable biochips. In *Proceedings of SPIE*, 2003.

[107] A. Wixforth and J. Scriba. Nano-Pumpen für das Chiplabor. *GIT Laborfachzeitschrift*, 5, 2002.

[108] M.H. Wright. Interior methods for constrained optimization. *Acta Numerica*, pages 341–407, 1992.

[109] S.J. Wright. *Primal-dual interior point methods*. SIAM, Philadelphia, 1997.

[110] H. Yserentant. On the multi-level splitting of finite element spaces. *Numer. Math.*, 49:379–412, 1986.

[111] H. Yserentant. Old and new convergence proofs for multigrid methods. *Acta Numerica*, pages 285–326, 1993.

[112] E. Zeidler. *Nonlinear functional analysis and its applications. II/A: Linear monotone operators*. Springer, Berlin, 1990.

[113] J. Zelenka. *Piezoelectric resonators and their applications*, volume 24 of *Studis in electrical and electronic engineering*. Elsevier, Amsterdam, 1986.

[114] X. Zhang. Multilevel Schwarz methods. *Numer. Math.*, 63:521–539, 1992.